SGP-TR-95

A Technical Review of Interference Testing with Application in the Ohaaki Geothermal Field

Jonathan D. Leaver

March 1986

Financial support was provided through the Stanford Geothermal Program under Department of Energy Contract No. DE-AT03-80SF11459 and by the Department of Petroleum Engineering, Stanford University

Stanford Geothermal Program
Interdisciplinary Research in
Engineering and Earth Sciences
STANFORD UNIVERSITY
Stanford, California

ACKNOWLEDGEMENTS

This project would not have been possible without the professional advice and support of Assoc. Prof. Abraham Sageev and Prof. Henry J. Ramey Jr. of Stanford University Petroleum Engineering Department.

The assistance of Mr. Paul F. Bixley, Ministry of Works and Development, Wairakei, New Zealand, and Dr. Malcolm Grant, Department of Scientific and Industrial Research, Wellington, New Zealand, in obtaining the data and background reports was also greatly appreciated.

Test data for the "C" series of tests was collected by Mr. David M. Wilson, M.W.D., Wairakei, and kindly filtered and supplied by Dr. Mark J. McGuinness, Applied Math. Division, D.S.I.R., Wellington.

Financial support was provided by M.W.D., New Zealand Energy Department, Stanford Geothermal Program, DOE Contract No. DE-AT02-80SF11459, and by Stanford University.

To

Cynthia

and

Trudie, Rosanne and Luke.

ABSTRACT

The chronology and mathematical development of interference testing and related earth tide and compressibility effects are reviewed. Hydrological information from field tests performed in the Ohaaki geothermal field since first development in 1965 is summarized.

Data from 12 interference tests (four on the same doublet) performed in the deep Ohaaki reservoir between 1979 and 1983 are analyzed using conventional log-log and semi-log type curve matching techniques along with recently developed semi-log type curve matdhing techniques which allow linear boundary detection without the necessity to develop two semi-log straight lines or the need to know reservoir parameters.

Data in nine tests were recorded using water level chart recording devices while data in the remaining three were recorded using quartz crystal pressure gauges. Both instruments have a resolution of about 100Pa.

Some tests show the presence of a no-flow boundary for which the inference ellipses have been located. Interpretation is made on the probable location of the no-flow boundary. A study of the significance of early time data and other factors shows that vastly different reservoir parameters can be obtained unless careful interpretation is made.

A hydrological model of the Ohaaki geothermal field is presented.

TABLE OF CONTENTS

LIST OF FIGURES

LIST OF TABLES

1. INTRODUCTION

Interference testing in geothermal fields is one of the principal tools used to determine bulk transmissivities (kh) and storativities ($\phi c_t h$) and to locate hydrological heterogeneities such as no-flow and pressure support boundaries. Changes in the hydrology of geothermal reservoirs in geologic time can be caused through mineral deposition, changes in the heat flux into or out of, the system, crustal movements, changes in fluid components (brine, gas) moving into or out of the reservoir and exploitation. Exploitation increases by orders of magnitude the rate of natural processes in the reservoir, with mineral deposition and reduction in the heat of the system being the most significant. Interference tests are both an essential and economical tool in assessment of the extractable heat capacity of a geothermal field and in monitoring changes in reservoir characteristics as exploitation proceeds. The past 50 years has seen steady progress in developing basic fluid flow theory to the practical techniques available in 1985. A brief chronology of the developments in interference testing is described below.

Theis [1935] published the line source solution based on heat transfer analogy and used time superposition to simulate a finite flow period. The stated assumptions were:

> *"(i) Entirely homogeneous bodies.*
>
> *(ii) Infinite areal extent.*
>
> *(iii) Well penetrates the entire thickness of the water body.*
>
> *(iv) Coefficient of transmissibility is constant at all times and in all places.*
>
> *(v) Pumped well has infinitesimal diameter.*
>
> *(vi) Applicable only to unconfined water bodies in which the water in the volume of sediments through which the water table has fallen is discharged instantaneously with the fall of the water table."*

Theis [1935] also noted that:

> *"The effect of boundaries can be considered by more elaborate analyses once they*

are located."

However the formal publication of these analyses awaited a further 17 years.

Jacob [1941] circumspectly used the term "interference testing" to describe the change in pressure in a shut-in well caused by changes in flow rate at other wells:

> ***"The interference of two wells, in the technical sense, is determined by a comparison of the flow of one of two wells when both are flowing freely, with He flow of each well when the other is shut off."***

Jacob also makes mention of the match between data and a theoretical type curve providing the parameters required to determine permeability and porosity thereby possibly being the first to use type curve matching techniques.

Muskat [1937] used space superposition to sum pressure changes from each individual well at any point in a reservoir at steady state thereby finding the total pressure change at that point. *Kazmann* [1946] used space superposition of source and image wells to determine the distance to a recharge boundary. ***Van Everdingen*** and ***Hurst*** [1949] showed that reservoir fluid flow could be described by the Diffusivity equation. The use of Laplace transforms was shown to simplify the solution process for many problems. ***Stallman*** [1952] presented type curves which included the effect of a no-flow boundary during drawdown. ***Hurst*** [1960] as a corollary to work on interference between oil fields showed how to determine pressure variations due to two wells in a single layer heterogeneous reservoir. ***Barenblatt*** and ***Zheltov*** [1960], and ***Barenblatt et al.*** [1960] introduced the concept of a double porosity model containing matrix and fissures. Fluid was assumed to flow from the matrix to the fissures under pseudo steady state conditions. Mathematical development utilized the average matrix and fissure pressures measured at the same reservoir location. *Hantush* [1960] analytically derived type curves for the pressure response in a reservoir bounded above by a leaky aquifer. The difference between these curves and the line source solution was small for compressible systems which generally meant the properties of the caprock could not be determined. ***Witherspoon*** [1962] resolved this problem by using well measurements in the aquifer overlying the main reservoir to determine

the leaky caprock properties. ***Ferris*** et ***al.*** [1962] presented methods for modelling linear fault combinations in a single homogeneous isotropic medium. ***Warren*** and ***Root*** [1963] simplified the analysis of double prosity systems by describing the pressure distribution in terms of only two parameters - the interporosity flow parameter (λ) and a storativity ratio (ω). *Davis* and *Hawkins* [1963] used the semi-log doubling of slope characteristic for wells of constant skin in a semi-infinite homogeneous isotropic medium to locate the position of a no-flow boundary. The technique used a semi-log dimensionless pressure-time graph on which the intersection point of the two straight lines occurred at the same dimensionless time regardless of the distance to the barrier. It was applicable to both drawdown and buildup tests. ***Papadopulos*** [1965] produced a solution for the analysis of interference tests in homogeneous anisotxtopic reservoirs. ***Ramey*** [1970] developed the solution of ***Papadopulos*** for application to petroleum engineering problems. ***Kazemi et al.*** [1969] extended the ***Warren and Root*** double porosity model for a single well test to include the pressure response at an observation well. System characteristics were determined from the difference in early time behavior between the double porosity and isotropic homogeneous models. ***Earlougher*** and ***Ramey*** [19731 published the solution for interference effects in bounded systems. Tables were presented of dimensionless pressure and dimensionless time for various reservoir shapes and pressure observation points. *Koefoed* [1974] continued the work of ***Witherspoon*** by publishing type curves for determining the leakage factor of a reservoir with a caprock. ***Jargon*** [1976] used a finite difference numerical simulator to generate interference test data with wellbore storage and skin at the source well. Resul showed that neglecting wellbore storage causes underestimation of transmissivity and overesti mation of storativity. Increased skin damage was shown to prolong wellbore 'storage effects. *Vela* [1977] described the location of a linear boundary detected from a single interference test as a tangent to an inference ellipse. ***Najurieta*** [1979] continued work on double porosity systems and included the effect of transient interporosity flow in the analysis. ***Deruyck*** et ***al.*** [1982] presented two type curves for double porosity reservoirs. These could be used to determine whether the flow from the less permeable to the more permeable medium was transient or

pseudo steady state and also to find the nature of the double porosity system. The curves were equally applicable to either single layered fractured or multilayered homogeneous reservoirs. *Sageev et al.* [1985] mathematically collapsed a semi-log version of *Stallman's* type curves to produce a single semi-log type curve applicable for drawdown tests. The technique allowed the inference ellipse of a constant pressure or a no-flow boundary to be determined without requiring any knowledge of reservoir parameters. The method is applicable for boundaries located more than $5r_1$ from either the source or observation well. Fox [1984] used the unpublished technique of *Sageev et al.* [1985] to produce a single semi-log type curve which was applicable for buildup tests. Graphs were developed using both total time and *Horner* time. *Eipper* [1985] extended *Stallman's* work and produced a set of log-log type curves showing the effect of either a no-flow or constant pressure boundary on both drawdown and buildup. *Sageev* [1985] examined the effects of a steam cap near a doublet and produced a method for determining the probable location of the steam cap based on the transmissivity and storativity value obtained from conventional techniques.

2. MATHEMATICAL DEVELOPMENT

The development of fundamental equations for type curves relies upon the assumption that fluid flow in the reservoir can be described by the diffusivity equation. In radial coordinates this is:

$$\frac{\partial^2 p}{\partial r^2} + \frac{1}{r}\frac{\partial p}{\partial r} = \frac{\phi \mu c_t}{k}\frac{\partial p}{\partial t} \tag{2.1}$$

The equation is derived using conservation of mass, *Darcy's* Law, and an equation of state, and is a second order linear homogeneous partial differential equation. Due to the linear property, multiples of any solution to the diffusivity equation and its associated boundary conditions will also be solutions. Hence space superposition of constant rate line sources is possible allowing the generation of single and multiple linear boundaries. Important assumptions in the development of the diffusivity equation are:

(i) Horizontal radial flow,

(ii) Negligible gravity effects.

(iii) Homogeneous isotropic porous medium.

(iv) A single fluid of small and constant compressibility.

(v) *Darcy* flow in the formation.

(vi) Permeability, compressibility, viscosity and porosity are independent of pressure.

2.1. LOG-LOG TYPE CURVES

2.1.1. Line Source *(Theis)*

The solution of the pressure response at any point in an infinite reservoir due to the discharg of a well of infinitesimal diameter at constant rate was given by *Theis* [1935]:

$$p_D = -\frac{1}{2}Ei\left[\frac{-r_D^2}{4t_D}\right] \tag{2.2}$$

The exponential integral (Ei) is defined as:

$$Ei(-x) = \int_{x}^{\infty} \frac{e^{-u}}{u}\, du \qquad (2.3)$$

A dimensionless pressure-time graph is shown in Figure 2.1.

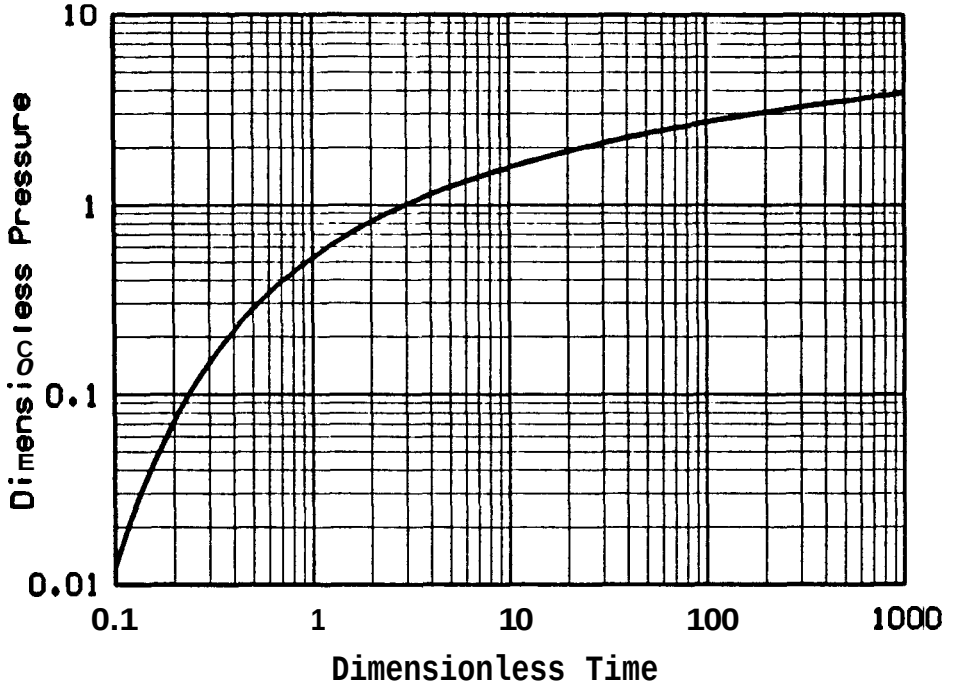

Fig. 2.1 Log-log drawdown response of a Line Source Well in an infinite reservoir (after *Theis* 1935).

2.1.2. Linear Boundary Drawdown (*Stallman*)

The solution of the pressure response at any point in a semi-infinite reservoir was given by *Stallman* [1952] superposing an image source in space to create the effects of a bear no-flow boundary. The dimensionless pressure at any spatial point in the reservoir will be the sum of the pressures due to the source and the image wells.

$$p_D = p_D\left[\frac{t_D}{r_{D_1}^2}\right] + p_D\left[\frac{t_D}{r_{D_2}^2}\right] \qquad (2.4)$$

where:

$$r_{D_1} = \frac{r_1}{r_w} \qquad r_{D_2} = \frac{r_2}{r_w}$$

Substituting the exponential integral gives: Figure 2.2 is a portion of the figure presented by ***Stallman*** [1952].

$$p_D = -\frac{1}{2}\left[Ei\left[\frac{-r_{D_1}^2}{4t_D}\right] + Ei\left[\frac{-(r_2/r_1)^2\, r_{D_1}^2}{4t_D}\right]\right] \tag{2.5}$$

A dimensionless pressure-time graph which is a portion of the figure presented by ***Stallman*** [1952], is shown in Figure 2.2.

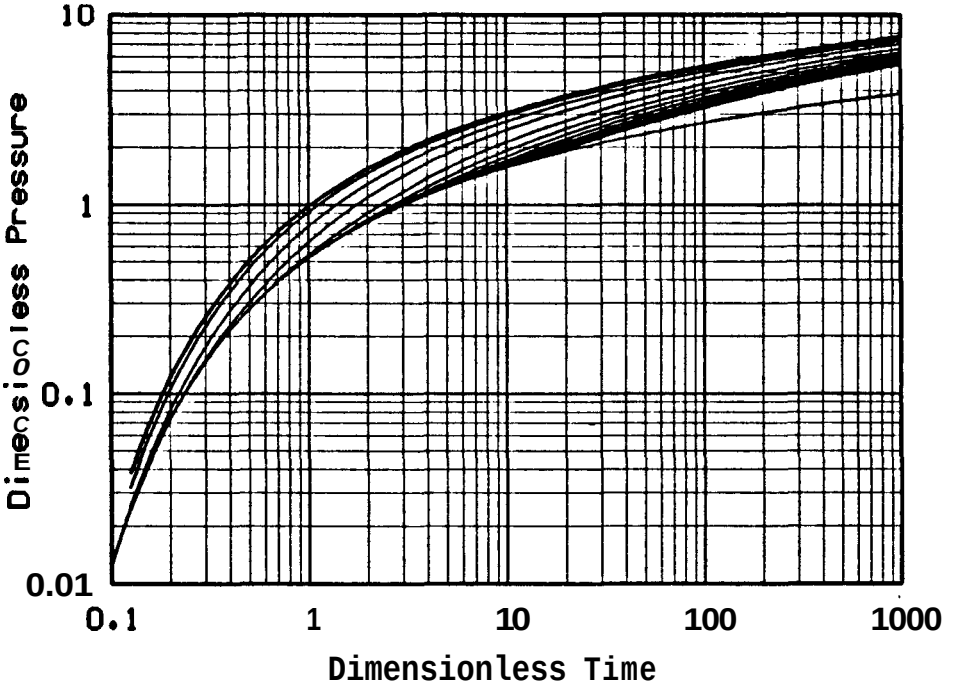

Fig. 2.2 Log-log drawdown response for reservoir with linear boundary (after *Stallman* **1952).**

The lower most curve is the line source curve for a r_2/r_1 ratio of infinity, while the upper most curve is for a pressure point at the boundary, $r_2/r_1 = 1$. Figure 2.2 is a portion of the figure presented by ***Stallman*** [1952].

2.1.3. Linear Boundary Drawdown and Buildup *(Eipper)*

Buildup behavior is incorporated into the response by using superposition in time. Zero flow rate is reflected mathematically by adding at the time of shut-in (t_p) the pressure response of source and image wells which have equal and opposite flow rates to the doublet used during drawdown:

$$p_D = p_D\left[\frac{t_D}{r_{D_1}^2}\right] + p_D\left[\frac{t_D}{r_{D_2}^2}\right] + p_D\left[\frac{t_D - t_{pD}}{r_{D_1}^2}\right] + p_D\left[\frac{t_D - t_{pD}}{r_{D_2}^2}\right] \tag{2.6}$$

Substituting the exponential integral gives:

$$p_D = -\frac{1}{2}\left\{ Ei\left[\frac{-r_{D_1}^2}{4t_D}\right] + Ei\left[\frac{-(r_2/r_1)^2\, r_{D_1}^2}{4t_D}\right] + Ei\left[\frac{-r_{D_1}^2}{4t_D} - \frac{r_{D_1}^2}{4t_{pD}}\right] + \left[\frac{-(r_2/r_1)^2\, r_{D_1}^2}{4t_D} - \frac{(r_2/r_1)^2\, r_{D_1}^2}{4t_{pD}}\right]\right\} \tag{2.7}$$

A dimensionless pressure-time log-log graph is shown in Figure 2.3.

2.2. SEMI-LOG TYPE CURVES

2.2.1. Linear Boundary Drawdown *(Sageev et al.)*

Semi-log type curves enable better matching of late time data as the higher pressure and late time scales are expanded from the log-log scale. ***Sageev et al.*** **[1985]** noted the similarity in the shape of semi-log graphs of the ***Stallman*** type curves (Figure 2.4) for r_2/r_1 ratios greater than 10. These curves and those for a constant pressure boundary were mathematically collapsed giving a single semi-log type curve which could be used to determine the inference ellipse for any linear boundary. The semi-log curves were arbitrarily collapsed onto the curve for r_2/r_1 = 100. The new curves used modified dimensionless pressure-time parameters which are defined as follows:

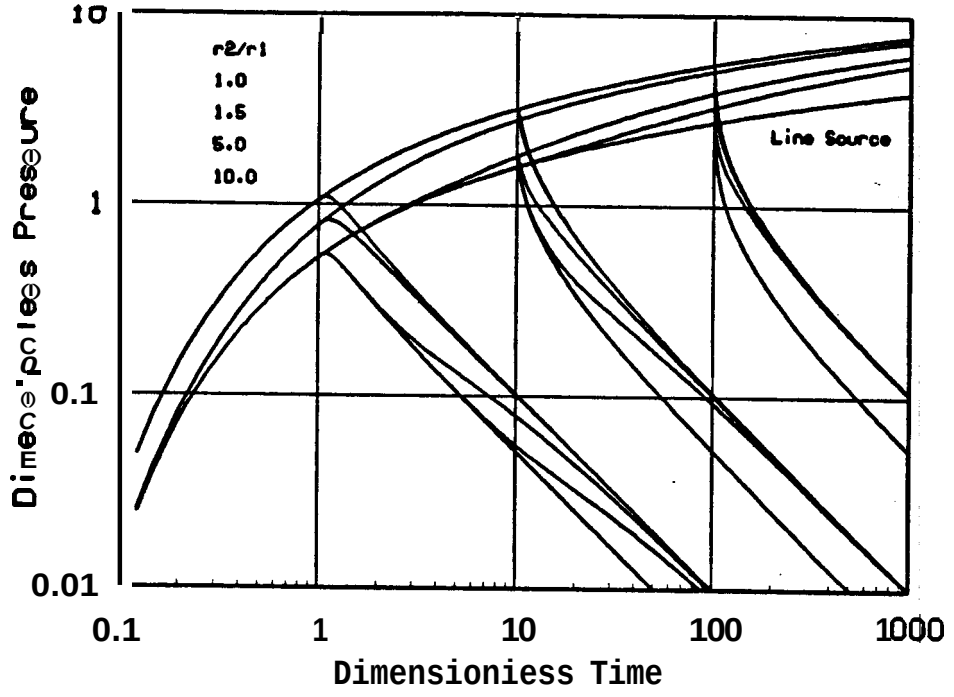

Fig. 2.3 Log-log drawdown and buildup response for reservoir with linear boundary (after Eipper 1985).

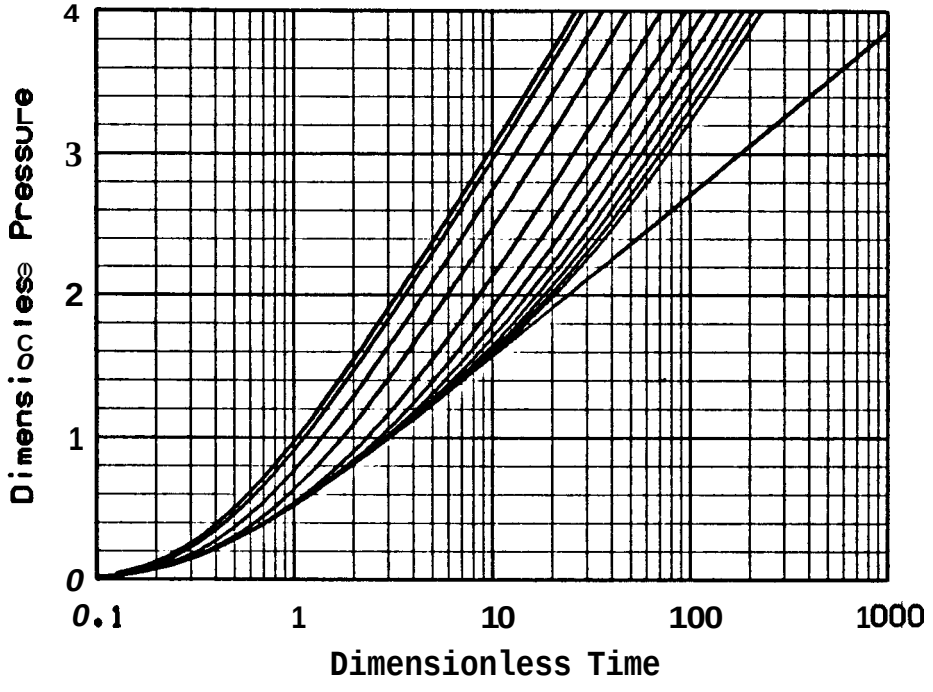

Fig. 2.4 Semi-log drawdown response for reservoir in a semi-infinite system.

$$p_D^* = p_D + \ln\left[\frac{100-1}{r_2/r_1}\right] \tag{2.8}$$

$$t_D^* = t_D\left[\frac{100-1}{r_2/r_1}\right]^2 \tag{2.9}$$

A dimensionless pressure-time semi-log graph is shown in Figure 2.5.

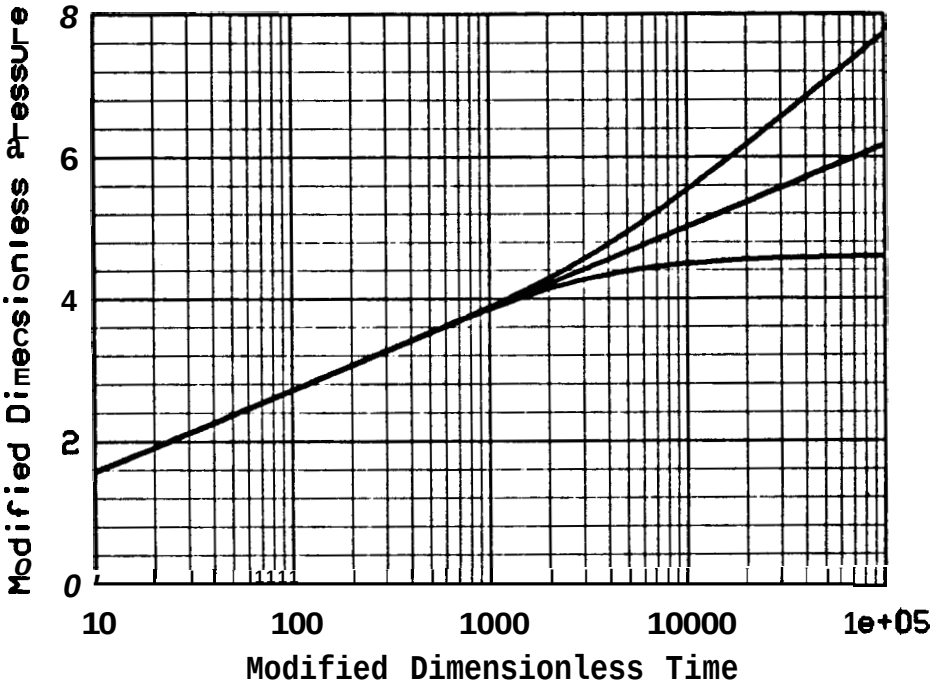

Fig. 2.5 Semi-log drawdown response for reservoir with linear boundary (after *Sageev* 1985).

2.2.2. Linear Boundary Buildup *(Fox)*

Fox [1984] used the unpublished technique of *Sugeev et al.* [1985] to produce a single type curve to analyze buildup data. Mathematical development used the log approximation to the line source solution to simplify the exact solutions. The behavior for buildup data in a semi-infinite system is characterized by two semi-log straight lines. *Fox* equated the amount by which each of the two straight lines was required to be shifted in pressure and *Horner* time at the point of intersection of the two. The semi-log curves were arbitrarily collapsed onto the curve for $r_2/r_1 = 100$. This gave two equations from which the modified dimensionless parameters were determined :

$$p^*_{DH} = p_D + \ln\left[\frac{100\,(r_2/r_1)^2}{4t_{pD}}\right] \tag{2.10}$$

$$t^*_{DH} = t_H\left[\frac{100\,(r_2/r_1)^2}{4t_{pD}}\right] \tag{2.11}$$

A dimensionless pressure-time graph is shown in Figure 2.6.

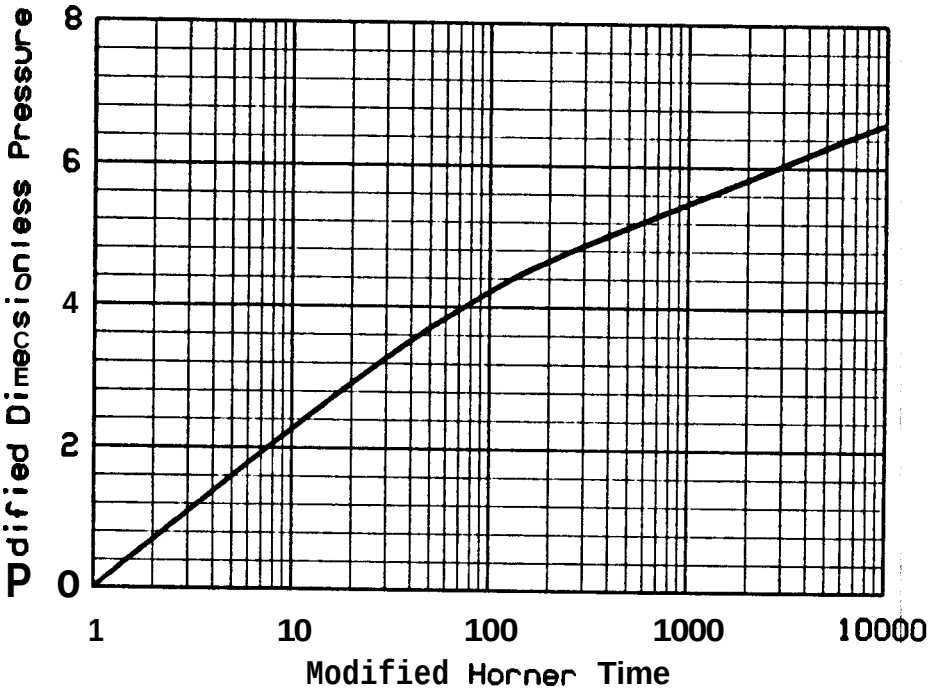

Fig. 2.6 Semi-log buildup response for reservoir with linear no-flow boundary (after Fox 1984).

2.3. INFERENCE ELLIPSE

Vela [1977] proved that in a homogeneous isotropic semi-infinite reservoir the linear boundary is located tangent to an inference ellipse. The wells are the focii of the ellipse. Vela's equation is redefined below using the *x–y* origin at the source well (Figure 2.7).

$$\frac{(2x/r_1 + 1)^2}{(r_2/r_1)^2} + \frac{(2y/r_1)^2}{(r_2/r_1)^2 - 1} = 1 \tag{2.12}$$

A schematic layout for notation used in linear boundary detection with the inference ellipse is shown in Figure 2.7.

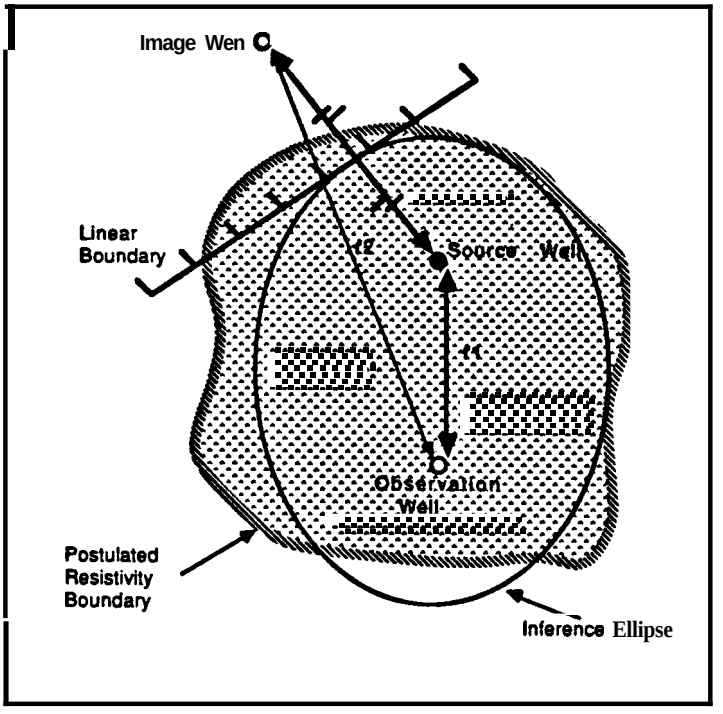

$$kh = \frac{1.01325\times10^{12}\ \mu\ p_{Dmatch}}{2\pi\ p_{Smatch}}\quad d\text{–}m \tag{13}$$

$$\phi c_t h = \frac{3600\ t_{match}\ p_{Dmatch}}{2\pi\ (t_D/r_D^2)_{match}\ r_1^2\ p_{Smatch}}\quad m/kPa \tag{14}$$

where:

$$1\ m^2 = 1.01325\times10^{12}\ \ darcy$$

3. BAROMETRIC AND EARTH TIDE EFFECTS

3.1. INTRODUCTION

The increased use of sensitive quartz crystal gauges for pressure measurements has meant greater emphasis on filtering out earth tide and barometric effects to obtain a clean interference pressure response. The response of reservoirs to barometric pressure, earth and oceanic tides and rainfall has long been observed with the magnitude of the pressure response depending on the fluid viscosity , permeability, porosity and total compressibility.

Barometric variations can produce reservoir responses of more than 8 *kPa* while earth tide responses in the reservoir are usually less than 1 *kPa*.

Studies of barometric and earth tide effects have been carried out since the beginning of the century. *Young* [1913] examined the responses of fluid levels in bore holes with a tidal variation. *LaRocque* [1941] observed fluctuations of water levels in wells during periods of strong earthquake activity. *Jacob* [1944] correlated ground water levels with rainfall. *Bredehoeft* [1967] and *Bodvarsson* [1970] studied the relation between rock characteristics and amplitude of the pressure response in an open aquifer. *Thorsteinsson* and *Eliasson* [1970] correlated pressures in the Laugarnes geothermal field in Iceland with oceanic tides. *Khurana* [1976] and *Strobel et* al. [1976] showed that tidal phenomena also affect closed systems. *Arditty* [1978] developed the following expression for the amplitude of the pressure response of a closed system to earth tides. The equation has been adapted to petroleum notation:

$$p_w = p_c \frac{4G_m(c_t-2c_f)}{3+4G_m(c_t-c_f)} \left[1 - \frac{1}{1+\frac{4k(1+\sqrt{ir_w^2\omega\mu S^*/k})}{\mu r_w d_w (c_t-c_f)}} \right] \qquad (3.1)$$

Sensitivity of the response to the forcing frequency and total compressibility was also examined.

33. BAROMETRIC PRESSURE CORRECTION

To calculate pressure changes in the reservoir from water level measurements correction must be made for changes in barometric pressure. A force balance in the wellbore gives:

$$p_{res} = \rho_w g h_w + \eta_b p_{atm} \tag{3.2}$$

where:

$$h_w = d_{pz} - d_{wl} \tag{3.3}$$

and:

η_b = barometric efficiency

$$\eta_b = \frac{\phi c_t}{\phi c_t + c_f} \tag{3.4}$$

The barometric efficiency is determined by comparing changes in reservoir pressure due to barometric fluctuations under steady state conditions with the barometric changes recorded at the surface. The barometric efficiency used for these tests was 0.85 after Grunt [1980].

An important assumption in determining the reservoir pressure from water level measurements is that the density (ρ_w) of the fluid column in the wellbore remains constant. Regular temperature or pressure profiles are recommended during pressure monitoring in the observation well to monitor drift which may lead to incorrect interpretation. Pressure measurements during drawdown in Test B2 may have been affected by changing wellbore density although other factors cannot be ruled out (refer § 7.2.2).

33. EARTH TIDES (*Sageev* et *al.* 1986)

The effects of earth tides may be significant during the early time response of an observation well. On a dimensionless match to the line source, there are three parameters that determine the importance of earth tides: the amplitude, the phase with respect to the start of the test, and the frequency. Figure 3.1 presents a record of the barometric pressure at the Ohaaki field during the the time that the flow test was carried out. The first ten days of this record are presented in Figure 3.2. In the five day period between 24 and 144 hours a linear overall decline of

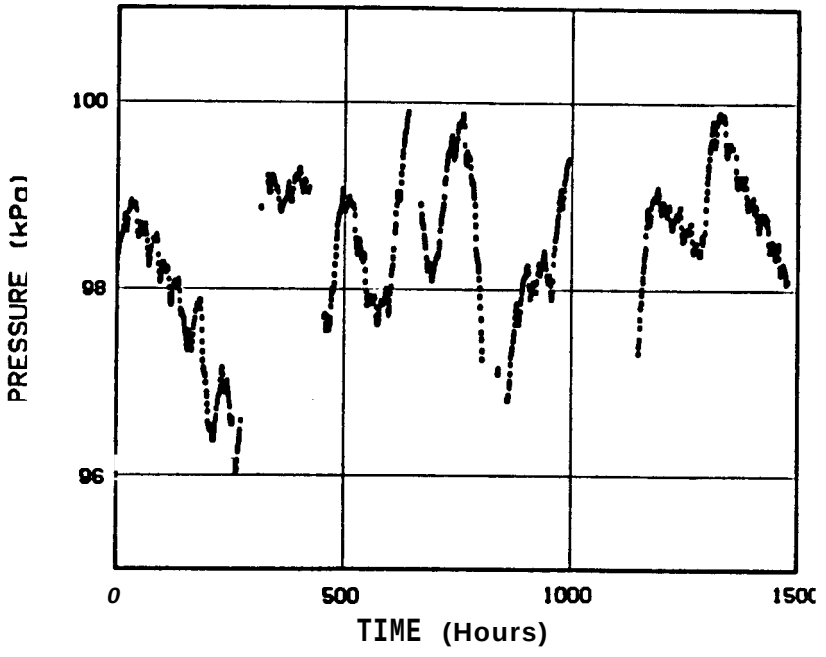

Fig. 3.1 Atmospheric pressure variations during the " C Tests.

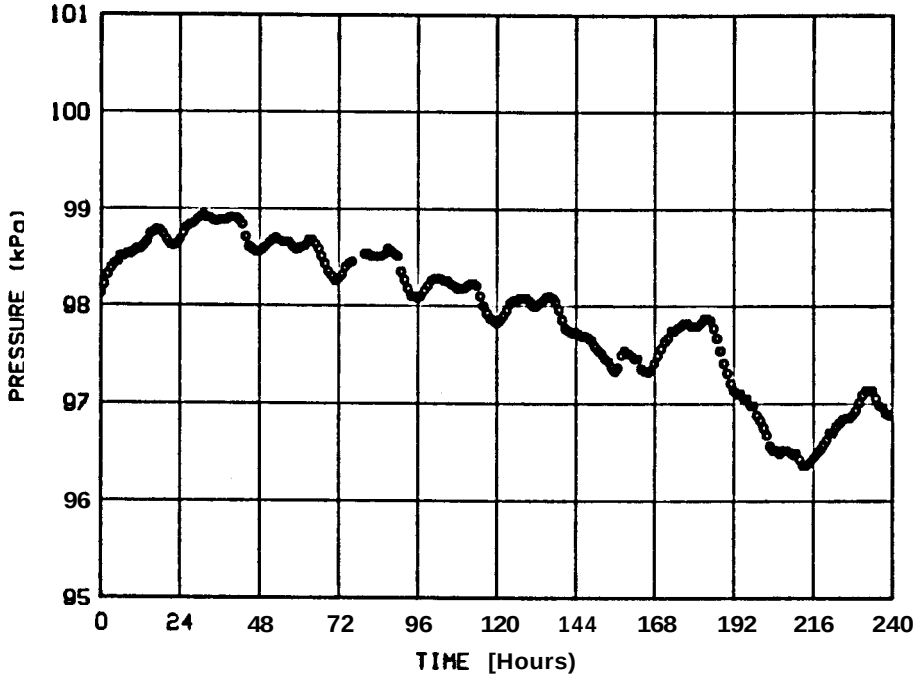

Fig. 3.2 Barometric and earth tide fluctuations during the "C" Tests.

the barometric pressure is evident. In addition, the daily oscillations are distinct, and are a combination of two sine waves with different amplitudes.

The first sine wave has a daily cycle, and the second sine wave has two cycles per day. This second sine wave with the higher frequency is responsible for the small depressions at the top of each pressure cycle that occurs at noon time in each of the five days. Hence, there is one linear overall pressure decline that represents the regional barometric trend, and two oscillatory pressure functions, superimposed on the linear pressure trend, caused by the sun and the moon.

Figure 3.3 presents a simulated pressure response of these three pressure

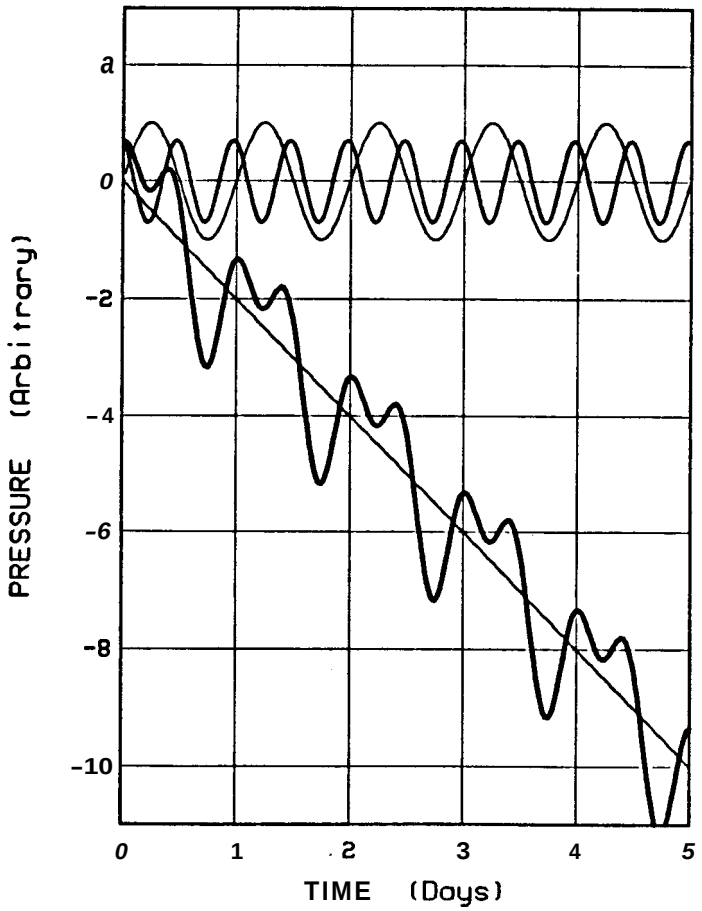

Fig. 3.3 Modelling of the earth tide response using two superposed sine waves on a linear barometric trend (after *Sageev et al.* 1986).

functions. The thick oscillating curve that displays similar characteristics tu the Ohaaki barometric record, is the sum of the three other curves on the figure. The amplitude of the

high frequency wave is 0.7 the amplitude of the low frequency wave. Also, there is a phase shift of 0.6π assigned to the high frequency wave.

Figure 3.4 presents a match of the simulated barometric pressure of

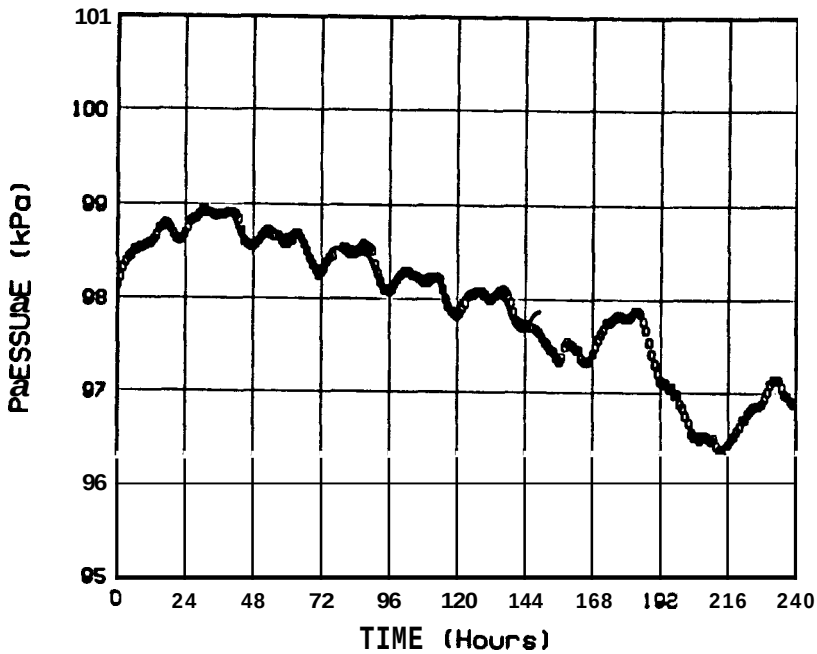

Fig. 3.4 Match of the synthetic and real **earth** tide responses (after ***Sageev et*** al. **1986).**

Figure 3.3 to the five day record presented in Figure 3.2. The match is quite good. The intention is to demonstrate that knowing the barometric pressure during the flow test,, and matching it to simulated responses may help in the **future** to filter out their effects from reservoir pressure data. Also, it may be possible after deconvolving the barometric pressure into its components, to evaluate reservoir properties such as storativity and transmissivity. Figure **3.5** presents three hypothetical earth tide effects superimposed on the line source curve. The curve denoted by A has a dimensionless pressure (p_D) amplitude of 0.05, a zero phase,, and a dimensionless time (t_D) frequency of 0.2. The large amplitude causes the oscillations of the pressure **to** extend up to a dimensionless time of **1.** The other two curves denoted with B and C have a dimensionless pressure amplitude of 0.01, and there are no oscillations present. **Both** these curves have a zero phase, but have different frequencies. Curve B has double the frequency of curves A and C. With combinations of different phases and frequencies it is possible to get os-

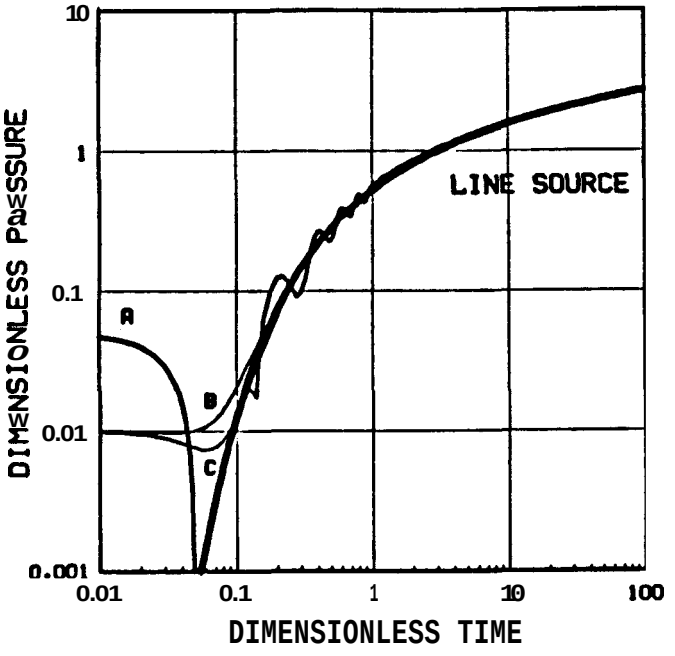

Fig. 3.5 Superposition of the Line Source with a single sine wave (after *Sageev et al.* 1986).

cillations at early time even with low amplitudes.

The first data of the log-log matches from Test C3 (Figure 3.6) indicate a dimensionless pressure amplitude of 0.01 and a dimensionless time frequency of 0.2. This is one of the reasons for deviation of early time data below a specific pressure level of about 40 $kPa\text{-}s/m^3$ (§ 3.4) from the line source. The linear barometric pressure decline was not considered since it had a smaller effect than the earth tide effects. Some processing methods may call for smoothing of pressure data or clipping of anomalies where the pressure declines unexpectedly. The magnitude of interference pressure changes in the early time flow period may be of the same order of magnitude as the earth tide and barometric pressure changes. Under such conditions, smoothing or clipping may lead to loss of information.

3.4. PRESSURE SIGNIFICANCE LEVEL

The pressure level at which the data can be considered significant can be determined from the magnitude of the earth tide response as the data have been corrected for barometric pressure variations only. Figures 3.3 and 3.4 show that the amplitude of the earth tide fluctuations dur-

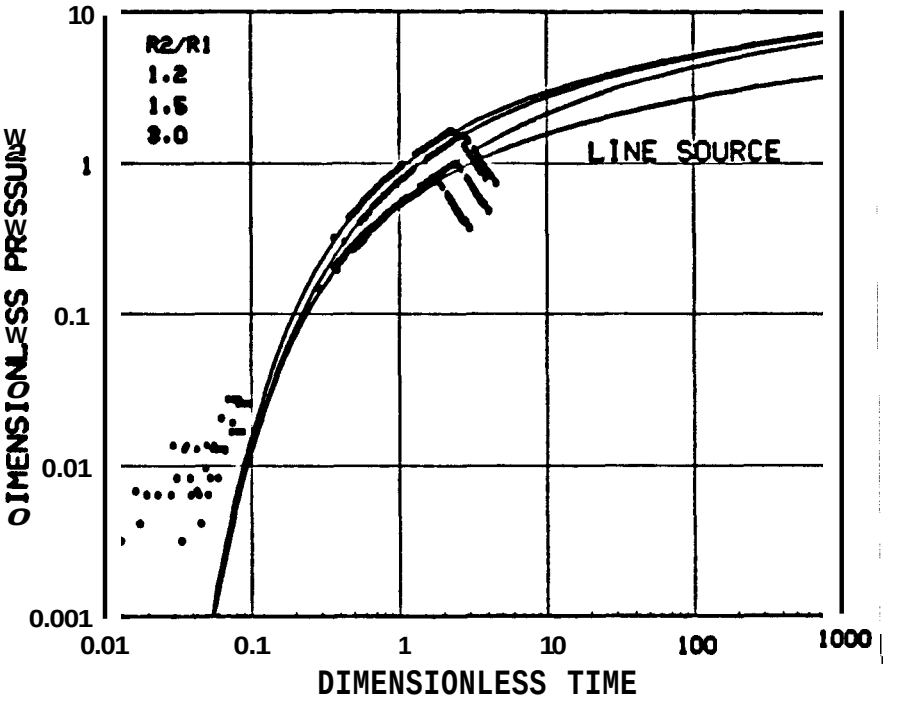

Fig. 3.6 Test C3: Log-log matches of data to *Stallman* **type** curves.

ing the "C" series of tests was about 500 Pa. Fluctuations of more than about a tenth of a log cycle cause problems in obtaining a unique match to the line source solution. Therefore the magnitude of the measured pressure fluctuations is required to be approximately **5** times the **earth** tide variation in order to be significant. That is the pressure change in the reservoir must be a minimum of 3 *kPa*. Since test data is normalized against **flow** rate before plotting the specific pressure significance level for each test must be determined by dividing the minimum absolute pressure change of **3** *kPa* by the flow rate. For most tests the flow rate was about 70 *l/s* which means the specific pressure significance level is **40** $kPa\text{-}s/m^3$.

4. COMPRESSIBILITY

Determination of the effective compressibility of both the reservoir fluid and the formation is an important factor is ensuring accurate data analysis. Several publications have contributed to the more accurate determination of total compressibility for multiphase systems.

Perrine [1956] used the following expression for two phase total system compressibility:

$$c_t = S_w c_w + S_g c_g + c_f \tag{4.1}$$

Martin [1959] developed a more exact expression for total compressibility:

$$c_t = -\frac{S_w}{B_w}\left[\frac{\partial B_w}{\partial p}\right]_T - \frac{S_g}{B_g}\left[\frac{\partial B_g}{\partial p}\right]_T + c_f \tag{4.2}$$

Ramey [1964] used the correlations of *Standing* [1952] to obtain approximations to the partial derivatives reducing the amount of work required to calculate compressibilities. *Horne* [1980] developed graphs showing the variation in water and steam compressibilities with temperature and pressure. These graphs are presented in Figures 4.1 and 4.2 . *Grant* and *Sorey* [1979] used conservation of mass and energy to derive the total compressibility for phase change alone in a two phase geothermal system:

$$c_{ph} = \frac{\left[(1-\phi)\rho_f C_f + \phi S_w \rho_w C_w\right](\rho_w - \rho_g)}{\rho_w \rho_g \phi h_{fg}\,(dp_{sat}/dT)} \tag{4.3}$$

A useful approximation to this equation using the *Clausius-Clapeyron* equation was also given.

$$c_{ph} = \frac{4.01\times10^{-2}}{\phi}\left[(1-\phi)\rho_f C_f + \phi S_w \rho_w C_w\right] p^{-1.66} \tag{4.4}$$

Grant et al. [1982] give a modification to this equation for non-condensible gases.

$$\frac{1}{c_{ph}} = 9.97\times10^{-7}\,\phi\, p_{sat}^{1.66} + 2.13\times10^{-2}\, p_g\, p_{sat}^{-0.21} \tag{4.5}$$

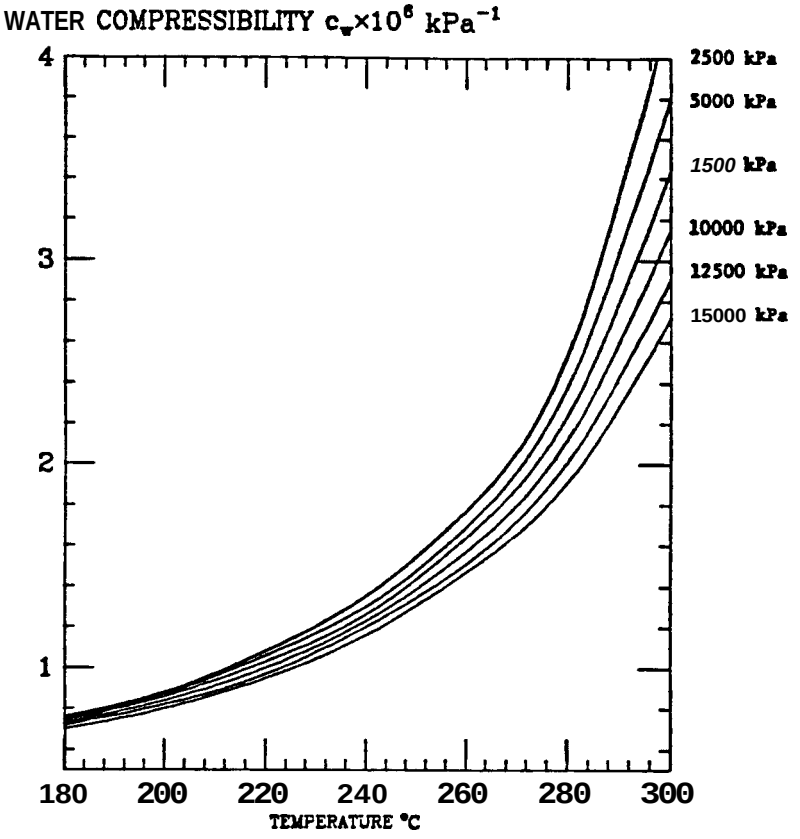

Fig. 4.1 Variation in water compressibility with temperature and pressure (after *Horne* 1980).

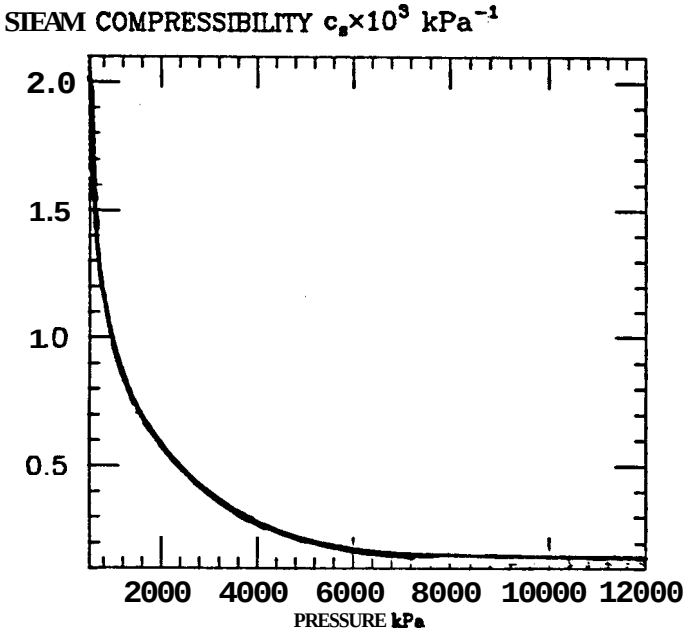

Fig. 4.2 Variation in steam compressibility with pressure (after *Horne* 1980).

5. EARLY TIME DATA MATCHING

(Sugeev et al. 1986)

5.1. THEORY

The dimensionless pressure responses of semi-infinite systems bounded by an impermeable linear boundary are presented in Figures 5.1 and 5.2.

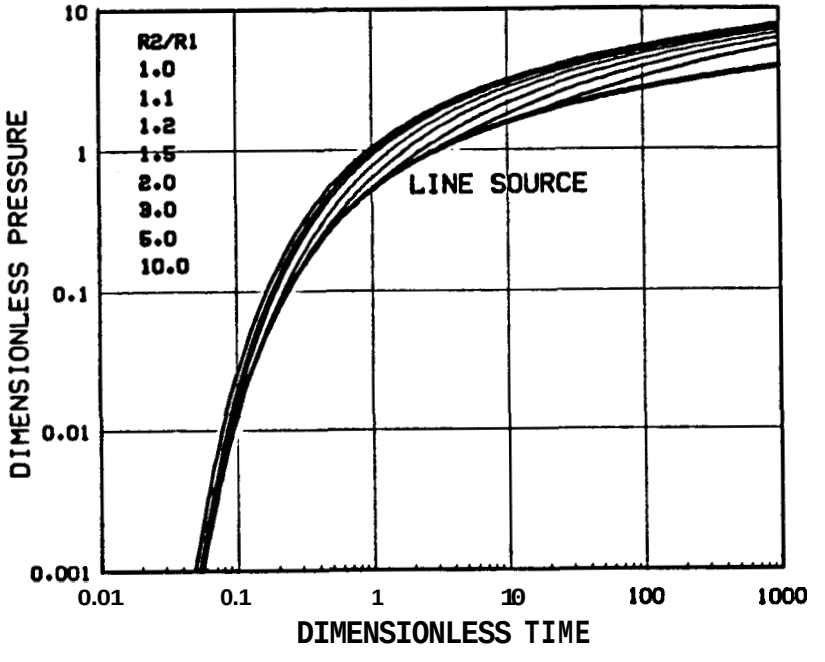

Fig. 5.1 Log-log type curve for a semi-infinite system (after *Stallman,* 1952).

Figure 5.1 is similar to the log-log *Stallman* [1952] type curve. The ratio r_2/r_1 varies between 1 and 10. The lowermost curve in Figure 5.1 represents the *Theis* line source solution. The uppermost curve represents a semi-infinite system where the observation point is adjacent to the boundary, yielding an r_2/r_1 of unity. In view of Equation 2.4, this curve is a sum of two identical exponential integrals, and is shifted by a factor of 2 in the vertical direction from the line source curve. As the value of the ratio r_2/r_1 increases, the dimensionless pressure response departs from the line source solution at later times, as the effects of the impermeable boundary become significant at the observation point.

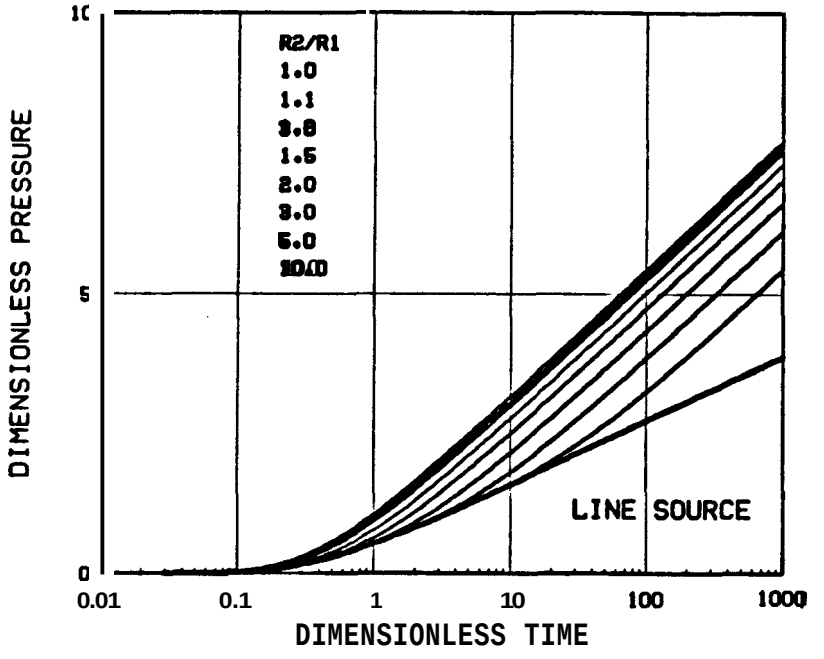

Fig. 5.2 Semi-log type curve for a semi-infinite system.

Figure 5.3 is a semi-log presentation of the same data as in Figure 5.1. The curves having r_2/r_1 ratios between 1 and 1.5 are closely spaced in both Figures 5.1 and 5.2, making log-log and semi-log type curve matching difficult,

The similarity of the curves for small values of the distance ratio is presented in Figure 5.3. In this figure, the line source curve is translated along the time and pressure axes by factors of 1.075 and 1.96 respectively, to match the curve for an r_2/r_1 of 1.1. The two curves match well. The square of the difference between these two curves is presented in the lower thin curve in Figure 5.3. The two minima in the error curve represent the fact that the two matched curves cross each other twice. The difference between the two curves is smaller than the resolution expected even from very sensitive pressure recording devices. Hence, transient pressure data from wells near an impermeable linear boundary with an r_2/r_1 ratio of 1.1 can be matched successfully to the line source solution, Based on the translation of the line source curve, this match would yield almost the correct storativity but a transmissivity which is a factor of 2 lower. No indication of the presence of an impermeable boundary would be present.

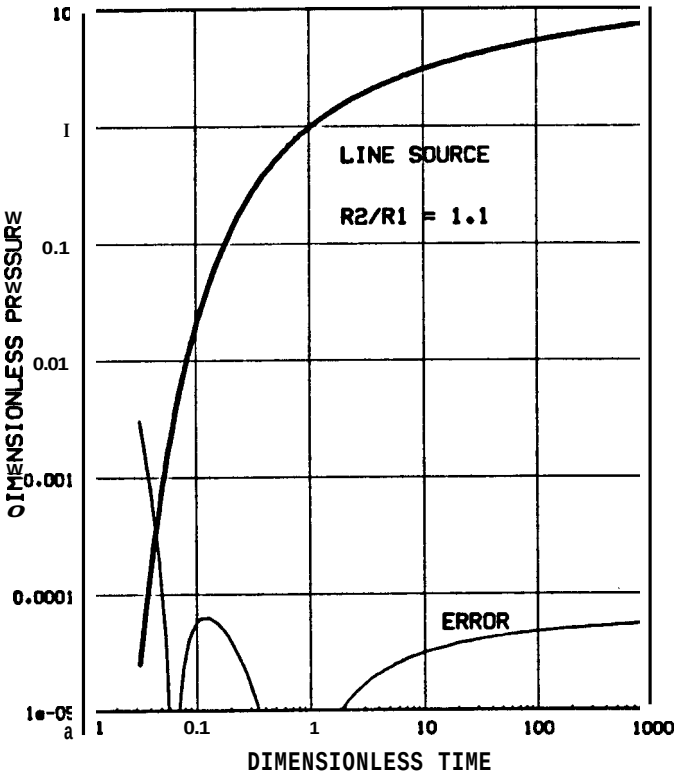

Fig. 5.3 Log-log match of the Line Source to the curve for $r_2/r_1 = 1.1$ (after *Sugeev et al.* 1986).

A standard procedure in analyzing interference pressure data that match the line source solution is to evaluate the minimum reservoir area that is free of any boundaries. In the case of a linear boundary, this area is elliptical in shape, as described by *Vela* [1977]. This analysis with interference data coming from a configuration with a distance ratio less than about 2 will over estimate the reservoir area free of boundaries. The magnitude of this over estimation depends on the duration of the test. For example, if a pressure response with a distance ratio of 1.1 matches the line source up to a dimensionless time of 20, the minimum distance ratio determined from this match would be 10. This match would locate the linear boundary at a distance ten times further than the actual boundary location.

The results from an interference test with a distance ratio smaller than 2 should be compared with results from other responses in observation wells or the source well. In the case of the source well, the distance ratio is large and the distance ratio and transmissivity may be estimated. The difference between the transmissivities of the source well and the observation well may

indicate the correct match of the interference data.

Although the curves for r_2/r_1 ratios of 1.1 and 1.5 are very similar to the line source, the curve for an r_2/r_1 ratio of 2 is unique, and cannot be matched to the line source curve. Figure 5.4 presents the two curves without any translation. This yields

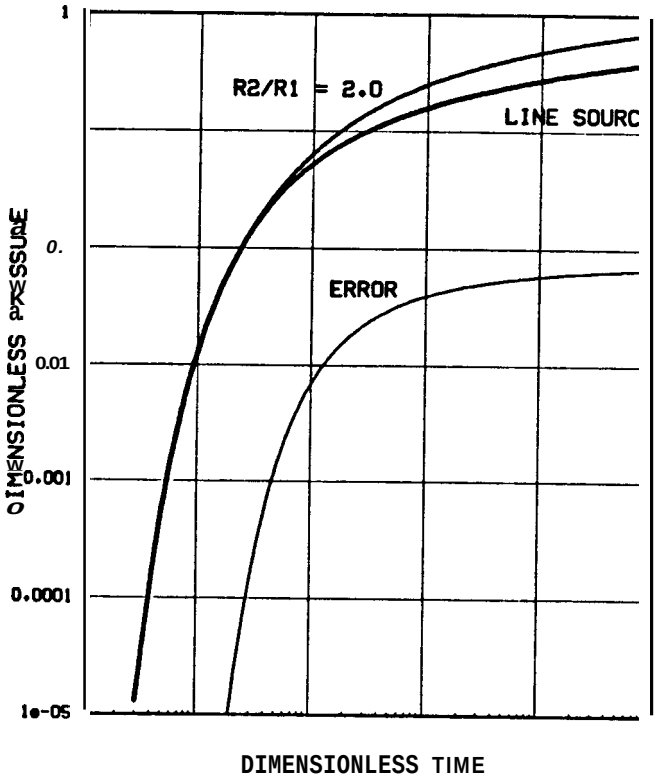

Fig. 5.4 Log-log response of the Line Source and a semi-infinite system with r_2/r_1 = 2.0 (after *Sugeev* et al. 1986).

an early time match to the infinite acting line source response, but after a dimensionless time of 1, the two curves are different. This can also be seen in the error curve. The error is small at early time, and increases rapidly with time. Figure 5.5 presents a late time match of the line source to the curve for an r_2/r_1 ratio of 2. Here, the early time line source behavior is not matched, as described by the error curve. The minimum in the error curve is caused by the two curve crossing one another. Hence, the line source curve cannot match simultaneously the early time and the late time responses of an observation well with a r_2/r_1 ratio of 2, and the detection of a linear boundary is possible.

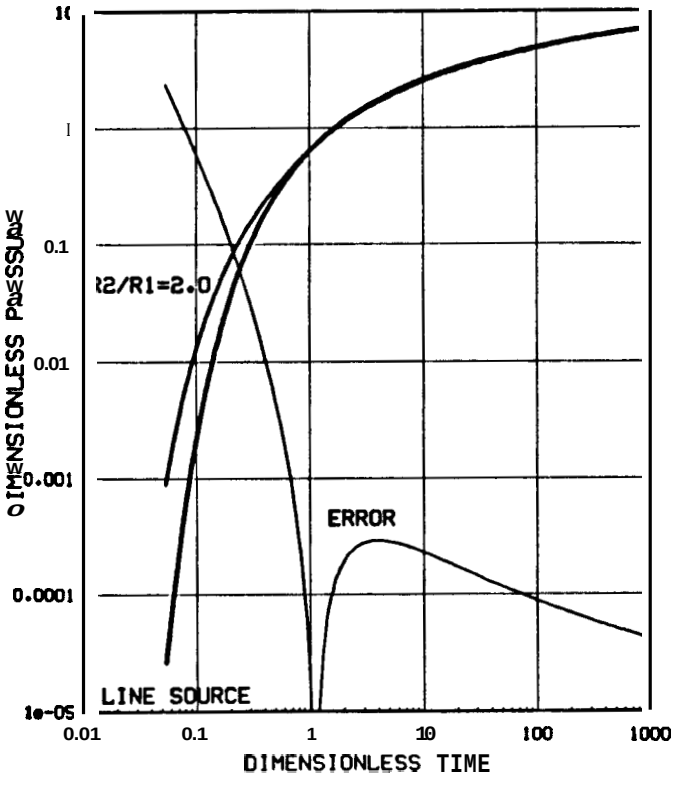

Fig. 5.5 Log-log match of the Line Source and a semi-infinite system with $r_2/r_1 = 2.0$ (after *Sugeev* et al. 1986).

The log-log and the semi-log responses are summarized in Figure *5.6.* The upper family of curves represents the log-log pressure responses, as presented in Figure 5.1. The lower family of curves, translated by a factor of *5* for display purposes, represents the semi-log pressure derivatives. From the pressure derivative curves, it is clear that for r_2/r_1 ratios greater than *5* the semi-log type curve matching technique is applicable because there is a distinct transition between the infinite and the semi-infinite behaviors. Pressure responses from cases with r_2/r_1 ratios between 2 and *5* can be analyzed using the type curves presented here, since these responses are significantly different from the line source. Also, pressure responses with r_2/r_1 ratios smaller than 2 can be matched to the line source curve, and may lead to erroneous estimations of some reservoir parameters.

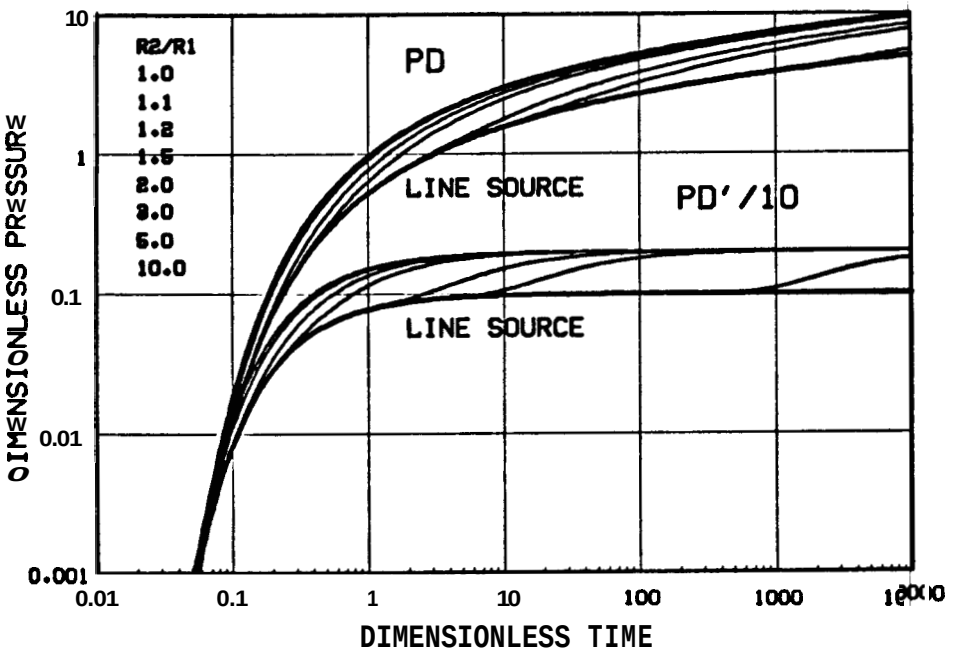

Fig. 5.6 Log-log type curve for dimensionless pressures and semi-log dimensionless derivatives for a semi-infinite system (after *Sageev* et al. 1986).

5.2. MISSING DATA

The detection of linear boundaries from transient pressure tests is based upon the transition between the infinite acting and semi-infinite acting pressure responses. If this transition is not present little can be done to detect the linear boundary. Some tests may have the required time span for the detection of a linear boundary, but, for human or mechanical reasons, some of the pressure data are missing. Local sampling problems that arise from discretizing the time and pressure domains are not considered. Local sampling is assumed adequate. Concern is with a time period of missing pressure data that is significantly longer than the sampling intervals required for transient pressure analysis.

Figure 5.7 presents an example of missing pressure data from Test C3 in the Ohaaki geothermal field. Test C3 was started on May 1, 1984 and the drawdown portion of it lasted for 339 hours. The active well, BR20, produced at a constant rate of 84 *l/s*, and pressures were measured with a quartz crystal gauge at the observation well, BR34. The distance between the two wells is 1145 meters (Table 7.16). The pressure scale in Figure 5.7 is normalized by the flow

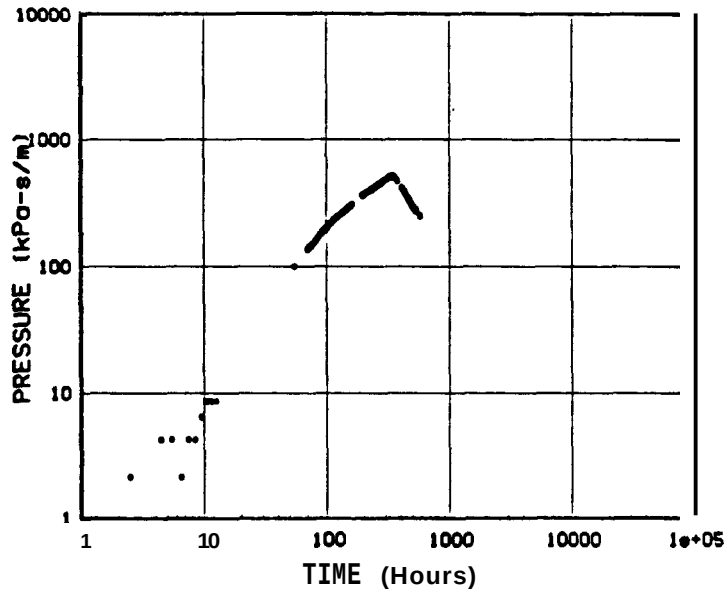

Fig. 5.7 Log-log plot of data From Test C3.

rate measured during the test. Pressures were not recorded from the 12th to the 54th hour of the test. The early time data of this test below a specific pressure level of 10 $kPa-s/m^3$ are affected by earth tides and baromemc pressure changes.

To determine the significance of the missing data in Test C3 consider a hypothetical case of the interference pressure response from a semi-infinite reservoir with a distance ratio of 2. Figure 5.8 presents four cases of pressure responses, three of which have missing pressure data. Figure 5.8A is the complete response that spans the transition flow period, and can be successfully analyzed for the detection of the linear boundary. In Figure 5.8B, a log cycle of the data during the transition is missing. Yet, the early time infinite acting response and the late time semi-infinite response are well defined. The two portions of the pressure data cannot be matched to the line source simultaneously, and the data can still be successfully analyzed for detecting the linear boundary.

The pressure response presented if Figure 5.8C has a longer period of missing data than the response of Figure 5.8B. Yet this pressure response can be successfully analyzed since the infinite and the semi-infinite responses are well defined. In the pressure response presented in Figure 5.8D, all the infinite acting pressure response is missing. The late time semi-infinite

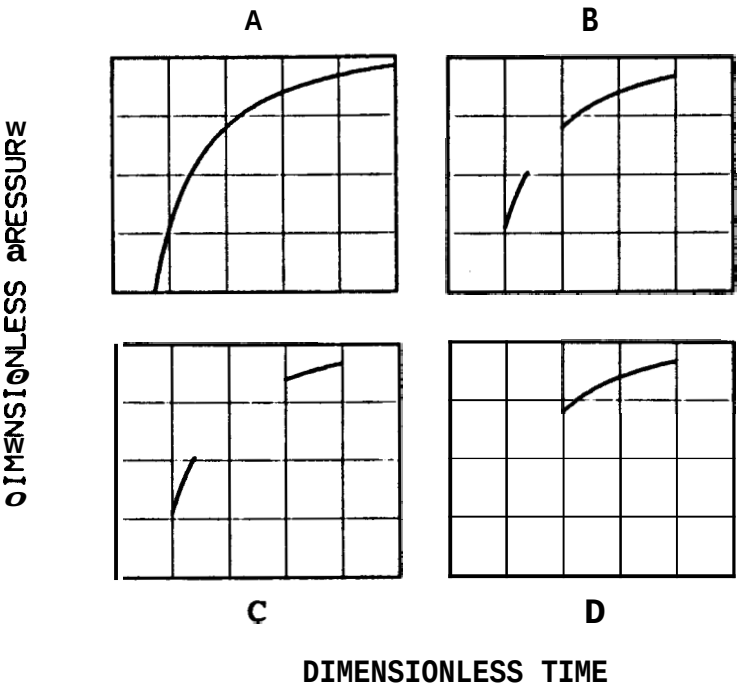

Fig. 5.8 Hypothetical cases for missing pressure data for $r_2/r_1 = 2.0$ (after *Sugeev* et al. 1986).

response can erroneously be matched to the line source curve, hence, yielding incorrect reservoir parameters, and providing no indication of the presence of a linear boundary.

The first ten hours of the test from **Cheaki** are influenced by earth tides and barometric pressures, making the condition of data in this test similar to the response presented in Figure 5.8D. Various matches of the drawdown data of this test are presented in Figure 5.9. The distance ratio varies between **1.2** and **infinity** (for the line **source).** The storativities derived from the log-log match vary by a factor of less than 2, but the transmissivities vary within an order of magnitude. Without information from other flow test, the analysis of the pressure data is ambiguous. In this case, the pressure data are missing in the time period that is required to establish the infinite acting response of the reservoir, and the late time data represent the semi-infinite behavior. Hence, **a** unique analysis of this tests is not possible.

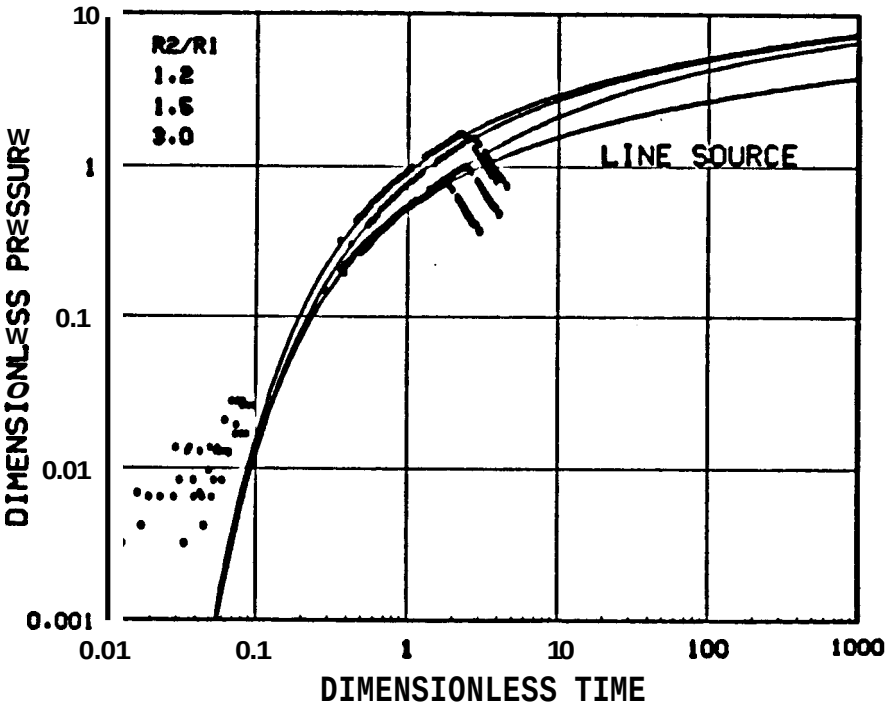

Fig. 5.9 Four **possible log-log matches of Test C3 data to the** *Stallman* type *curves.*

6. HYDROLOGY OF THE OHAAKI GEOTHERMAL FIELD

6.1. BACKGROUND

The Ohaaki geothermal field is located in the Taupo volcanic zone, 30 *km* north-east of Lake Taupo, near the center of the North Island of New Zealand (Figure **6.1).**

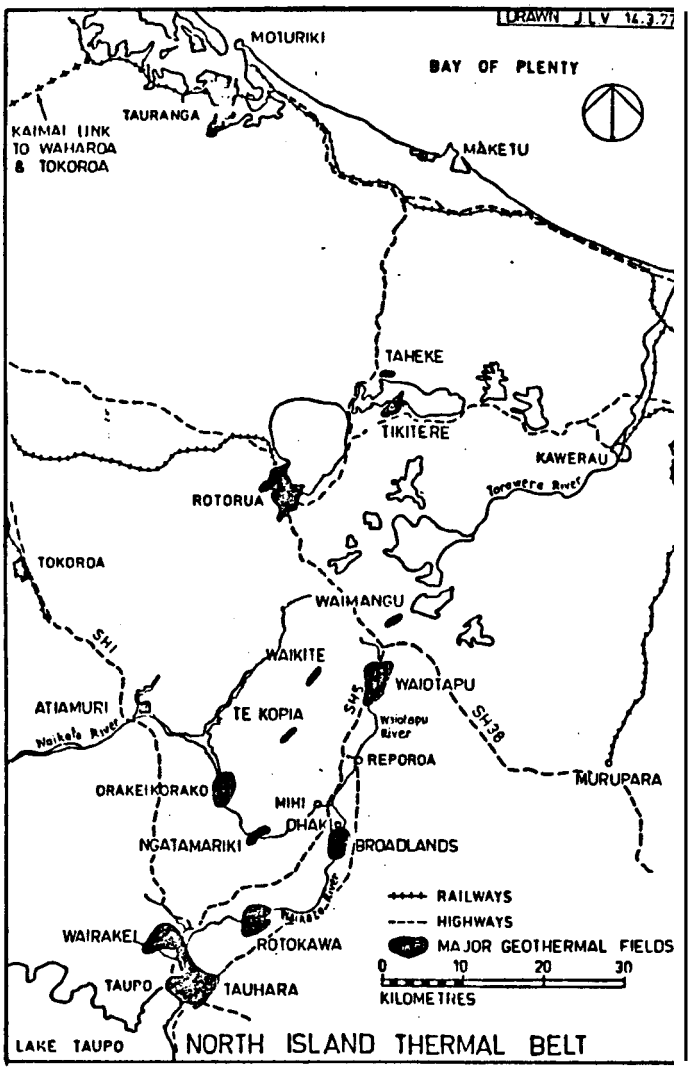

Fig. 6.1 Locality map for the Ohaaki Geothermal Field.

The Waikato River, the largest in the North Island, bisects the field in a north-east south-west direction. A total of **44** wells have currently been drilled (Figure 6.2). These range in depth

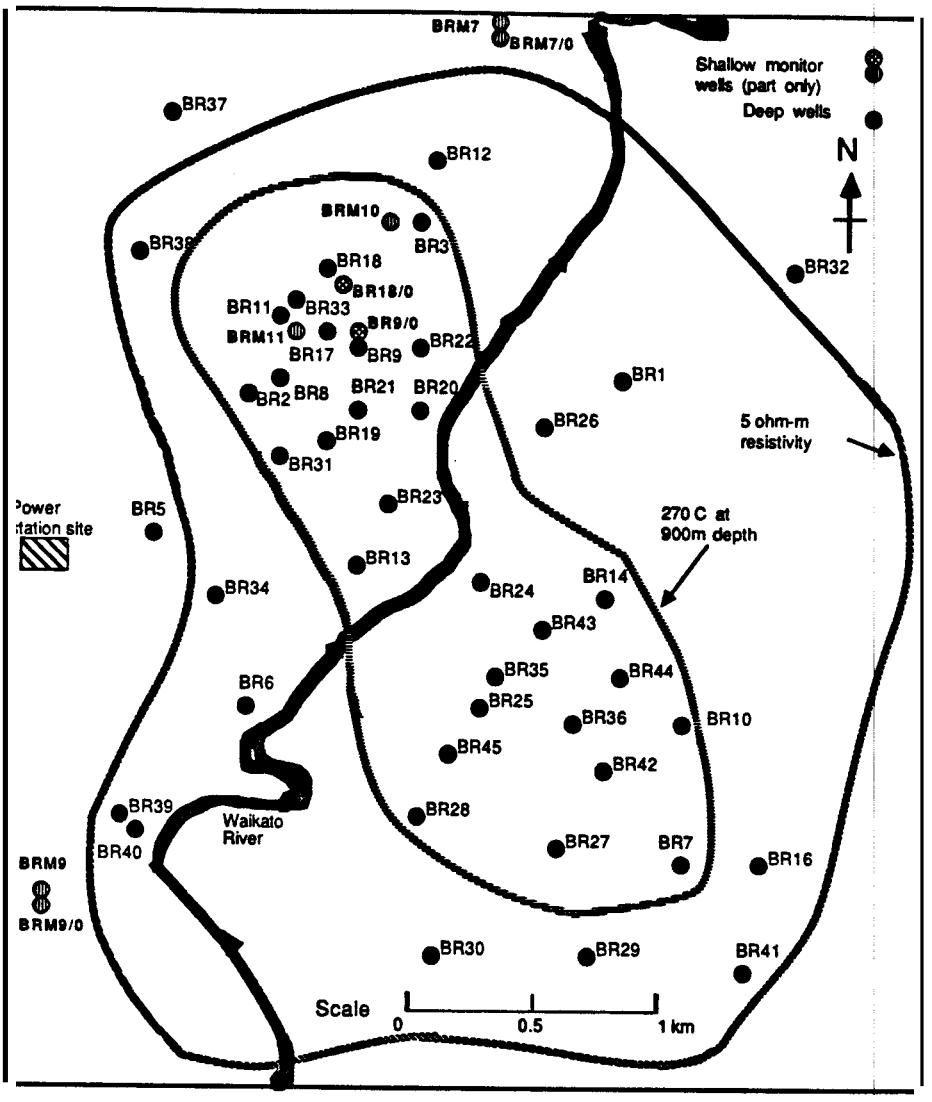

Fig. **6.2** Well layout of the Ohaaki Geothermal Field.

from 358 meters to 2587 meters with an average of 1256 meters ***(Hedenquist*** 1985). The east bank land area contains 13 productive wells and is known as Broadlands. The west bank land area which contains 17 productive wells and includes the power station site, is known as Ohaaki. The term Ohaaki is used in this report to designate the total geothermal system as a consequence of the siting of the power station.

Drilling began in the west bank of Ohaaki at well BR1 in 1965. The first well to be successfully discharged was BR2 in 1966. Between 1967 and 1971 large scale discharge testing of the field was undertaken with 35 *Mt* of fluid being withdrawn from the reservoir (***Hunt and*** *Hicks*

1975). Reservoir pressures in the producing area dropped during this period by 1.2-1.8 *MPa*. From 1971 to 1973 the field was at near shutdown as other energy projects tookldevelopmental priority. Then, between 1974 and 1983, discharge testing continued with 19 *Mt* of fluid being produced of which 5 *Mt* was reinjected. Reservoir pressures during this period recovered by 600-800 *kPa* (Grunt *et al*. 1982).

6.2. GENERAL

Hydrologically, the Ohaaki field consists of three reservoirs (Grunt *et al*. 1983, *McGuinness* 1985). The main reservoir is located in the Rangitaiki ignimbrite and Rautawiri breccia formations below 500 meters depth (Figure 6.3). Geologically, the lower limit

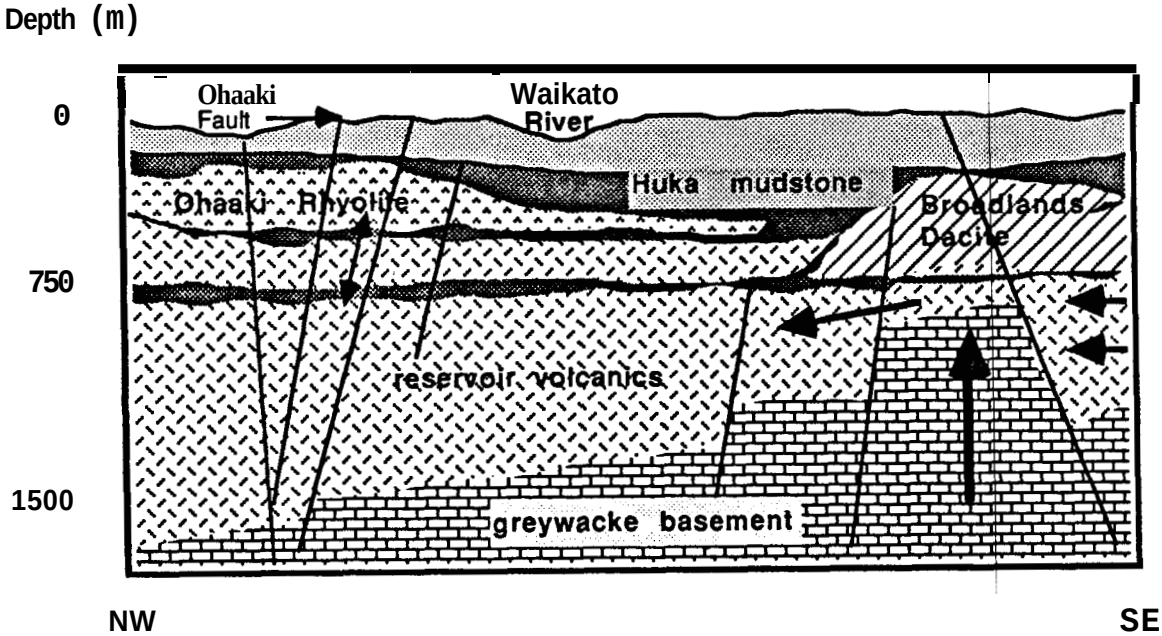

Fig. 6.3 North-west south-east geologic cross section showing postulated flows in the Ohaaki reservoir.

of the reservoir could be defined by the upper limit of the basement greywacke which extends from 1000 meters depth in the east at BR7 to over 1700 meters depth at BR15 in the west (*Grindley* and *Browne* 1968, Browne 1973). During discharge and subsequent recovery of the field between 1967 and 1979 noticeable changes in pressure and temperature occurred only above 1000 meters depth. This may represent the exploitable limit of the field, although a temperature saddle below 1000 meters between the east and west banks may be an indication of

flow below that depth *(Grunt* 1983). Pressure gradients in the reservoir indicate that vertical permeability is much lower than horizontal permeability. Vertical permeability was roughly estimated at about 3 millidarcies *(Grunt* 1983).

63. EAST BANK

On the east bank, upflows of hot fluid from depth may occur near wells BR36 and BR43 as temperatures show a continued increase with depth in this area *(Grunt* 1983). High temperature chloride waters are saturated with silica and calcium carbonate with the average carbon dioxide concentration in the water at depths of 400 - 800 meters being 0.6% by weight. The partial pressure of carbon dioxide in the reservoir varies from 0.8 - 3 *MPa,* but at depths below 1000 meters partial pressures are probably over 10 *MPa.* The high gas concentrations appear to be related to the basement greywackes and argillites. This is confirmed by higher gas concentrations found in those wells which penetrate the basement rocks. *(Ellis and Mahon* 1977). Most rising hot fluid on the east bank probably travels west because only there, in the Ohaaki pool, does any significant surface discharge of reservoir fluid occur. Steeper pressure gradients in the region near BR24 and BR26 indicate a possible flow barrier to this area. Shallow ground waters in the Broadlands dacite above the postulated east bank upflow zone (Figure 6.3) show steam dilution effects but no significant addition of deep chloride water. The estimated minimum fluid temperature in the upflow zone is 310°C. Geochemical analysis of fluid from east bank production wells show evidence of both boiling and dilution with bicarbonate rich condensates *(Hedenquist* 1983). Condensates can be formed by the deep 310°C fluid flowing upward to the base of the sealing mudstone and siltstone at 500 meters depth. There the pressure reduction would cause about 10% of the total mass to flash off into the overlying Broadlands dacite *(Grunt* 1983) while the other 90% is assumed to travel to the west bank within the hot permeable region of the field. Lumped parameter modelling of the east bank *(Grunt* and *Iles* 1982) showed the flow from the east to the west was about *3.5 kt/yr-kPa.* Modelling also showed that total recharge to the east bank was about 4 *kt/yr-kPa* while recharge to the west bank not including that from the east bank was about 1.5 *kt/yr-kPa.* Hence the east bank has

better recharge than the west bank *(Grunt* 1983).

6.4. WEST BANK

On the west bank total heat discharge from 1965 to 1979 was 5×10^{16} *J*. Changes in well temperature profiles indicate that only 20% of the enthalpy of the discharged fluid was not replaced *(Grunt* 1983). Pressure and temperature profiles measured in the central west bank show no evidence of recharge of brine from directly below. Profiles measured in wells BR2, 17, 18 have shown some signs of the existence of upflow in the past but these have 'not persisted. Geochemical analysis of production fluid from the west bank indicated that boiling with minor dilution is taking place in the production zone *(Hedenquist* 1983).

Outside the field pressure gradients were 400 *kPa* below reservoir pressures before exploitation ensuring that during early drawdown of the reservoir no significant recharge of cold water was likely *(Grunt* 1982). Detailed analysis of pressure measurements in nearly all west bank wells (Figure 6.4) both before and after exploitation showed that the wells fell into three groups each with a characteristic linear formation pressure profile (*Bixley* 1982). Wells with the smallest pressure gradients were contained within the 270°C contour at 900 meters depth and this was considered to define the productive area of the field (Figure 6.5). Wells included were BR5, 8, 11, 12, 13, 14, 19, 21, 24, 28. Wells offset more than 500 meters from this contour showed the greatest formation pressure gradients and were considered very poorly connected to the deep reservoir. Wells included in this group were BR6, 32, 33, 37, 39. Some wells showed formation pressure gradients which were intermediate between the previous two cases and were considered to be poorly connected to the deep reservoir. Wells included were BR10, 16, 29, 34, 38. Wells BR5, 12, 34 were exceptions to the rule showing fair connection to the deep reservoir possibly as a consequence of north-east trending faults in this region.

Gravity changes indicate that total recharge to 1983 to both east and west banks is about 25 Mt or about half the total mass discharge. Gravity changes affected an area greater than that covered by the 5 *ohm-m* resistivity boundary and were consistent with a reservoir of 1.5 *km* radius and thickness of 500 meters *(Hunt* 1985). A persistent negative trend in gravity measure-

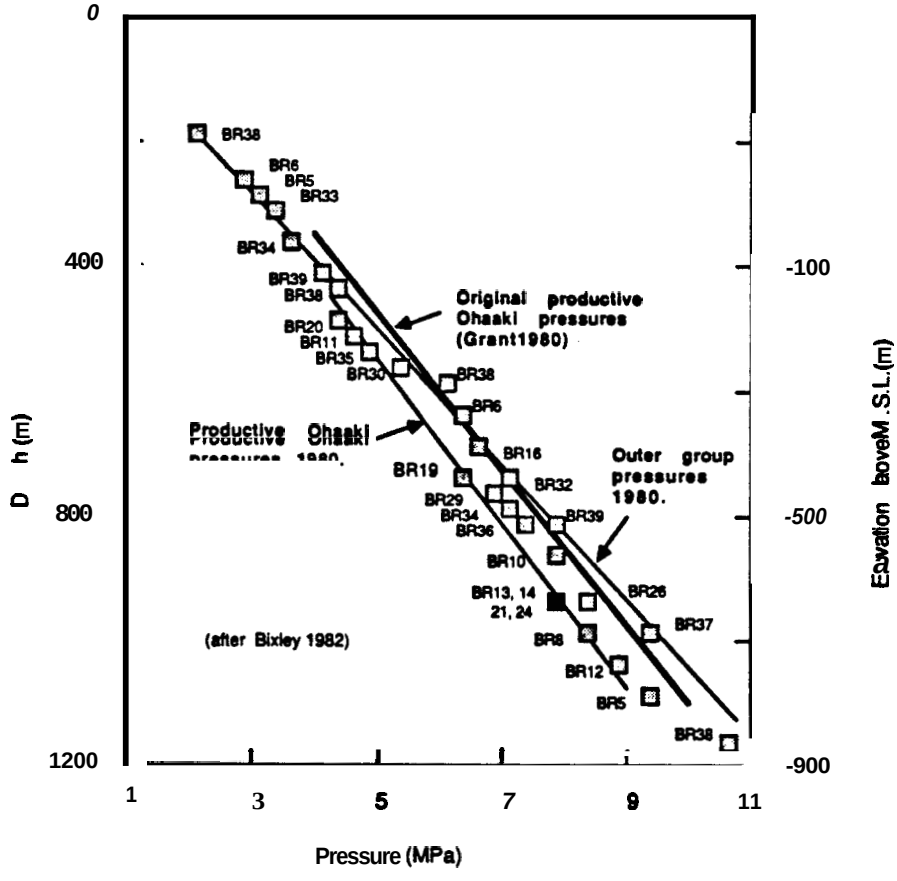

Fig. 6.4 West Bank well pressure profiles (after *Bixley* 1982).

ments extending up to 2 *km* west of a line bounded by wells **BR38** and **BR39** may indicate that the main reservoir is hydrologically connected to this part of the field (Figure 6.6). The fact that gravity surveys show a continued loss of mass in this area could be due tu the buffering effect of a deep two phase zone and/or low permeability which has delayed response *to* earlier reservoir drawdown. Measurements in the east of the field between **BR14** and BR32 reflect a similar trend.

6.5. BROADLANDS DACITE *(McGuinness* 1985)

Overlying the Ohaaki field south of a line joining wells **BR** 3, **14,** M6 is the second reservoir unit, the Broadlands dacite. This formation contains liquid brine at about 140°C, has transmissivity about **370** *d–m* and storativity of about 3.0×10^{-4} *m/kPa*. A 35 day interference test in January **1984** in which source well **BR40** was produced at **44** *kg/s* and pressures observed at

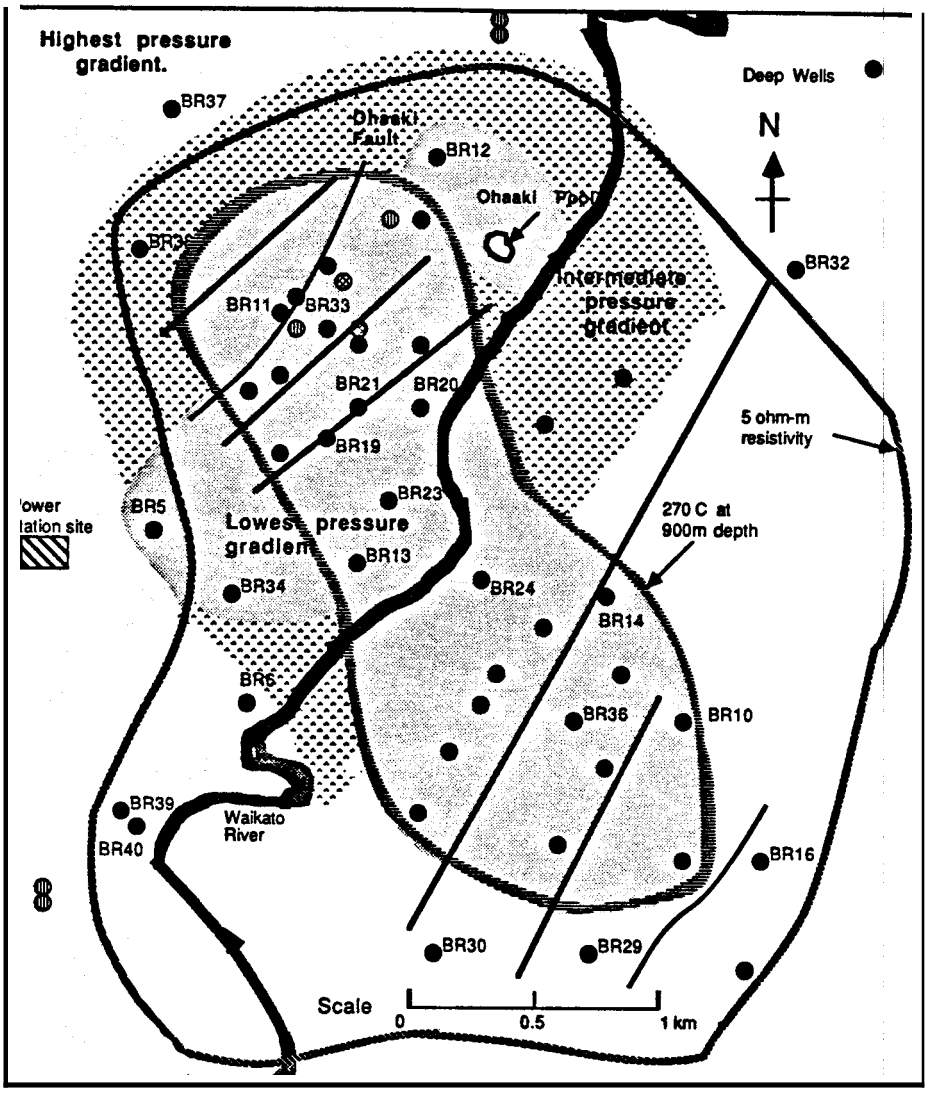

Fig. 6.5 West Bank well grouping from pressure gradient characteristics (after *Bixley* 1982).

well BR5, both with permeable zones in the Broadlands dacite showed no observable boundary effects. The region of influence covered a radius of about 2.5 *km* around BR5 and BR40. No response in wells BR33, M10, M11, 9/0 with permeable zones in the Ohaaki rhyolite implies near isolation of this geological unit form the Broadlands dacite. The upper bound permeability estimate in the barrier was about 10 *md.*

The Broadlands dacite shows no connection with the deep reservoir as discharge of well BRM9 with permeable connection in the Broadlands dacite produced no observable response in wells BR13, 23 having connection to the deep reservoir. Due to its hydrological isolation from

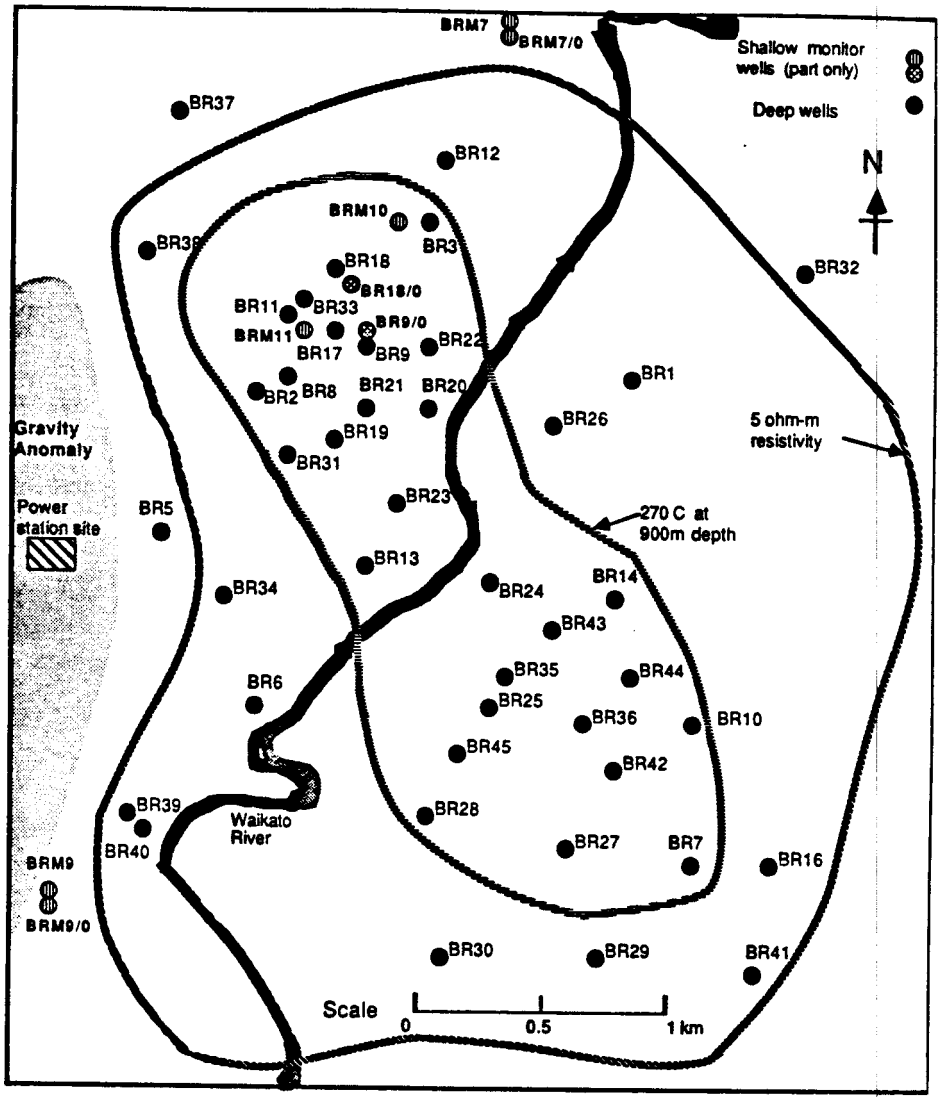

Fig. 6.6 Areal view of the Ohaaki Field showing West Bank gravity anomaly.

the deep reservoir and apparent large extent the Broadlands dacite has been mooted for reinjection of waste fluid from the power station.

6.6. OHAAKI RHYOLITE

Overlying the west bank is the third reservoir unit, the Ohaaki rhyolite. Interference tests were carried out from November 1983 - May 1984 in which the response of wells BR12, 33, 37, M7, M10, M11, 9/0 was monitored to the discharge of wells BR11, 22, 33, 40, M9 (Figure 6.7). Wells BR12, 37, M7 showed no response to production confirming their poor hydrologi-

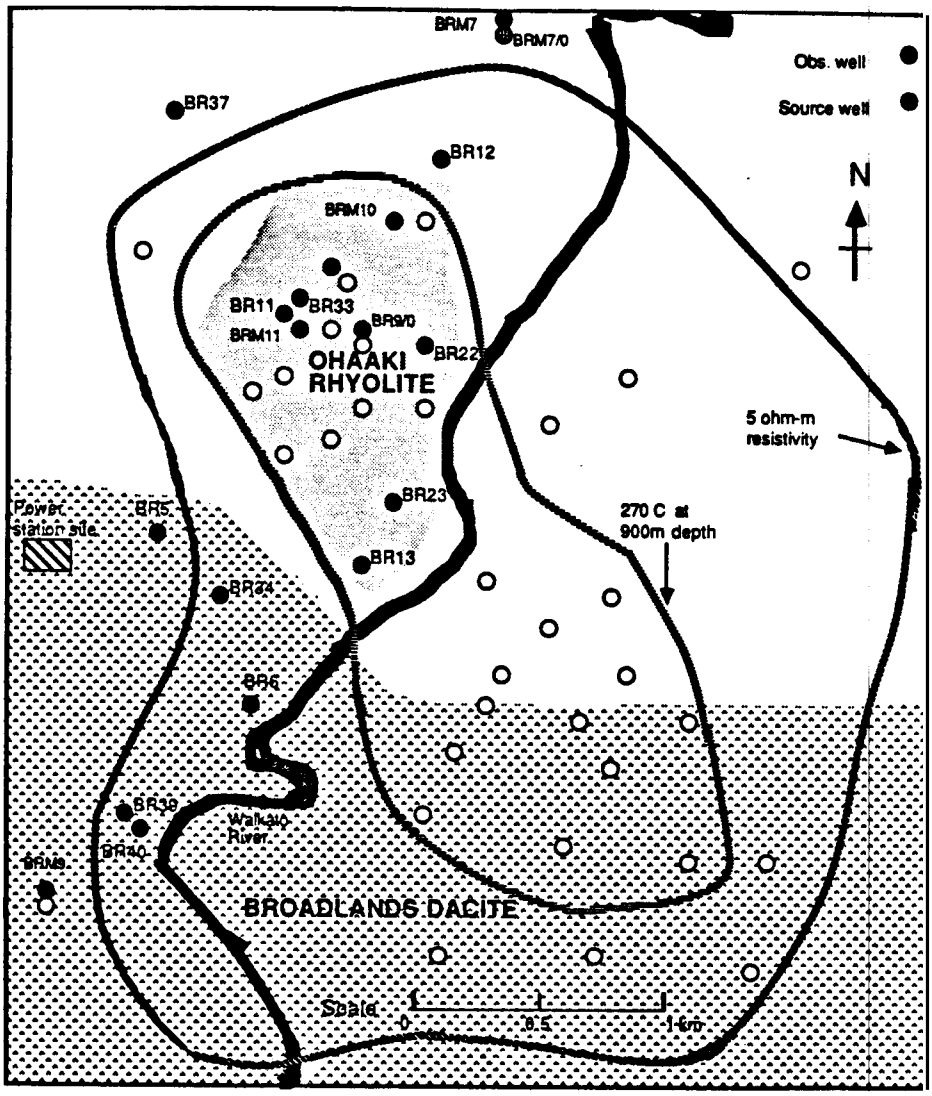

Fig. 6.7 Areal view of the Ohaaki Field showing significant geology and Well Layout for West Bank Rhyolite interference tests *(after McGuinness* 1985).

cal connection to the deep west bank reservoir. A response to drawdown in the Ohaaki rhyolite was measured in shallow ground water well BR9/0 with slow pressure recovery during buildup. The linear drawdown pressure response of observation wells BR33, M10, M11, 910 and the slow buildup, indicated that the Ohaaki rhyolite was an open tank reserkoir with poor recharge *(McGuinness* 1985). Analysis of interference test data gave the porosity area (ϕA) of the open tank as 0.23 km^2 assuming that the box is filled with liquid water at 140° C. Ground water well BR9/0 is known to have the same response as the Ohaaki Pool, the single major

chloride spring in the Ohaaki field. However ground water wells further than about 500 meters radius from BR9/0 on the west bank have shown little response and east bank shallow ground water wells show no response to discharge of the deep reservoir.

Between 1970 and 1974 pressure rises were measured at the base of the Ohaaki rhyolite at 450 - 540 meters depth indicating the existence of a two phase zone in this region (Grunt 1983). This zone disappeared after 1974. Pressure changes at the surface in the Ohaaki pool were 5 - 10 times less than those occurring at the base of the Ohaaki rhyolite. The Ohaaki rhyolite and the deep west bank reservoir were assumed to be separated by an aquitard consisting of low permeability siltstones and Huka mudstones (Grunt 1983). Pressures in the Ohaaki rhyolite appear to be buffered either by a lateral connection to another near surface reservoir or by a two phase zone within the rhyolite. Lack of evidence of large lateral flows in the rhydlite make the two phase zone option more credible.

6.7. COMMENT

At present, a 110 *MW(e)* power station is under construction on the west bank at Ohaaki with generation expected to commence 1989. Despite over 20 years of researchi during field development, enigmas remain. Two phase zones and isolated areas of low permeability in the main hydrological units complicate interference test interpretation. The role of faulting in connecting and distributing colder recharge fluid to the deep reservoir has not been fully established. The gravity anomaly west of the 5 *ohm-m* resistivity boundary on the west bank has not been explained by independent measurements. The lower limit of the deep reservoir is tentatively assumed as 1000 meters however evidence of pressure drawdown in BR38 extends to nearly 1200 meters and cores from BR34 show hydrothermal mineral deposition in low permeability veins in the basement greywacke at 2590 meters (*Braithwaite* 1979). The extent and type of connections of the Ohaaki rhyolite and Broadlands dacite reservoir units with formations outside the primary production area have not been established. The answers to these enigmas may have to await the next decade when large scale production will inevitably provide enough data to obtain solutions to the complex problems involved.

7. ANALYSIS OF INTERFERENCE TESTS DATA IN THE OHAAKI WEST BAN

7.1. MEASUREMENT ACCURACY

Two types of instruments were used to measure pressures in the interference tests. These were:

(i) Water level chart recording devices.

(ii) Quartz crystal gauges.

The water level chart recorder has an accuracy of about 100 Pa. and was used in the observation wells for the "B" series of tests. Barometric pressures for this series of tests were measured using a barograph which also has an accuracy of about 100 Pa.

Quartz crystal gauges were used in the "C" series of tests. The accuracy of the quartz crystal gauges varies depending on the pressure range, but is typically 10^{-5} of the maximum range. Atmospheric pressures were monitored with an accuracy of 1 Pa, while reservoir pressures had an accuracy of 100 Pa.

7.2. WELL LOCATION

The locations of observation and source wells for the interference tests are shown in Figure 7.1.

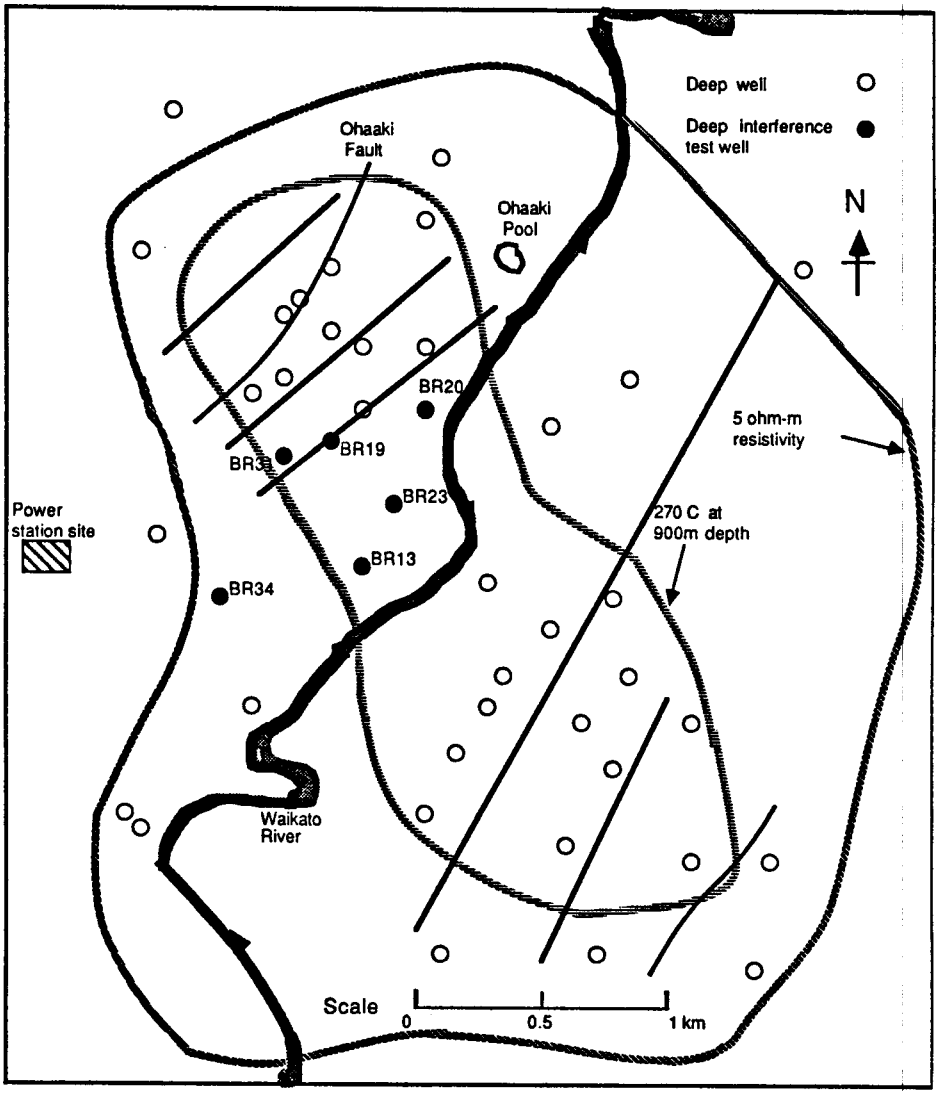

Fig. 7.1 Source and observation well location for interference tests .

73. DATA FROM WATER LEVEL CHART RECORDERS

73.1. TEST B1: BR13 RESPONSE TO BR23 *(Leaver et al.* 1985)

Specific pressure verses time data for this test are presented in Table **B1** and plotted in cartesian form in Figure **7.2.** Test specifications are presented in Table **7.1.**

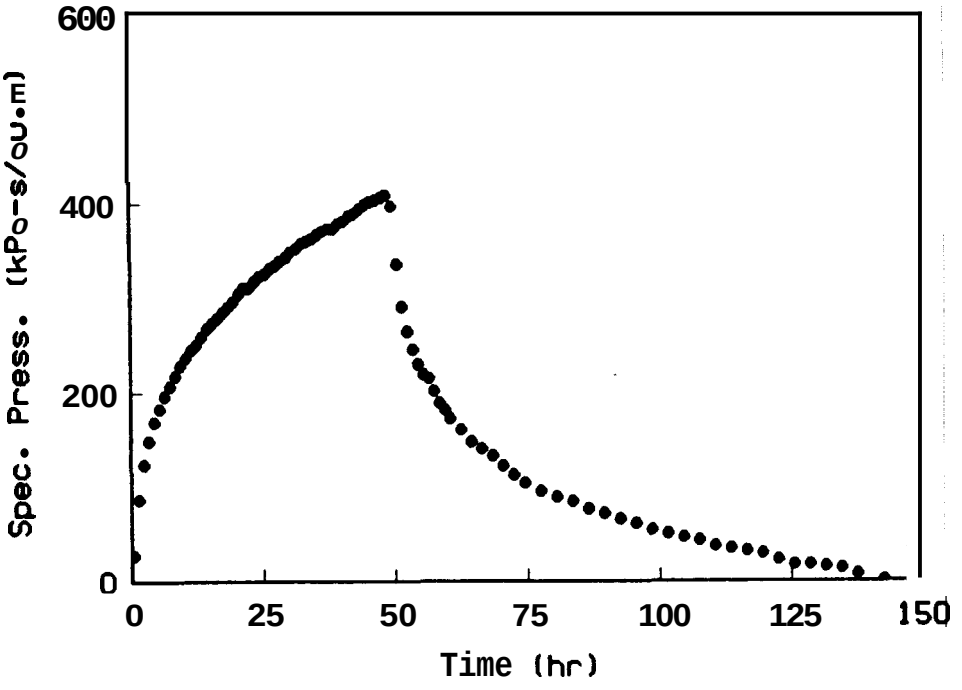

Fig. 7.2 Cartesian graph of the interference data (after *Leaver* et *al.* 1985).

For a minimum pressure significance level of **3** *kPa* (refer §3.4) and an average early time flow rate of **84** *l/s* the minimum specific pressure significance level is 60 $kPa\text{-}s/m^3$.

7.3.1.1. **Log-log** Analysis

A log-log pressure-time graph of the data is drawn and matched on the Eipper /dimensionless pressure-time graph of the same scale (Figure **7.3).** Dimensionless pressure and dimensionless time are defined as:

$$p_D = \frac{2\pi kh(p_i - p)}{q\mu} \qquad (7.1)$$

TABLE 7.1

TEST B1: BR13 RESPONSE TO BR23 DISCHARGE

TEST SPECIFICATIONS

	Observation Well	Source Well
Well No.	BR13	BR23
Coordinates (Broadlands Grid)	S 79705.90 *ft* W 45687.30 *ft*	S 78923.12 *ft* W 45215.27 *ft*
R.L. (C.H.F.) (*Moturiki* Datum)	293.5 *m*	291.8 *m*
Permeable Depth	915 ± 30 *m*	1015 - 1055
Drilled Depth	1081 *m*	1097 *m*
Open Hole Diam.	197 *mm*	194 *mm*
Interwell Distance	279 *m*	
Discharge Rate	52.4 *l/s*	
Discharge Temp.	245°C	
Discharge Enthalpy	1050 *kJ/kg*	
Recording Meter	Water Level Chart Recorder	
Flow Start Time	1230 Dec. 12 1979	
Drawdown Period	49.5 *h*	
Total Test Time	142.5 *h*	

$$t_D = \frac{kt}{\phi \mu c_t r_w^2} \qquad (7.2)$$

The graph contains three curves. Curve 1 represents the line source solution, while curves 2 and 3 represent type curves for drawdown and buildup which include the presence of a no-flow boundary *(Stallman* 1952) with $r_2/r_1 = 9.25$. The early time data is matched to the line source solution giving a match point of:

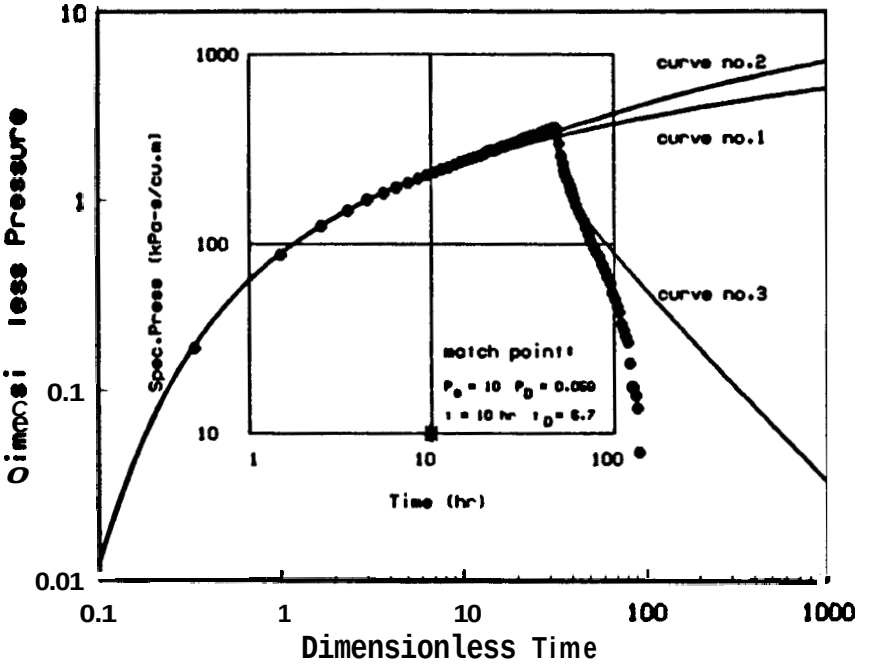

Fig. 7.3 Log-log match of data to Eipper type curves (after *Leaver et al.* 1985).

$$p_s = 10\ kPa\text{-}s/m^3 \qquad p_D = 0.059$$

$$t = 10hr \qquad \frac{t_D}{r_D^2} = 6.7$$

Values of transmissivity and storativity derived from the match point are presented in Table 8.1.

In conventional log-log analysis the late time data is matched to the appropriate *Stallman* type curve and the distance to the no-flow boundary or the ratio r_2/r_1 determined. From Figure 7.3 it can be seen that there is insufficient late time data to make an accurate match to one of the *Stallman* curves, yet the early time infinite acting response matches reasonably well to the line source solution.

The buildup portion of the test initially follows the log-log buildup curve up to about 70 hours. Then, the pressure builds up faster than expected for a system with one no-flow linear boundary. This rapid buildup indicates the presence of pressure support in the system. This could

be caused by:

(i) Recharge to the system.

(ii) A two phase region in the reservoir.

(iii) Injection into the reservoir at the time of testing.

(iv) Instrument error.

The effect of this pressure support is not apparent in the drawdown portion of the test, suggesting that the distance between the source well and the pressure support is greated than the distance between the source well and the no-flow boundary. This boundary effect does not appear in Test C2 and Test C1 shows a possible further barrier effect at late time. Further consideration of this trend is therefore not considered warranted.

7.3.1.2. Semi-log Analysis

Conventional analysis involves matching the data to a semi-log *Stallman* plot which has the effect of expanding the log-log graph in the higher pressure and time ranges. Figure 7.4 shows that definition of the r_2/r_1 ratio is still difficult.

Better definition can be obtained using the type of *Sageev et al.* [1985]. This analysis involves using the semi-log type curve formed by mathematically collapsing the semi-log plots of *Stallman's* type curves. The method gives accurate boundary definition providing the r_2/r_1 ratio is greater than 10 and definition to 20% of the true ratio for values greater than 5. The graph uses modified dimensionless coordinate axes for pressure and time (Figure 7.5). Modified pressure and time are defined respectively as:

$$p_D^* = p_D + \ln\left[\frac{100-1}{r_2/r_1}\right] \tag{7.3}$$

$$t_D^* = t_D\left[\frac{100-1}{r_2/r_1}\right]^2 \tag{7.4}$$

Figure 7.5 presents a semi-log match of the dimensionless pressure data to the type curve

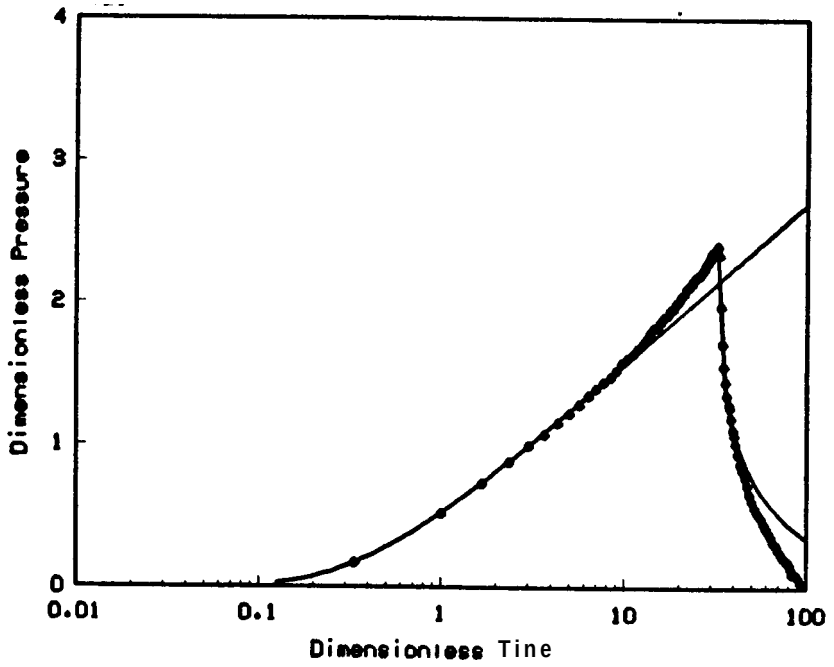

Fig. 7.4 Semi-log match of data to semi-infinite type curves (after *Leaver et al.* 1985).

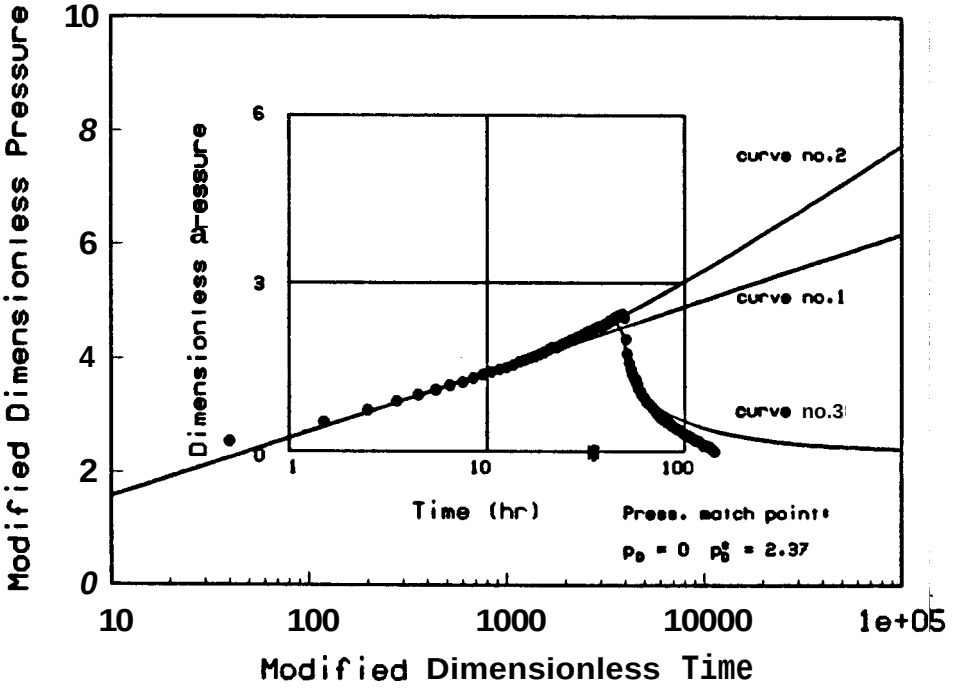

Fig. 7.5 Semi-log match of drawdown data to *Sageev et al.* type curves (after *Leaver et al.* 1985).

presented by ***Sageev et al.*** [1985]. The pressure match point is:

$$p_D = 0.0 \qquad p_D^* = 2.37$$

Substituting the semi-log pressure match point into Equation 7.3 and solving for the ratio r_2/r_1 yields:

$$r_2/r_1 = \exp\left[(p_D - p_D^*) + ln(100-1)\right] \tag{7.5}$$

$$r_2/r_1 = \exp(0.0 - 2.37 + ln99) = 9.25 \tag{7.6}$$

From the semi-log graph it can be noted that in order to get a unique match, only one semi-log straight line and the transition period are required. The data show that during the drawdown period the first semi-log straight line and the transition developed, but the second semi-log straight line did not.

7.3.1.3. Horner Analysis

Figure 7.6 presents a conventional dimensionless pressure Horner plot of the buildup data with the buildup curve for a linear boundary at $r_2/r_1 = 9.25$ shown on the same graph.

An alternative ***Horner*** plot can also be used which enables the boundary distance to be determined from a single buildup type curve. This analysis involves using the semi-log type curve for long producing times (***Ramey et al.*** 1973) formed by mathematically collapsing the family of Horner curves describing buildup behavior affected by a linear no-flow boundary (Fox 1984). This graph uses modified dimensionless coordinate axes for pressure and Horner time. The modified pressure and modified Homer time are defined respectively as:

$$p_{DH}^* = p_D + \ln\left[\frac{100(r_2/r_1)^2}{4t_{pD}}\right] \tag{7.7}$$

$$t_{DH}^* = t_H \frac{100(r_2/r_1)^2}{4t_{pD}} \tag{7.8}$$

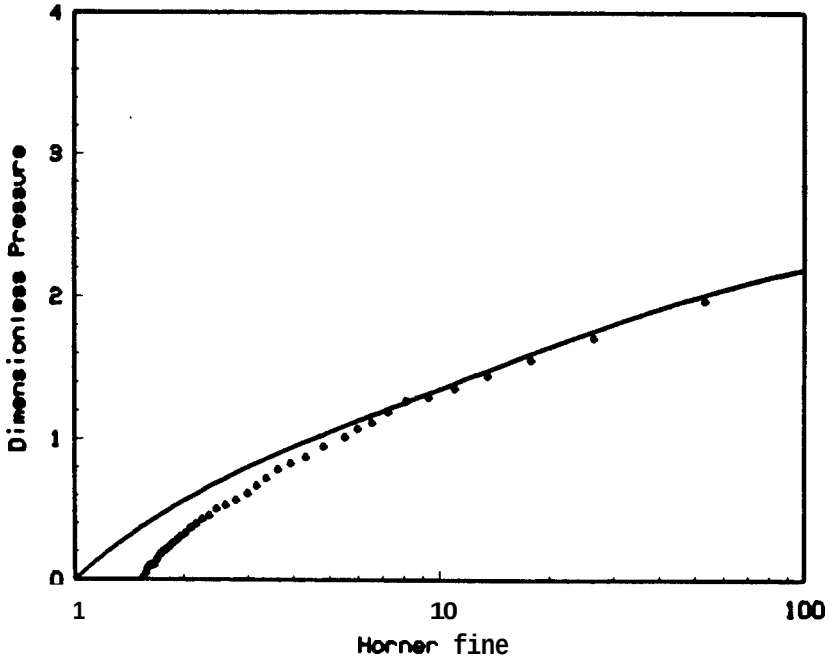

Fig. 7.6 Match of buildup data **on a *Horner* plot (after *Leaver et al.* 1985).**

and are arbitrarily defined for $d_D = 100$ ($d_D = \frac{r_3}{r_w}$) **and** $t_{pD} = 10^6$.

Type curve matching the data requires careful interpretation. A simple best fit of the data on the type curve would give a match point of (Figure 7.7):

$$p_D = 0.0 \quad p_D^* = 3.4$$

from Figure 7.3:

$$t_{pD} = (49.5)(0.67) = 33.17$$

from **Equation 7.8:**

$$r_2/r_1 = \left[4t_{pD} \frac{e^{(p^*_{DH} - p_D)}}{100} \right]^{0.5} \tag{7.9}$$

solving for r_2/r_1 **gives:**

$$r_2/r_1 = \left[(4)(33.17) \frac{e^{(3.4-0.0)}}{100} \right]^{0.5} = 6.3 \tag{7.10}$$

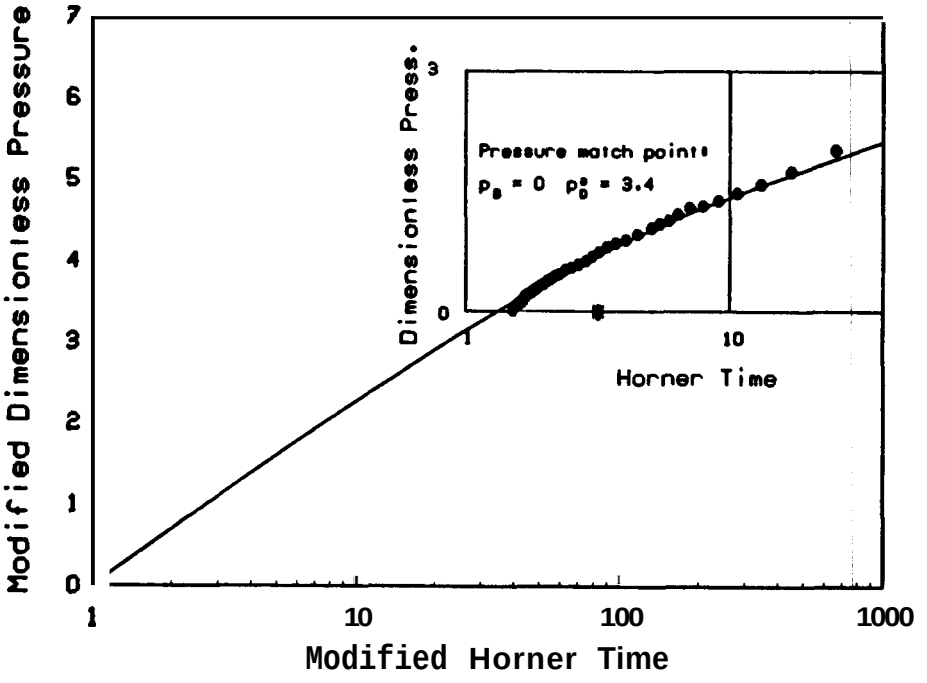

Fig. 7.7 Incorrect **Semi-log** match of **buildup** data to Fox **type** curve (after ***Leaver et al.*** **1985).**

This analysis is incorrect. The log-log analysis (Figure **7.3)** shows that the data after $t_D = 43$ $(t = 64hr)$ are influenced by the pressure support and that **only** the buildup data recorded before this time can be expected to match the type curve. Inspection of the semi-log plot (Figure **7.4)** shows that **only** the first semi-log straight line is present and that **the** transition **and** second semi-log straight lines are masked by the effect of the pressure support, Analysis of the drawdown data gives $r_2/r_1 = 9.25$. The correct match point for the buildup data can be determined by substituting this value in Equation 6. **This** gives:

$$p_{DH}^* = 0.0 + \ln\left[\frac{(100)(9.25)^2}{(4)(33.17)}\right] = 4.2 \qquad (7.11)$$

The correct match can now be made (Figure **7.8).**

For this test the semi-log and log-log graphs alone confirm the location of **the** no-flow **boundary.** The distance between the source well and the observation well, r_1, is 279 meters. Hence the distance between the observation well and the image well, r_2, is:

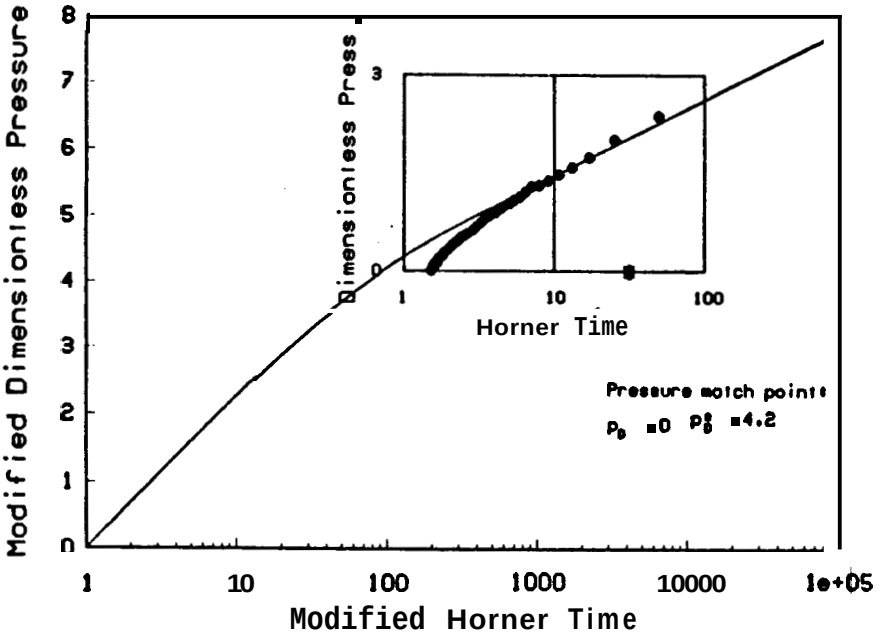

Fig. 7.8 Correct Semi-log match of buildup data **to** *Fox* type *curve* (after ***Leaver et al.*** **1985).**

$$r_2 = (279)(9.25) = 2582 \text{ meters} \qquad (7.121$$

The corresponding inference ellipse to which the postulated linear boundary is tangent is presented in Figure 7.9.

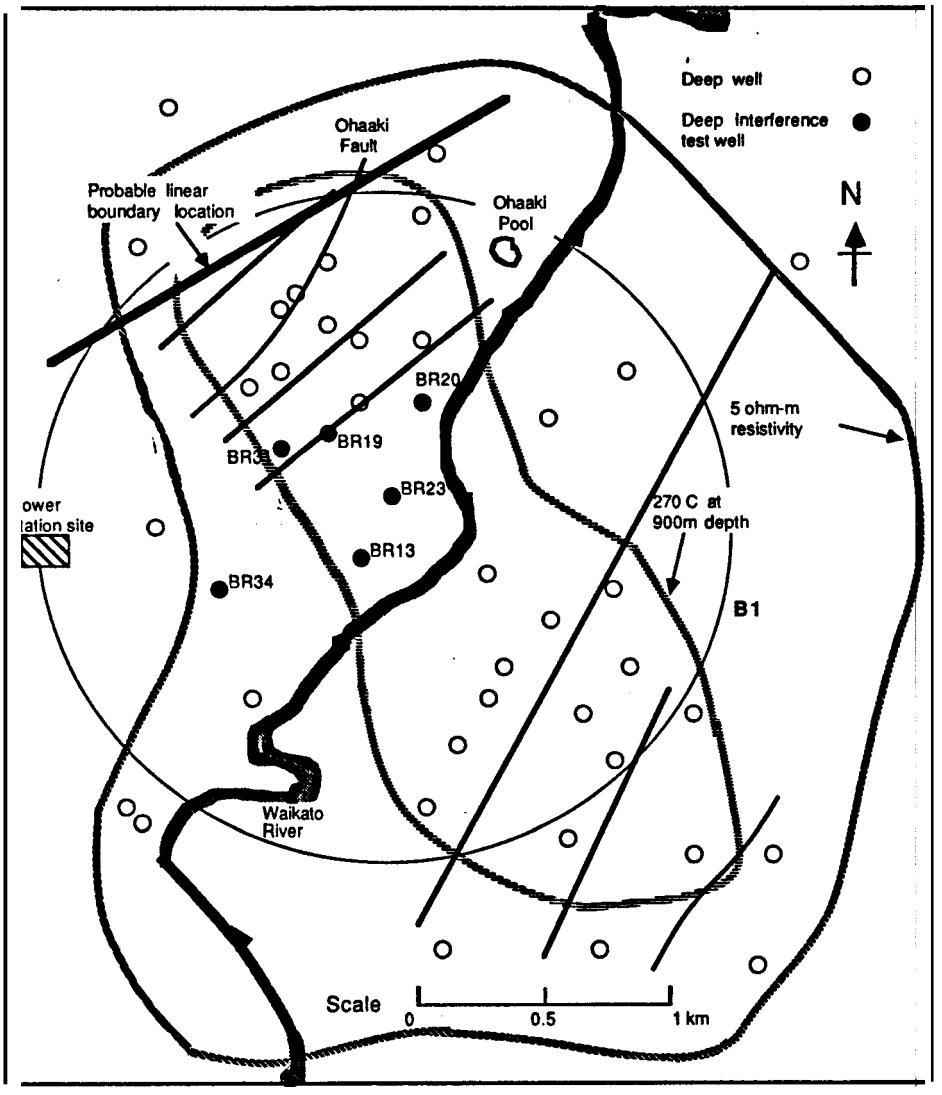

Fig. 7.9 Inference ellipse location (after *Leaver et al.* 1985).

73.2. TEST B2: BR23 RESPONSE TO BR13 DISCHARGE

Specific pressure verses time data for this test are presented in Table B2 and plotted in cartesian form in Figure 7.10. Test specifications are shown in Table 7.2 and

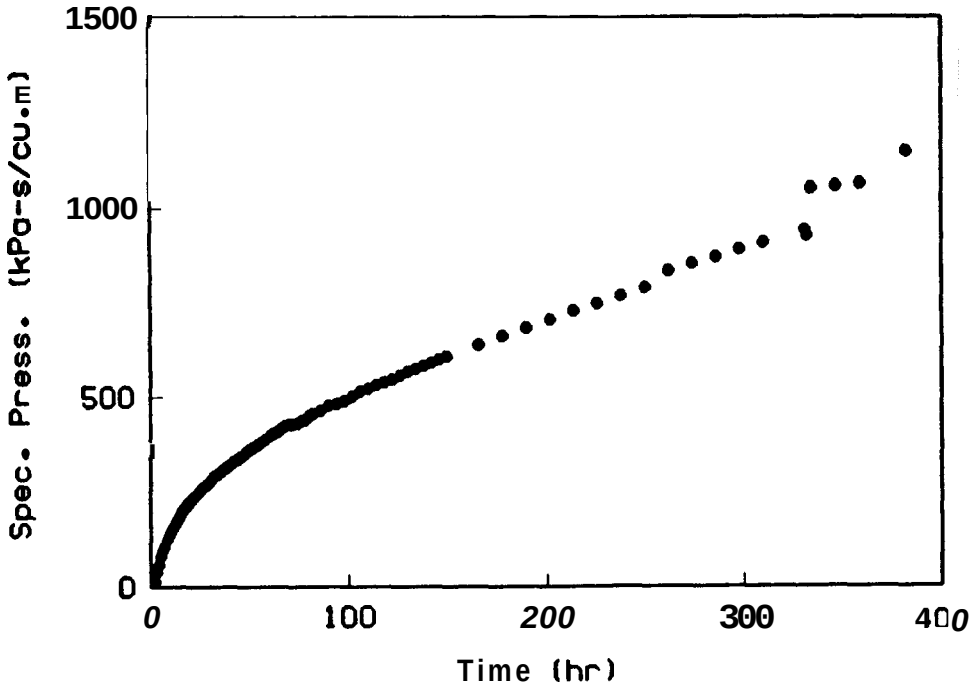

Fig. 7.10 Cartesian graph of the interference data

variations in flow rate are detailed in Table 7.3. The flow rate variation for the test period up to 190 hours fits the following correlation:

$$q = 0.0815 - 0.00361 \log\left[\frac{t}{3600}\right] \qquad (7.13)$$

For a minimum pressure significance level of 3 *kPa* (refer §3.4) and an average early time flow rate of 81 *l/s* the minimum specific pressure significance level is 37 $kPa\text{-}s/m^3$.

73.2.1. Log-log Analysis

A log-log pressure-time graph of the data is drawn and matched on the *Stallman* dimensionless pressure-time graph (Figure 7.11). On this graph, the lower curve is the *Theis* line source solution while the upper curve is that for a no-flow boundary with $r_2/r_1 = 4.5$. Early time data

TABLE 7.2

TEST **B2: BR23** RESPONSE **TO BR13** DISCHARGE

TEST SPECIFICATIONS

	Observation Well	Source Well
Well No.	**BR23**	**BR13**
Coordinates (*Broadlands* Grid)	S 78923.12 *ft* W 45215.27 *ft*	S 79705.90 *ft* W 45687.30 *ft*
R.L. (C.H.F.) (*Moturiki Datum*)	**291.8** *m*	**293.5** *m*
Permeable Depth	**1015 - 1055**	**915 ± 30 m**
Drilled Depth	**1097** *m*	**1081 m**
Open Hole Diam.	**194** *mm*	**197** *mm*
Interwell Distance	**279 m**	
Discharge Rate	refer Table **7.3**	
Discharge Temp.	**240°C**	
Discharge Enthalpy	**1040** *kJ/kg*	
Recording Meter	Water Level Chart Recorder	
Flow *Start* Time	**1400** Mar. **19 1980**	
Drawdown Period	**382 h**	
Total Test Time	**382** *h*	

fit well to the line **source** solution for times up to **40** hours and yield **a** match **point** of

$$p_s = 10\ kPa\text{-}s/m^3 \quad p_D = 0.038$$

$$t = 10\ h \qquad \frac{t_D}{r_D^2} - 1.10$$

TABLE 7.3

TEST B 2 BR23 RESPONSE TO BR13 DISCHARGE

DRAWDOWN FLOW RATE DATA

Time (*h*)	Flow Rate (*l/s*)
0.0	81.8
2.0	82.1
23.0	76.3
46.0	74.9
190.0	73.4
214.0	72.7
238.0	72.7
262.0	70.9
331.0	70.9
334.0	63.3
382.0	59.0

After 40 hours the data follow the pressure response for a boundary of $r_2/r_1 = 4.5$. After 120 hours the data show an upward trend above the response for this boundary. The trend in the data, if real, would indicate a further no-flow boundary. However it does not appear in any

(i) Temperature variations in the wellbore.

(ii) Discharge of another well in the field for which no record was kept.

(iii) Malfunction of the recording equipment.

7.3.2.2. Semi-log Analysis

A semi-log graph of the data is shown in Figure 7.12. The lower curve is the *Theis* line source solution while the upper curve is the solution for the linear no-flow boundary at $r_2/r_1 = 4.5$. In the semi-log plot the definition of the data match with the theoretical solutions is improved for higher values of pressure and time. The graph shows that the match of the data with the

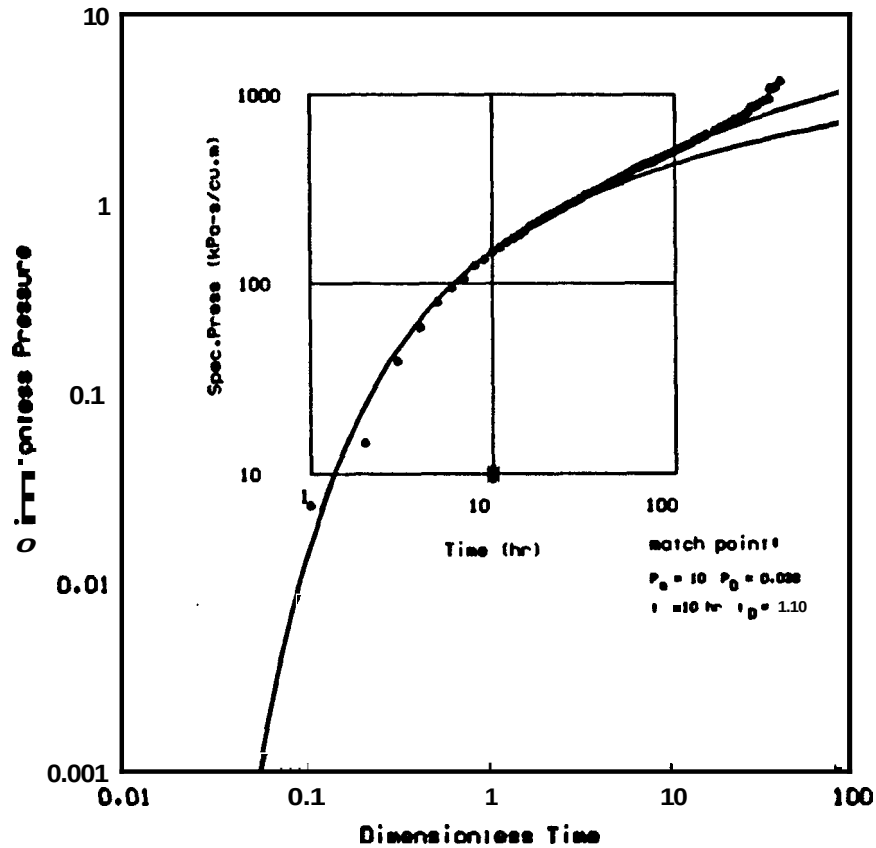

Fig. 7.11 Log-log match of data to ***Stallman*** **type** curves.

chosen boundary position is good for $t \leq$ **120 hours.**

While the semi-log graph confirms the position of the postulated no-flow boundary, the results from this analysis for transmissivity and the r_2/r_1 ratio are considered anomalous as the matched ratio was not in agreement with the value of **9.3** obtained from Tests B1 and B10. The results of this test are presumed to be affected by by one or more of the factors discussed in the previous section. The storativity value which is relatively insensitive to changes in the matched pressure level is retained for analysis.

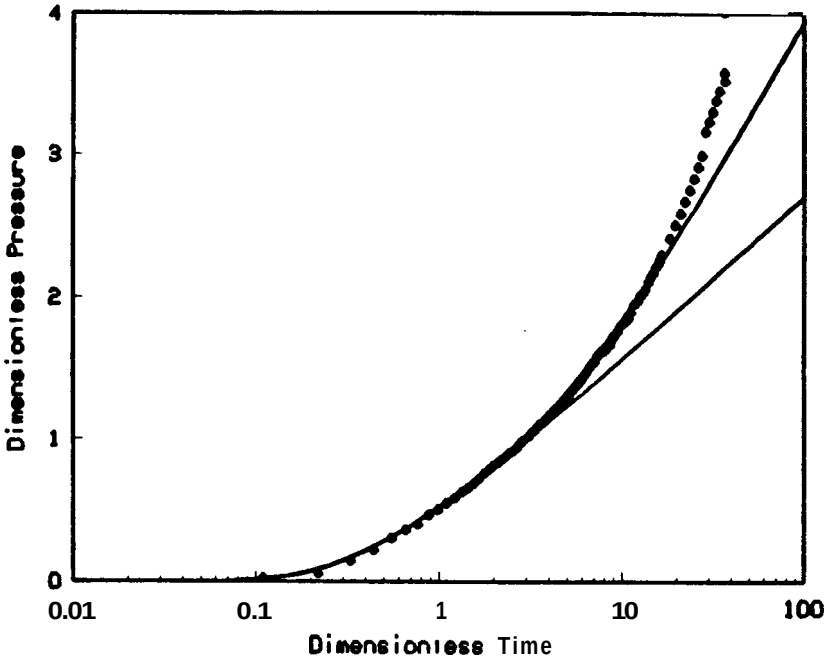

Fig. 7.12 Semi-log match of data to semi-infinite type curves.

7.3.3. TEST B3: BR23 RESPONSE TO BR19 DISCHARGE

Specific pressure verses time data for this test are presented in Table B3 and plotted in cartesian form in Figure 7.13. Test specifications are shown in Table **7.4.**

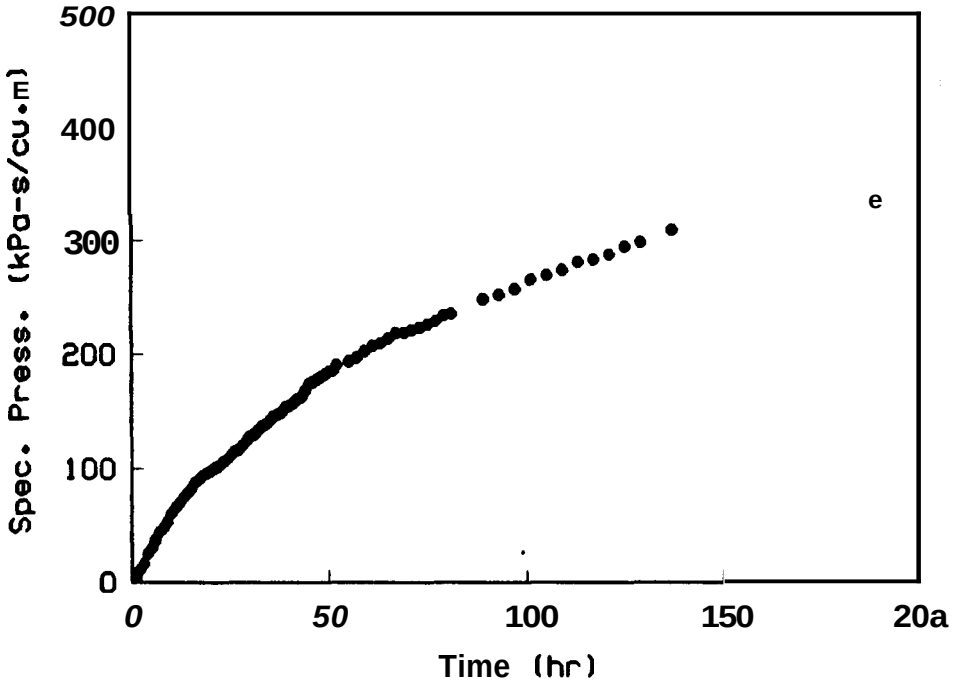

Fig. **7.13** Cartesian graph of the interference data.

For a minimum pressure significance level of 3 *kPa* (refer §3.4) and an average early time flow rate of 83 *l/s* the minimum specific pressure significance level is **36** $kPa\text{-}s/m^3$.

7.3.3.1. Log-log Analysis

A log-log pressure-time graph of the data is drawn and matched on the ***Stallman*** dimensionless pressure-time graph (Figure 7.14). On this graph, the lower curve is the ***Theis*** line source solution while the upper curve is that for a no-flow boundary with $r_2/r_1 = 2.8$. Early time data show some deviation from the line source solution for $t \leq 8$ hours. Data deviate from the line source solution for specific pressures of up to 60 $kPa\text{-}s/m^3$ which is above the minimum significance level of **36** $kPa\text{-}s/m^3$ and therefore the deviation cannot be attributable to earth tide effects. One explanation is that at early times the large pressure drop at the wellbore may cause

TABLE 7.4

TEST B3: BR23 RESPONSE TO BR19 DISCHARGE

TEST SPECIFICATIONS

	Observation Well	Source Well
Well No.	BR23	BR19
Coordinates (*Broadlands* Grid)	S 78923.12 *ft* W 45215.27 *ft*	S 78224.54 *ft* W 46154.80 *ft*
R.L. (C.H.F.) (*Moturiki* Datum)	291.8 *m*	294.4 *m*
Permeable Depth	1015-1055	600 - 1074
Drilled Depth	1097 *m*	1074 *m*
Open Hole Diam.	194 *mm*	194 *mm*
Interwell Distance	356 *m*	
Discharge Rate	83.2 *l/s*	
Discharge Temp.	-	
Discharge Enthalpy	1180 *kJ/kg*	
Recording Meter	Water Level Chart Recorder	
Flow Start Time	1500 April 5 1980	
Drawdown Period	189 h	
Total Test Time	189 h	

some non-*Darcy* flow resulting in a small two phase zone near the wellbore which would provide pressure support at early times only. Unfortunately no pressure data is available at the source well which could substantiate this effect. Whatever the reason the early time data is important in obtaining the match point to the line source solution. Linear boundaries with $r_2/r_1 \leq 10$ can only be accurately located from drawdown data once the infinite acting line source behavior has been observed. In Figure 7.14 the match to the line source only occurs

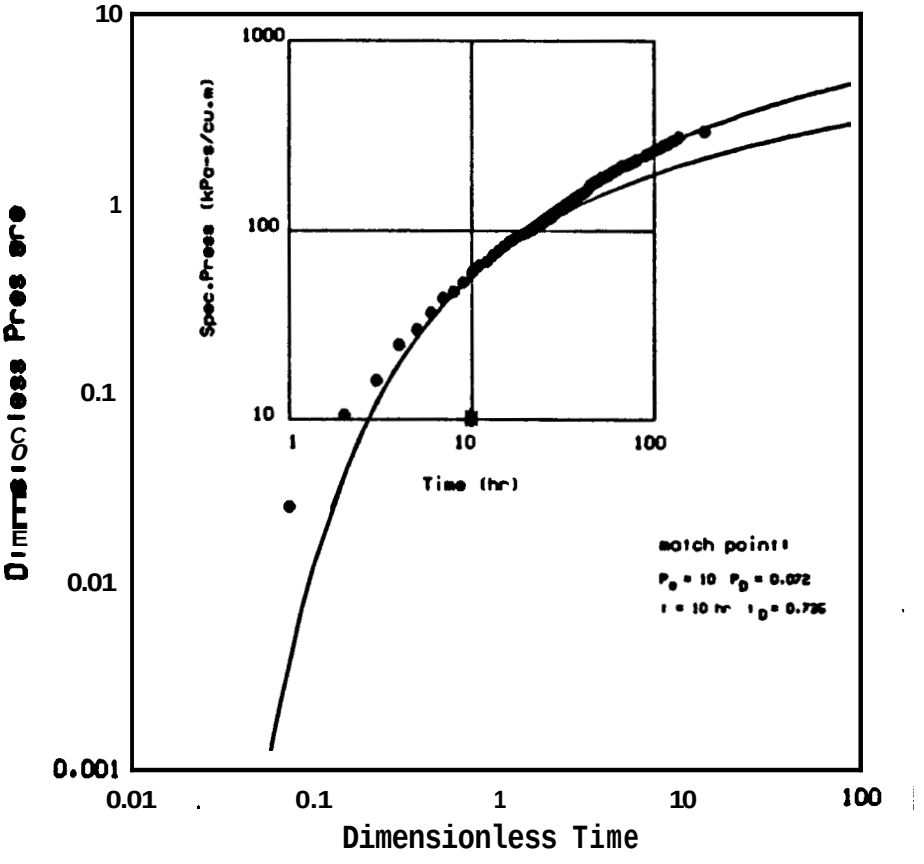

Fig. 7.14 Log-log match of data to *Stallman* type curves.

between times of 8 and 27 hours or half a log cycle.

Matching data between times of 8 and 27 hours yields a match point of:

$$p_s = 10\ kPa\text{-}s/m^3 \quad p_D = 0.072$$

$$t = 10\ h \qquad \frac{t_D}{r_D^2} = 0.735$$

Values of permeability and storativity derived from the match point are presented in Table 8.1.

After 27 hours the data show a good match to the pressure response for a boundary of $r_2/r_1 = 2.8$.

7.3.2. Semi-log Analysis

A semi-log graph of the data is shown in Figure **7.15.** The lower curve is

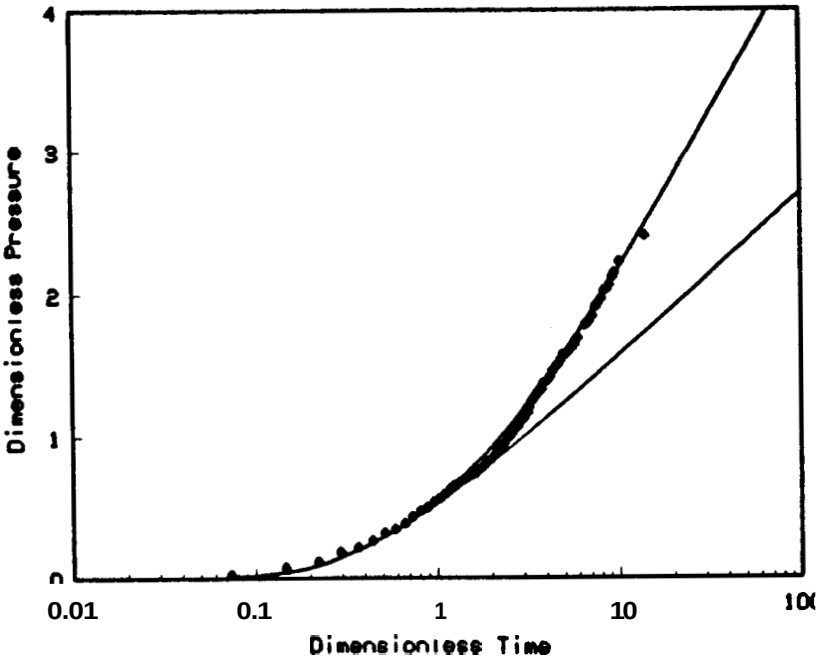

Fig. **7.15** Semi-log match of data to semi-infinite type curves.

the *Theis* line source solution while the upper curve is the solution for the linear no-flow boundary at $r_2/r_1 = 2.8$. In the semi-log plot the definition of the data match with the theoretical solutions is improved for higher values of pressure and time. The graph shows that the match of the late time data with the chosen boundary position is good.

The semi-log and log-log graphs confirm the location of the no-flow boundary. The distance between the source well and the observation well, r_1, is 357 meters. Hence the distance between the observation well and the image well, r_2, is:

$$r_2 = (357)(2.8) = 1000 \text{ meters}$$

The corresponding inference ellipse to which the postulated linear no-flow boundary is tangent is presented in Figure **7.16.**

There is an indication of either tidal or residual barometric effects in the data from the faint os-

cillations on the **fit** to the theoretical curves.

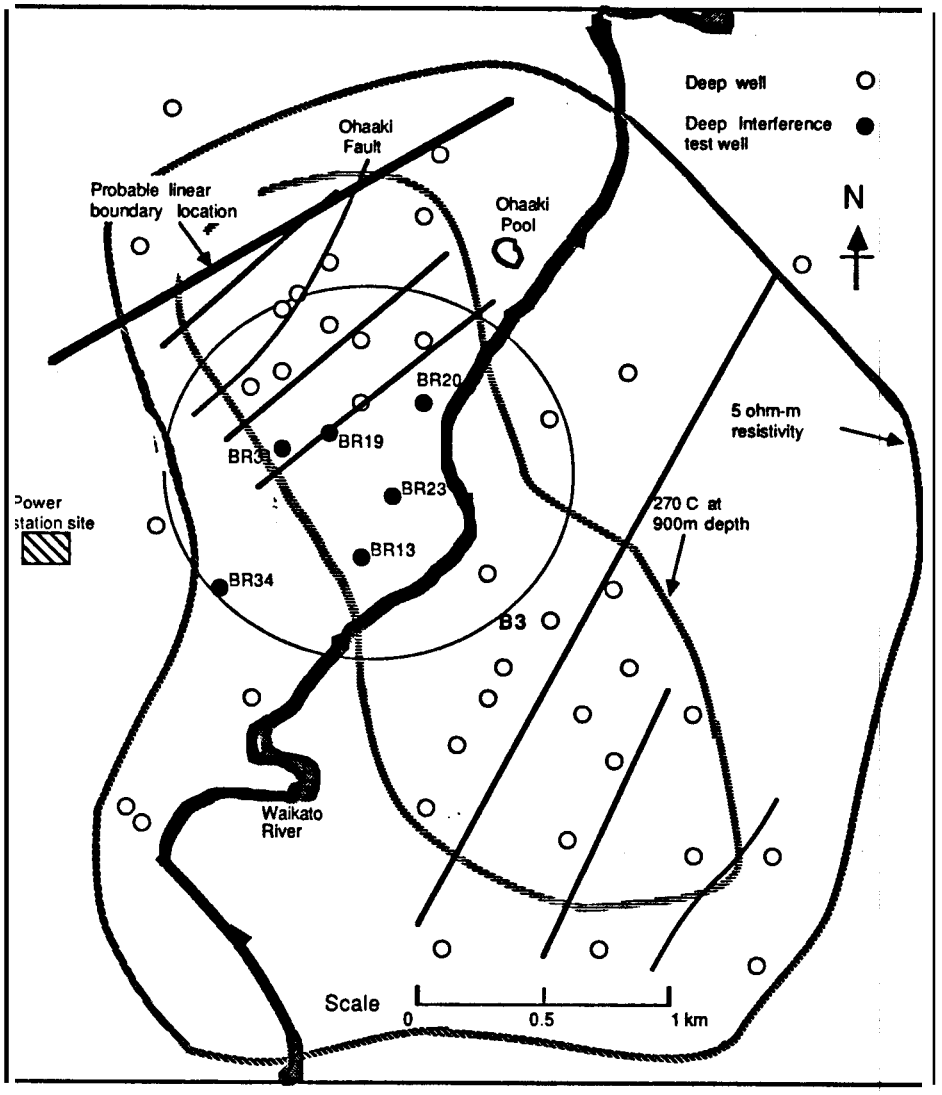

Fig. **7.16** Inference ellipse location.

73.4. TEST B4: BR23 RESPONSE TO BR13 INJECTION

Specific pressure verses time data for this test are presented in Table B4 and plotted in cartesian form in Figure 7.17. Test specifications are shown in Table 7.5.

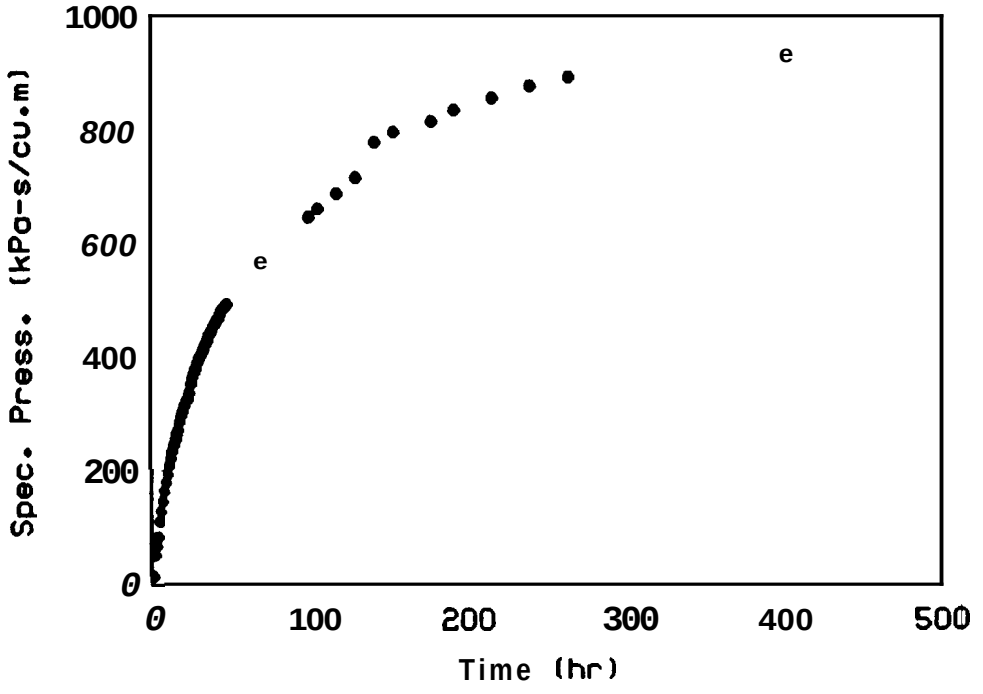

Fig. 7.17 Cartesian graph of the interference data.

For a minimum pressure significance level of 3 *kPa* (refer §3.4) and an average early time flow rate of 53 *l/s* the minimum specific pressure significance level is 57 $kPa\text{-}s/m^3$.

7.3.4.1. Log-log Analysis

A log-log pressure-time graph of the data is drawn and matched on the *Stallman* dimensionless pressure-time graph (Figure 7.18). On this graph, the lower curve is the *Theis* line source solution while the upper curve is that for a no-flow boundary with $r_2/r_1 = 3.0$. The data give a fair match to the line source for $t \leq 10$ hours and yield a match point of

$$p_s = 10\ kPa\text{-}s/m^3 \quad p_D = 0.0375$$

$$t = 10\ h \qquad \frac{t_D}{r_D^2} = 1.5$$

TABLE 7.5

TEST B4: BR23 RESPONSE TO BR13 INJECTION

TEST SPECIFICATIONS

	Observation Well	Source Well
Well No.	BR23	BR13
Coordinates (Broadlands Grid)	S 78923.12 ft W 45215.27 ft	S 79705.90 ft W 45687.30 ft
R.L. (C.H.F.) (Moturiki Datum)	291.8 m	293.5 m
Permeable Depth	1015 - 1055	915 ± 30 m
Drilled Depth	1097 m	1081 m
Open Hole Diam.	194 mm	197 mm
Interwell Distance	279 m	
Injection Rate	53.1 l/s	
Injection Temp.	162°C	
Injection Enthalpy	690 kJ/kg	
Recording Meter	Water Level Chart Recorder	
Flow Start Time	1400 May 13 1980	
Drawdown Period	402 h	
Total Test Time	402 h	

Between 10 and 200 hours the data show a good match to the pressure response for a boundary of $r_2/r_1 = 3.0$. After 200 hours the data assume a gradient very similar to that of the line source solution.

The match point of the early time data to the infinite acting curve agrees closely with that obtained from Tests B2 and B10. However the appearance of the boundary effect is known to ac-

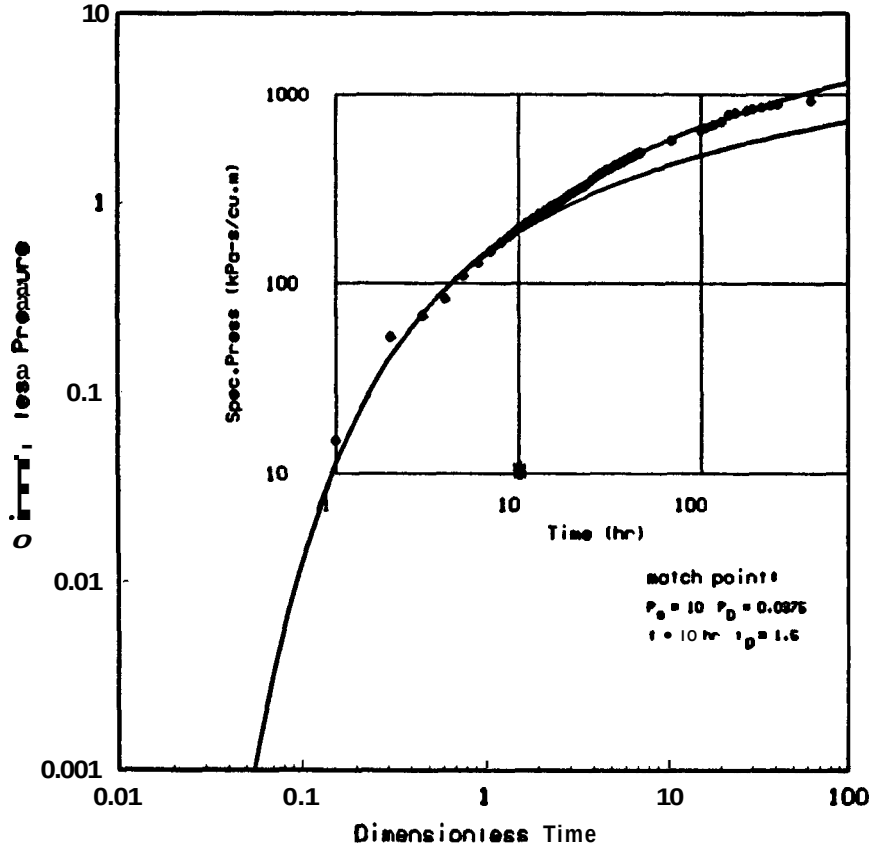

Fig. 7.18 Log-log match of data to ***Stallman*** type curves.

tually occur at r_2/r_1 = **9.3 as** shown in Tests B1 and B10. The significant deviation of this data from the known solution must be due to injection of brine. The difference in dimensionless pressure at the end of the test between the curve for r_2/r_1 = 3.0 and the line **source** is $\Delta p_D = 1$ or specific pressure difference $\Delta p_s = 267\ kPa\text{-}s/m^3$. **This** pressure difference is about 29% of **the** total pressure rise in the reservoir.

The difference may be due to a composite effect of the 162°C injected fluid moving into the reservoir predominantly at 270°C. Calculation of the radius of the bank of injected fluid shows that the amount of fluid injected represents **a** very small portion of the total fluid within the sphere of influence of the test:

$$Q = qt = \pi r_i^2 \phi h \qquad (7.14)$$

$$r_i = \sqrt{\frac{qt}{\pi\phi h}} \tag{7.15}$$

The permeable depth of **BR13** is at **915** meters. Colder fluid injected at this depth could conservatively be expected to occupy permeable thickness in the reservoir **at** or below this depth. The total permeable thickness in the Ohaaki reservoir is unknown but **a** maximum permeable depth of **1200** meters will be assumed. The effective permeable thickness seen by the injected fluid is then:

$$h = 1200 - 915 = 285 \ meters \tag{7.16}$$

A porosity **(ϕ)** of **20%** is arbitrarily assumed.

$$r_i = \sqrt{\frac{(0.0531)(402)(3600)}{\pi\ 0.2(285)}} \tag{7.17}$$

$$r_i = 21 \ meters \tag{7.18}$$

The distance between the source and observation wells **(r_1)** is **279** meters. The injected fluid front would not appear to have wide reaching thermal effects on the reservoir.

Fluid at **162°C** heated in the reservoir to **270°C** would undergo a specific volume change from **0.1104** m^3/kg to **0.1302** m^3/kg or a change of **18%** which would cause pressure changes of a similar amount.

Other factors affecting the response could include:

(i) Mineral deposition in the formation **(*Henley* and Harper, 1979).**

(ii) Permeability changes due to hydro-fracturing at the source well **(*Bixley* and Grant, 1980).**

(iii) Permeability changes due to thermal effects of the injected fluid on the formation.

(iv) Storativity changes due to condensation of any two phase fluid in the region of influence of the injected fluid.

The data appear to show oscillations about the theoretical curves which may **be** the result of earth tides or residual barometric fluctuations.

7.3.4.2. Semi-log Analysis

A semi-log graph of the data is shown in Figure 7.19. The lower curve is

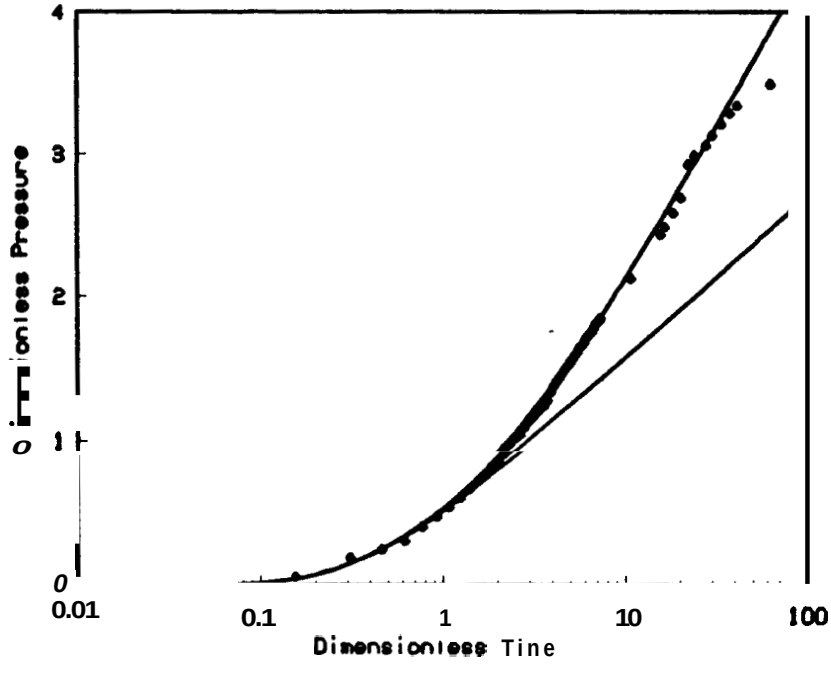

Fig. 7.19 Semi-log match of data to semi-infinite type *curves.*

the *Theis* line source solution while the upper curve is the solution for the linear 'no-flow boundary at $r_2/r_1 = 3.0$. In the semi-log plot the definition of the data match with the theoretical solutions is improved for higher values of pressure and time. The graph shows that the match of the data with the chosen boundary position is good for $t \leq 200$ hours. After this time the data show a flattening off. Reasons for this trend were discussed in the previous section however if the flattening of were "real" it would be indicative of contact with pressure support somewhere in the reservoir. This could be due to:

(i) A two phase zone.

(ii) Interaction with a "leak" within the reservoir.

(iii) Unknown discharge of another well in the reservoir.

(iv) Instrument error.

The apparent anomalous location of the no-flow boundary when compared to Tests B1 and B10 performed on the same doublet preclude further use of the results of this test. It is difficult to rationalize why the results appear to be so affected by the injection of a "small" amount of separated brine. Further study of this test using a thermal simulator may help resolve this problem.

73.5. TEST B6: BR23 RESPONSE TO BR20 DISCHARGE

Specific pressure verses time data for this test are presented in Table B5 and plotted in cartesian form in Figure 7.20. Test specifications are shown in Table 7.6.

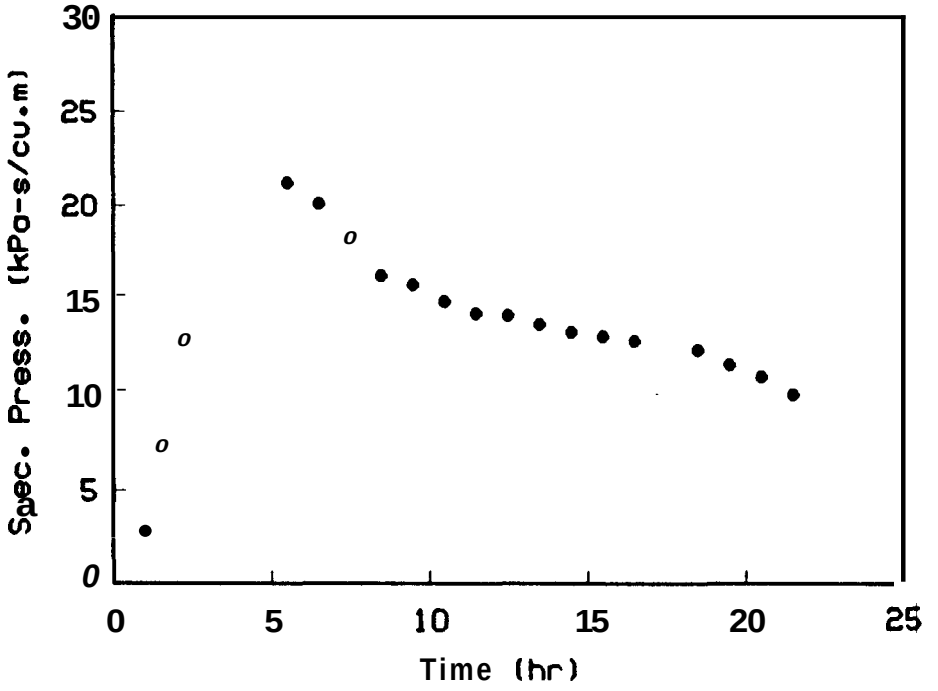

Fig. 7.20 Cartesian graph of the interference data.

For a minimum pressure significance level of 3 *kPa* (refer §3.4) and an average aarly time flow rate of 127 *l/s* the minimum specific pressure significance level is 24 *kPa-s/m*^{3}.

7.3.5.1. Log-log Analysis

A log-log pressure-time graph of the data is drawn and matched on the Eipper dimensionless pressure-time graph (Figure 7.21). A feature of this graph is the short test duration and the corresponding small pressure drawdown induced in the reservoir. The maximum specific pressure drop was 21.2 *kPa-s/m*^{3} (Table B5) which for a flow rate of 127 *l/s* (Table 7.6) corresponds to a pressure drop of only 2.7 *kPa*. This is less than the minimum specific pressure significance level of 3 *kPa*. Despite this the data have been crudely clipped of secondary effects and analysis proceeded with to demonstrate aspects particular to tests with small pres-

TABLE 7.6

TEST B6: BR23 RESPONSE TO BR20 DISCHARGE

TEST SPECIFICATIONS

	Observation Well	Source Well
Well No.	BR23	BR20
Coordinates *(BroadlandsGrid)*	S 78923.12 *ft* W 45251.27 *ft*	S 77671.308 W 44714.90 *ft*
R.L. (C.H.F.) *(MoturikiDatum)*	291.8 *m*	291.7 m
Permeable Depth	1015 - 1055 *m*	815 *m*, 945 *m*, 1085 *m*
Drilled Depth	1097 *m*	997 *m*
Open Hole Diam.	194 *mm*	194 *mm*
Interwell Distance	411 *m*	
Discharge Rate	127 *Us*	
Discharge Temp.	270°C	
Discharge Enthalpy	-	
Recording Meter	Water Level Chart Recorder	
Flow Start Time	1430 Oct.20 1980	
Drawdown Period	*6 h*	
Total Test Time	21.5 *h*	

sure drawdown.

The drawdown at early times is represented by the ***Theis*** line source solution as at early time fluid is drawn from close proximity to the wellbore and the existence of a boundary has little effect on the pressure response at the observation well. The magnitude of the pressure response increases with time.

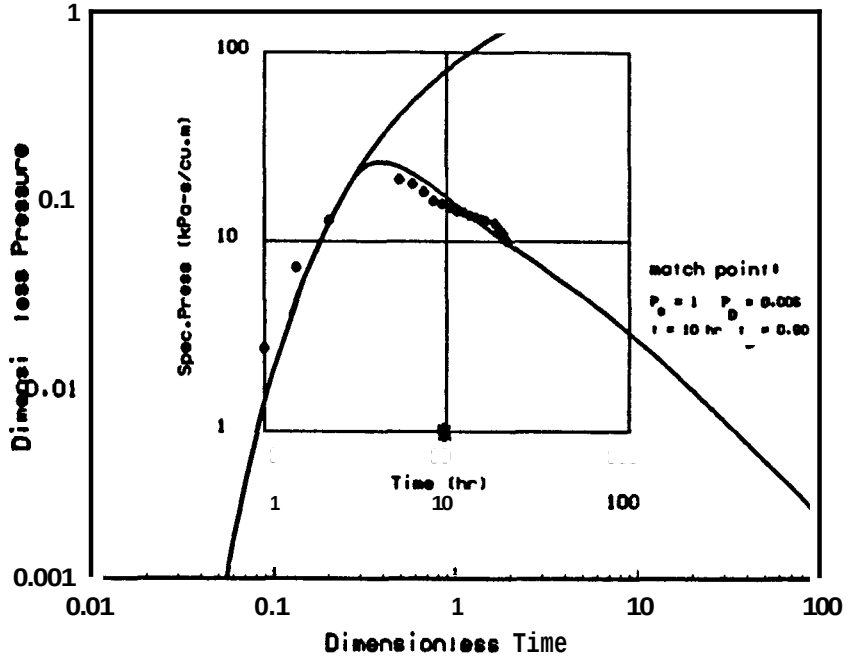

Fig. 7.21 Log-log match of data to Eipper type *curves* for r_2/r_1 =4.0.

$$\frac{t_D}{r_D^2} = \frac{kt}{\phi\mu c_t r_1^2} \tag{7.19}$$

$$t = \frac{\phi\mu c_t r_1^2}{k}\,\frac{t_D}{r_D^2} \tag{7.20}$$

High porosity, viscosity and compressibility and low permeability contribute to kxtending the time it takes for a given pressure change to occur in the reservoir and therefore these attributes help maintain pressures in the system.

Figure **7.21** shows that the effect of a boundary located at $r_2/r_1 = 4.0$ is felt at the observation well after $t_D/r_D^2 = 1$. The lower curve represents the *Theis* line source solution while the upper curve is the pressure response for the no-flow boundary at $r_2/r_1 = 4.0$. The data give a fair match to the theoretical curves and yield a match point of:

$$p_s = 1\,kPa\text{-}s/m^3 \quad p_D = 0.006$$

$$t = 10\,h \qquad \frac{t_D}{r_D^2} = 0.90$$

A feature of the short duration test is that the shape of the theoretical curves demonstrate how reservoir pressures continue to fall for a short time after the source well has stopped discharging. This feature is present for all the Eipper curves but is usually masked by the log-log scaling of the data.

While the match shown in Figure 7.21 appears to be satisfactory a non-uniqueness problems exist with the data. Only three points are shown on the drawdown with which to match to the line source solution. The determination of the existence of a boundary is largely reliant on the match of the buildup data. Figure 7.21 shows that a good match can be obtained for an r_2/r_1 ratio of 4.0. However an alternative match using the line source solution alone ils presented in Figure 7.22. Again the match looks plausible.

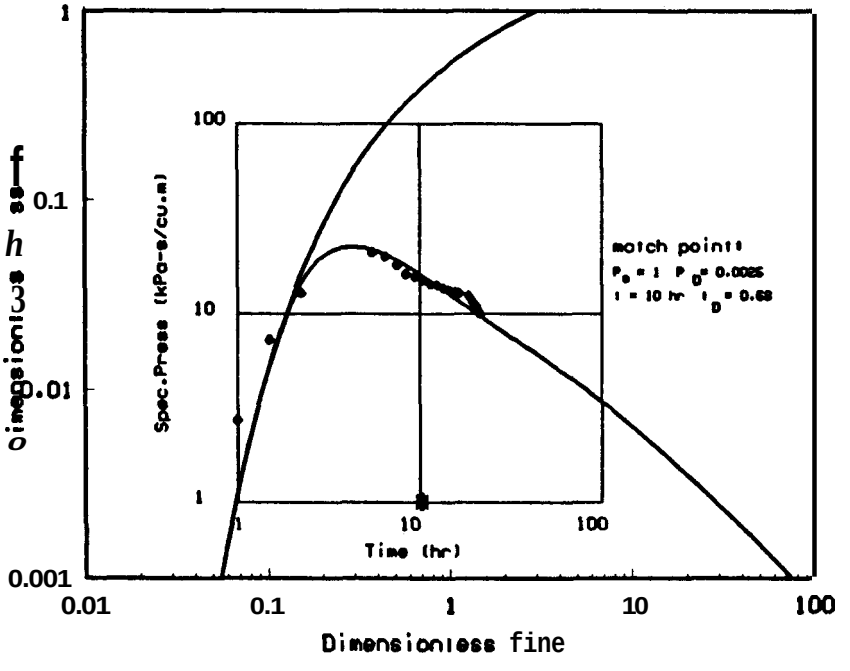

Fig. 7.22 Log-log match of data to line source solution.

Without additional data this problem could not be resolved. In this case the pressure match obtained from Test C2 on the same doublet could be used and the buildup data then fitted to the appropriate boundary curve (Figure 7.21). With the drawdown data matched at the same pressure level as Test C2 the buildup data match fairly to the pressure response for a boundary of

$r_2/r_1 = 4.0$.

73.53. Semi-log Analysis

Semi-log plots of the data are shown in Figures 7.23, 7.24.

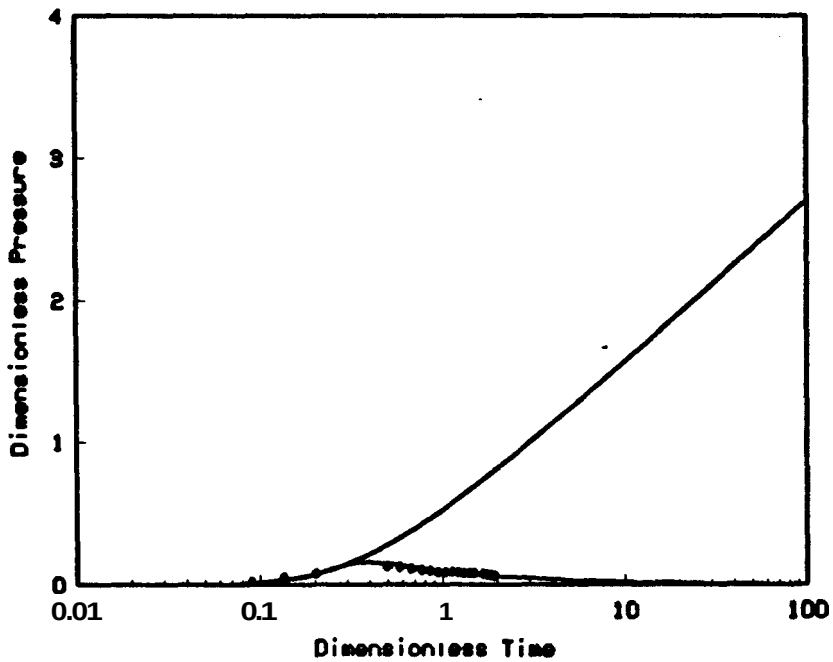

Fig. 7.23 Semi-log match of data to semi-infinite type curves for $r_2/r_1 = 4.0$.

The figures show the low pressure response level compared to other tests as all the semi-log dimensionless pressure-time plots are to the same scale. Both semi-log plots show a good match to the late time data emphasising the problem of non-uniqueness.

73.53. Horner Analysis

The *Horner* plot (Figure *7.25)* demonstrates the drawback of obtaining a significant match when data span less than one-fifth of a *Horner* time log cycle. The data show a good match to the theoretical buildup curve for $r_2/r_1 = 4.0$ but would also an equally good match to the line source solution.

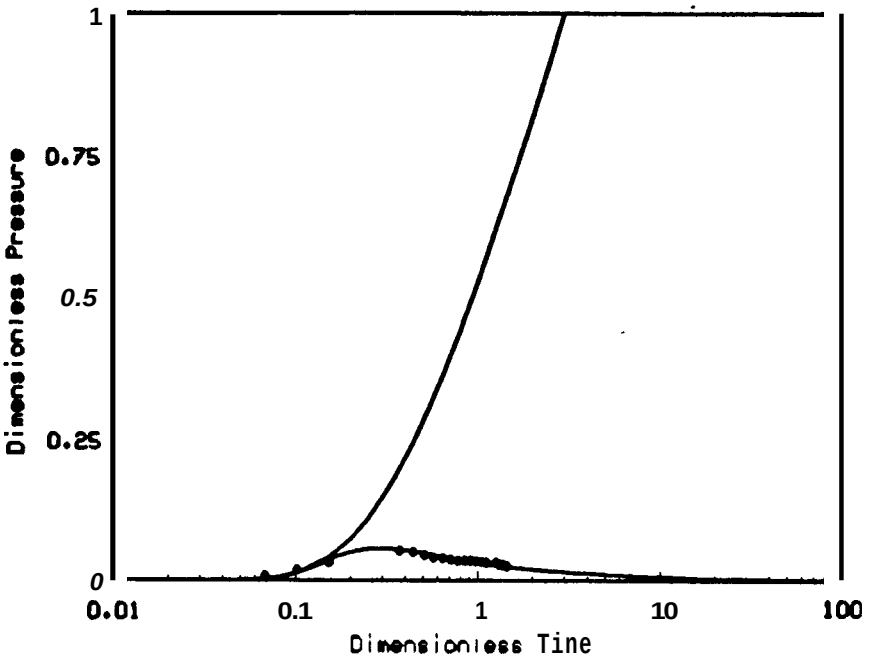

Fig. 7.24 Semi-log match of data to line source solution.

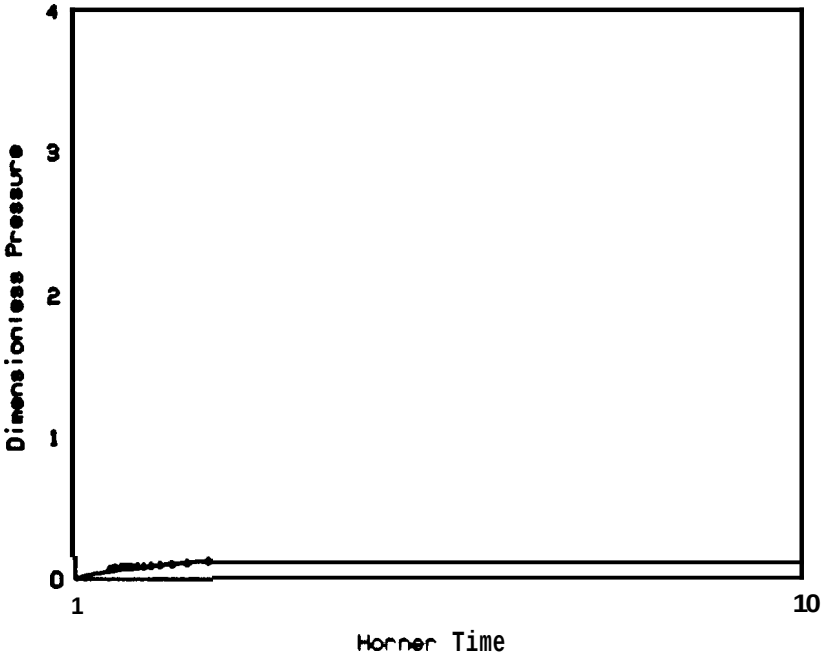

Fig. 7.25 Match of buildup data on a *Horner* graph.

73.6. TEST B7: BR34 RESPONSE TO BR31 DISCHARGE

Specific pressure verses time data for this test are presented in Table B6 and plotted in cartesian form in Figure 7.26. Test specifications are shown in Table 7.7 and

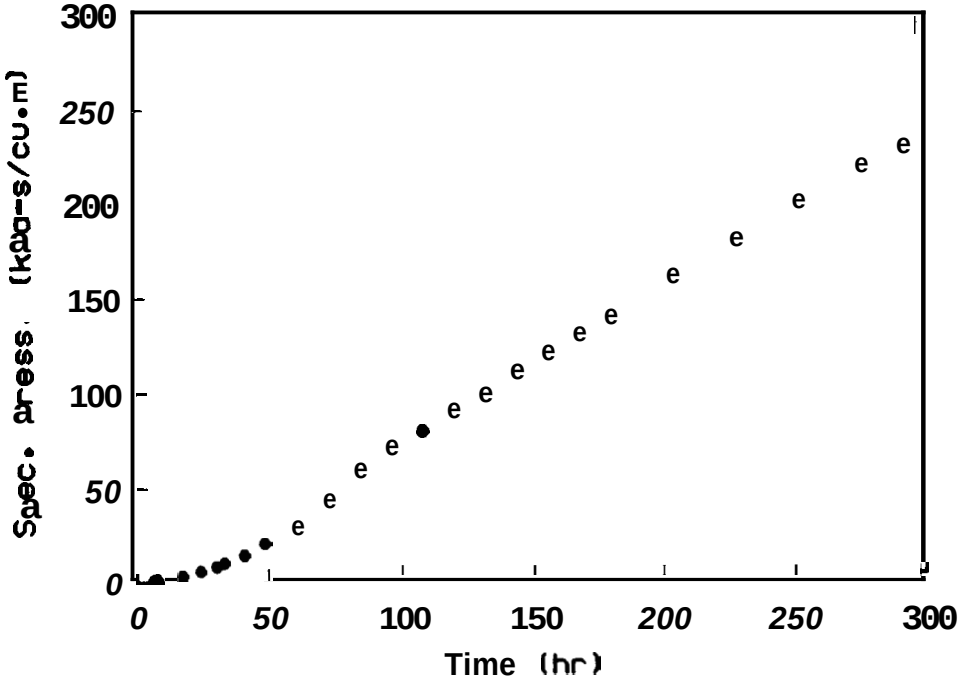

Fig. 7.26 Cartesian graph of the interference data.

variations in flow rate are detailed in Table 7.8.

For a minimum pressure significance level of 3 *kPa* (refer §3.4) and an average early time flow rate of 79 *l/s* the minimum specific pressure significance level is 38 $kPa\text{-}s/m^3$.

7.3.6.1. Log-log Analysis

A log-log pressure-time graph of the data is drawn and matched on the *Stallman* dimensionless pressure-time graph (Figure 7.27). On this graph, the lower Curve is the *Theis* line source solution while the upper curve is that for a no-flow boundary with $r_2/r_1 = 1.8$. The data show an early time deviation from the theoretical boundary curve until the specific pressure drawdown reaches about 10 $kPa\text{-}s/m^3$. Non-uniqueness of match is a problem with this data. The data has a marginal number of two points above the specific pressure significance level of 38

TABLE 7.7

TEST B7: BR34 RESPONSE TO BR31 DISCHARGE

TEST SPECIFICATIONS

	Observation Well	Source Well
Well No.	BR34	BR31
Coordinates (Broadlands Grid)	S 80200.84 *ft* W 47490.01 *ft*	S 78498.30 *ft* W 46766.50 *ft*
R.L. (C.H.F.) (Moturiki Datum)	308.8 *m*	297.7 *m*
Permeable Depth		730 *m*, 900 - 1000 *m*
Drilled Depth	2587 *m*	1252 *m*
Open Hole Diam.	216 mm	168 mm
Interwell Distance	564 *m*	
Discharge Rate	refer Table 7.8	
Discharge Temp.	-	
Discharge Enthalpy	1270 *kJ/kg*	
Recording Meter	Water Level Chart Recorder	
Flow Start Time	1130 Mar. 25 1980	
Drawdown Period	293 h	
Total Test Time	293 h	

$kPa\text{-}s/m^3$ which are matched to the line source. The match to the curve for $r_2/r_1 = 1.8$ is at the limit of resolution (refer §5.2). The final match was influenced by the need to have an excellent fit of the late time drawdown data which showed an upward trend that could not be fitted to the line source solution. The chosen match point gave an excellent fit to the data above the critical specific pressure level for a no-flow boundary located at $r_2/r_1 = 1.8$.

TABLE 7.8

TEST B7: BR34 RESPONSE TO BR31 DISCHARGE

DRAWDOWN FLOW RATE DATA

Time (h)	Flow Rate (l/s)
3.5	79.0
121.0	73.0
145.0	71.0
293.0	64.0

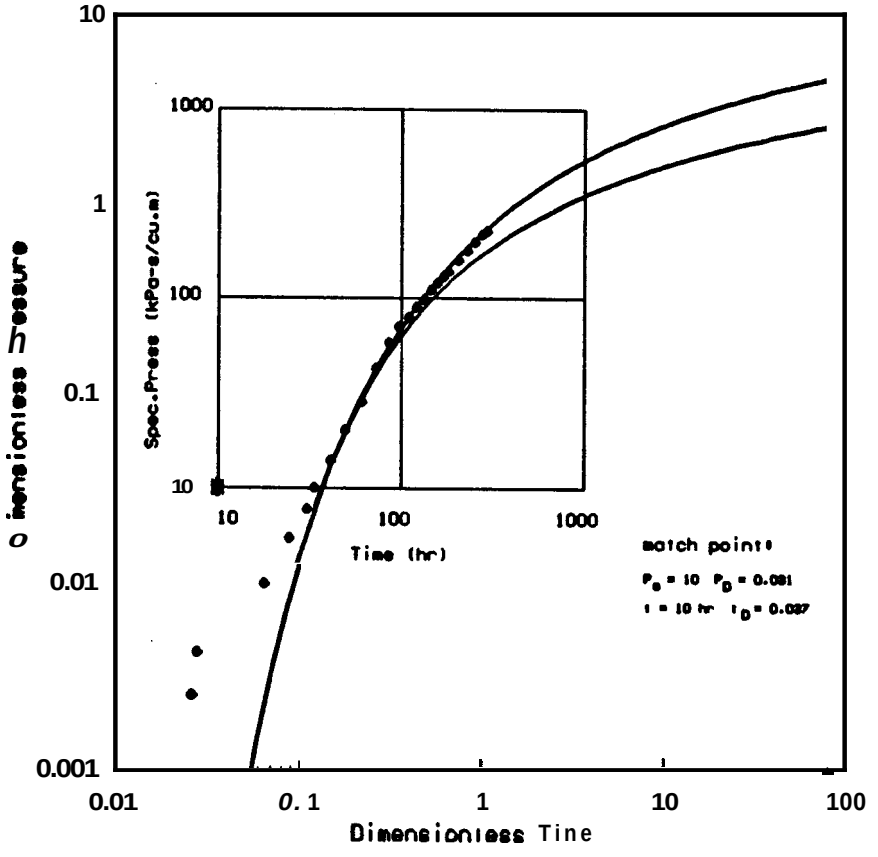

Fig. 7.27 Log-log match of data to *Stallman* type *curves.*

$$p_s = 10\ kPa\text{–}s/m^3 \quad p_D = 0.031$$

$$t = 10\ h \qquad \frac{t_D}{r_D^2} = 0.037$$

Values of permeability and storativity derived from the match point are presented in Table 8.1. The data show minor oscillations about the theoretical curves which may be the result of earth tides or residual barometric fluctuations.

73.6.2. Semi-log Analysis

A semi-log graph of the data is shown in Figure 7.28. The lower curve is

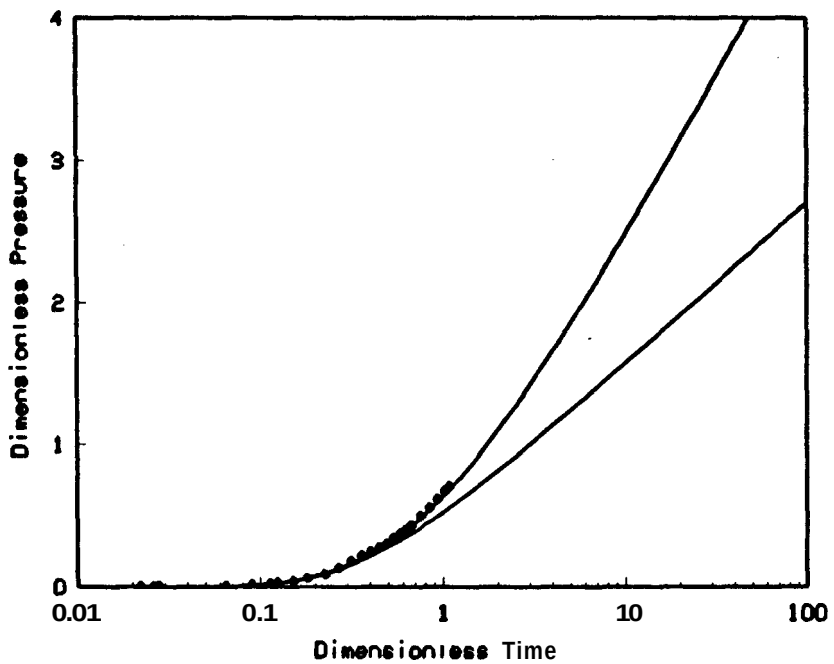

Fig. 7.28 Semi-log match of data to semi-infinite type curves.

the *Theis* line source solution while the upper curve is the solution for the linear no-flow boundary at $r_2/r_1 = 1.8$. In the semi-log plot the definition of the data match with the theoretical solutions is improved for higher values of pressure and time. The graph shows that the match of the late time data with the chosen boundary position is excellent.

The semi-log and log-log graphs confirm the location of the no-flow boundary. The distance between the source well and the observation well, r_1, is 564 meters. Hence the distance between the observation well and the image well, r_2, is:

$$r_2 = (564)(1.8) = 1015 \; meters$$

The corresponding inference ellipse to which the postulated linear boundary is tangent is presented in Figure 7.29.

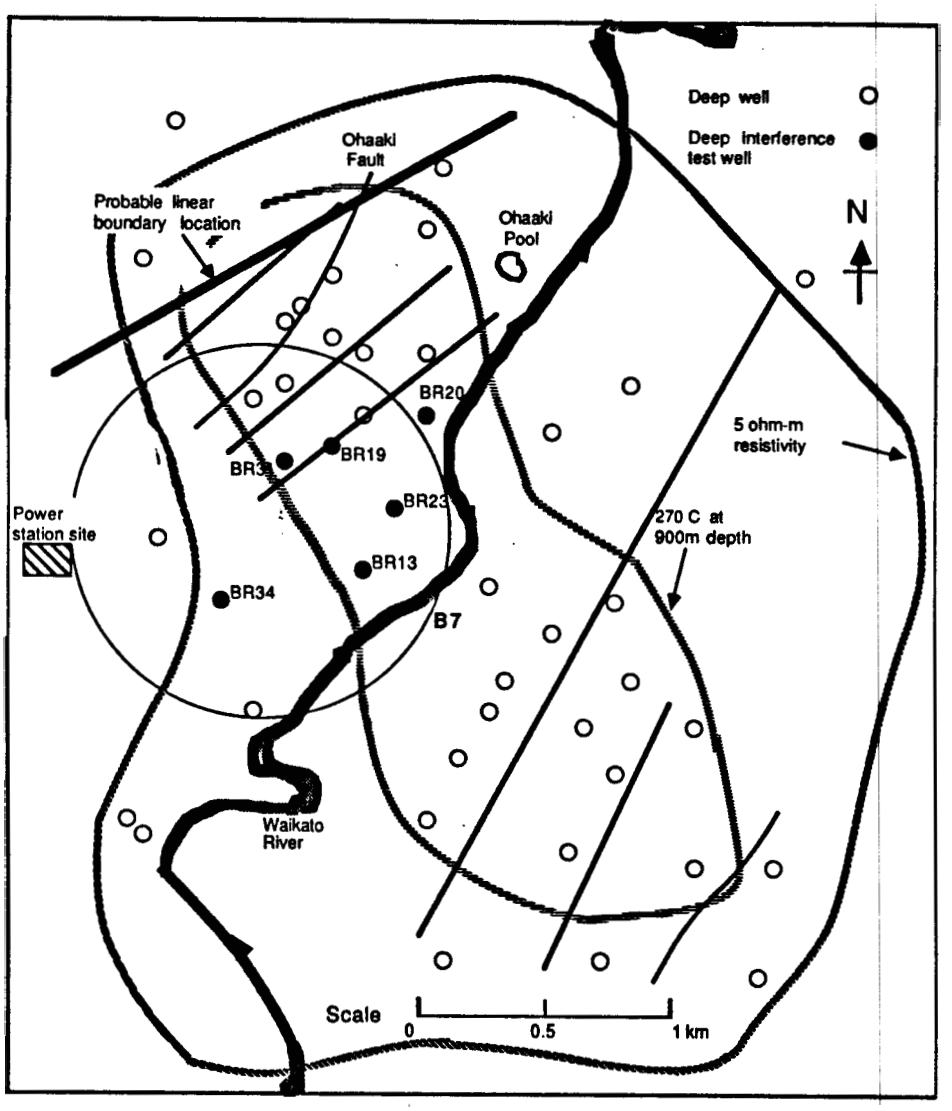

Fig. 7.29 Inference **ellipse location.**

73.7. TEST B8: BR34 RESPONSE TO BR23 DISCHARGE

Specific pressure verses time data for this test are presented in Table B7 and plotted in cartesian form in Figure 7.30. Test specifications are shown in Table 7.9 and

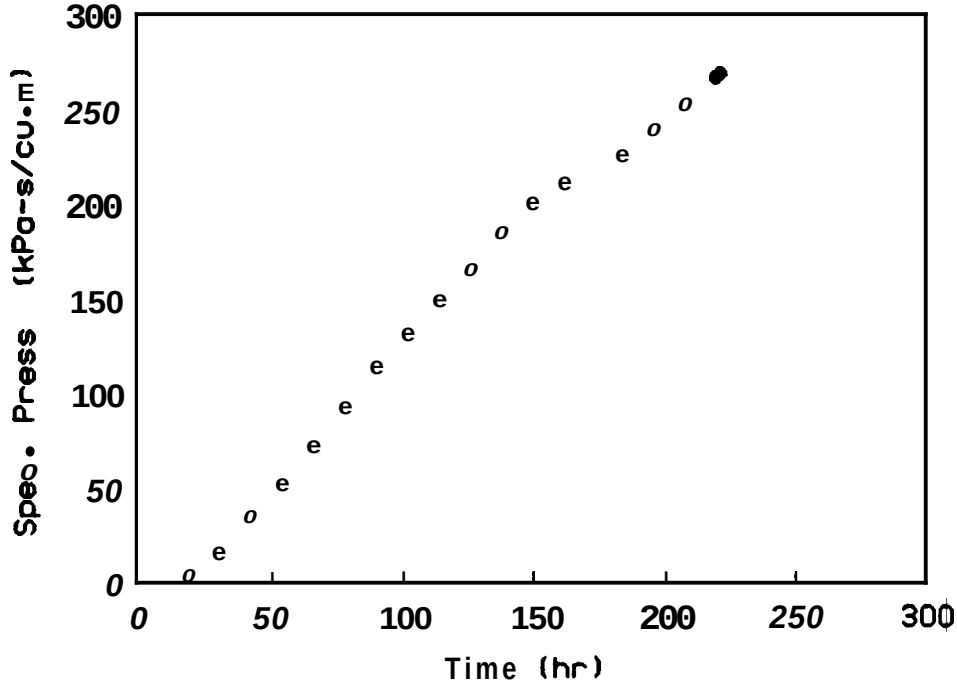

Fig. 7.30 Cartesian graph of the interference data

variations in flow rate are detailed in Table 7.10. A 32% drop in flow rate occurred in the final 10 hours of the test.

For a minimum pressure significance level of 3 *kPa* (refer §3.4) and an average early time flow rate of 71 *l/s* the minimum specific pressure significance level is 42 $kPa\text{-}s/m^3$.

73.7.1. Log-log Analysis

A log-log pressure-time graph of the data is drawn and matched to the *Theis* line source solution (Figure 7.31). The data show an excellent match to line source solution at \$11 times. The match is non-unique however as a match could also be obtained to that of a boundary with r_2/r_1 of less than 2 (refer §5.2). The match point for the line source solution is:

$$p_s = 10\ kPa\text{-}s/m^3 \quad p_D = 0.0204$$

TABLE 7.9

TEST **B8: BR34** RESPONSE TO **BR23** DISCHARGE

TEST SPECIFICATIONS

	Observation Well	Source Well
Well No.	**BR34**	**BR23**
Coordinates *[Broadlands* **Grid)**	**S 80200.84** *ft* W **47490.01** *ft*	**S 78923.12** *ft* W **45215.27** *ft*
R.L. (C.H.F.) (*Moturiki* Datum)	**308.2 m**	**291.8 m**
Permeable Depth		**1015-1055**
Drilled Depth	**2587 m**	**1097 m**
Open Hole Diam.	**216** *mm*	**194** *mm*
Interwell Distance	**795 m**	
Discharge Rate	refer Table **7.10**	
Discharge Temp.		
Discharge Enthalpy	**1209** *kJ/kg*	
Recording Meter	Water Level Chart Recorder	
Flow **Start** Time	**1650** Mar. **2 1981**	
Drawdown Period	**223 h**	
Total Test Time	**223 h**	

$$t = 10\ h \qquad \frac{t_D}{r_D^2} = 0.0046$$

The value **of** storativity which is relatively insensitive to the matched pressure level is present-*ed* in Table **8.1.**

TABLE 7.10

TEST B8: BR34 RESPONSE TO BR23 DISCHARGE

DRAWDOWN FLOW RATE DATA

Time	Flow Rate
223.0	70.9
233.0	48.5

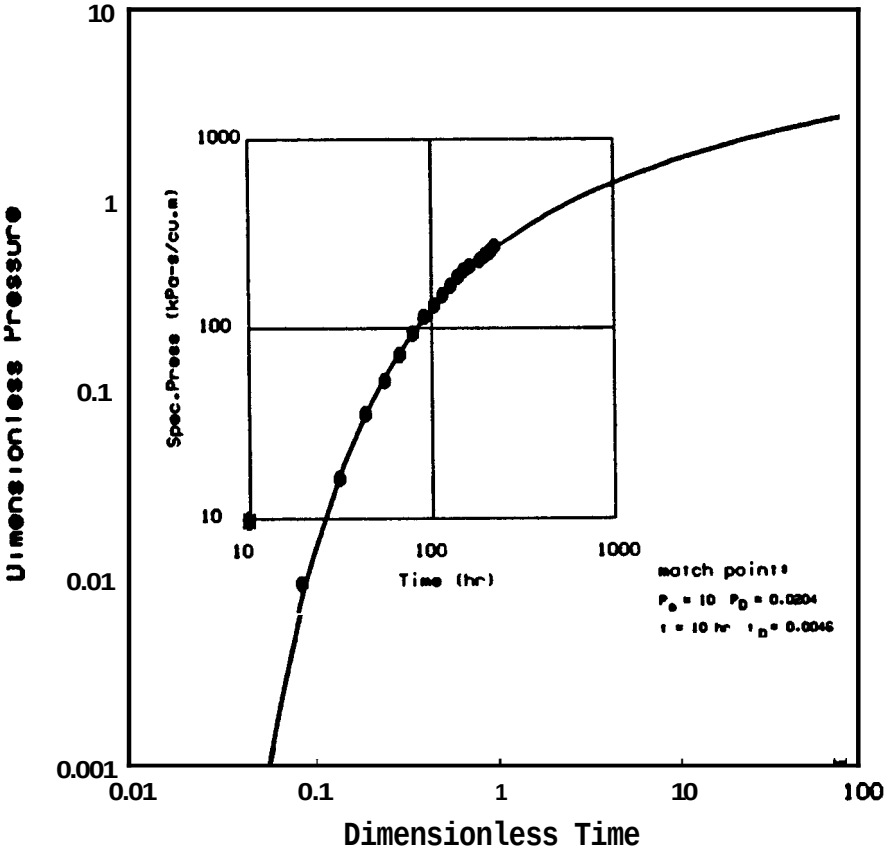

Fig. 7.31 Log-log match of data to *Theis* type curve.

7.3.7.3. Semi-log Analysis

The data show an excellent fit to the *Theis* line source solution but this match is non-unique for the reasons discussed in the previous section (Figure 7.32).

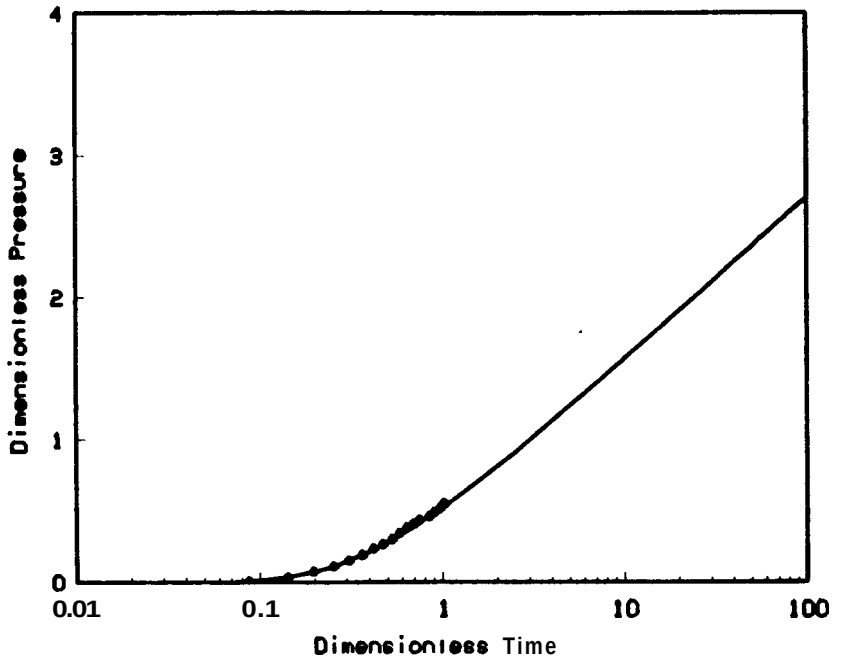

Fig. 7.32 Semi-log match of data to line source solution.

73.8. TEST B9: BR34 RESPONSE TO BR19 DISCHARGE

Specific pressure verses time data for this test are presented in Table B8 and plotted in cartesian form in Figure 7.33. Test specifications are shown in Table 7.11 and

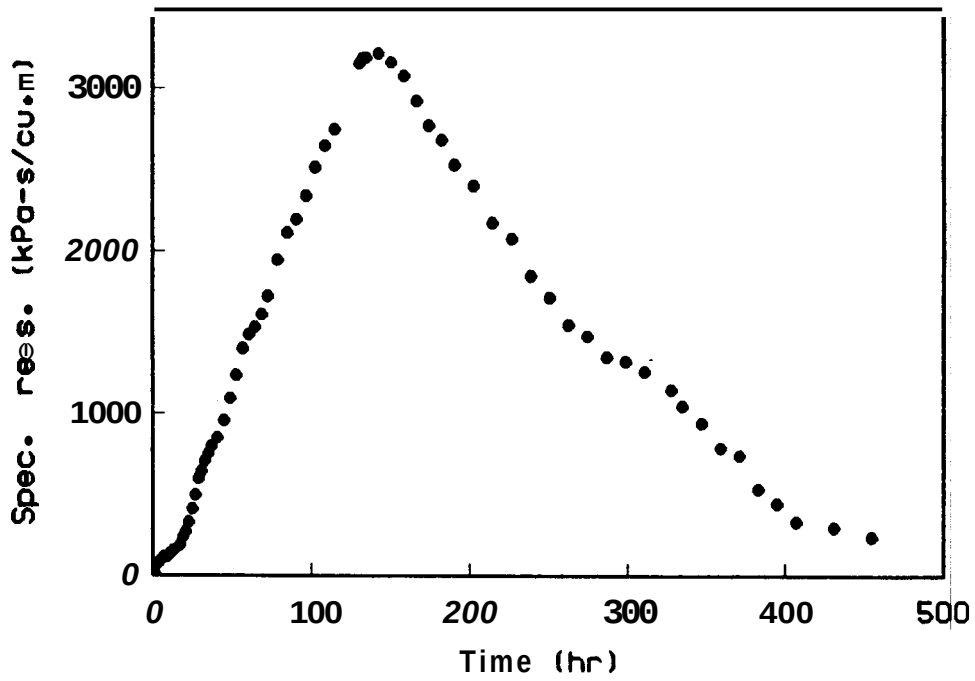

Fig. 7.33 Cartesian graph of the interference data

variations in flow rate are detailed in Table 7.12. The flow rate variation was fitted to the following correlation for the total discharge time:

$$q = 0.0749 - 0.0039 \log\left[\frac{t}{3600}\right] \qquad (7.21)$$

For a minimum pressure significance level of 3 *kPa* (refer §3.4) and an average early time flow rate of 70 *l/s* the minimum specific pressure significance level is 43 $kPa\text{-}s/m^3$.

7.3.8.1. Log-log Analysis

A log-log pressure-time graph of the data is drawn and matched on the ***Eipper*** dimensionless pressure-time graph (Figure 7.34). On this graph, the lower curve is the ***Theis*** line source solution while the upper curve is for a no-flow boundary with $r_2/r_1 = 1.5$. The drawdown data

TABLE 7.11

TEST **B9: BR34 RESPONSE** TO **BR19 DISCHARGE**

TEST **SPECIFICATIONS**

	Observation Well	Some Well
Well No.	**BR34**	**BR19**
Coordinates (Broadlands **Grid)**	**S 80200.84** *ft* W **47490.01** *ft*	**S 78224.54** *ft* W **46154.80** *ft*
R.L. (C.H.F.) (*Moturiki Datum*)	**308.2 m**	**294.4 m**
Permeable **Depth**	-	**600 - 1074** *m*
Drilled Depth	**2587 m**	**1074 m**
Open Hole Diam.	**216** mm	**194** mm
Interwell Distance	**727 m**	
Discharge Rate	refer Table **7.12**	
Discharge Temp.	-	
Discharge Enthalpy	**1180** *kJ/kg*	
Recording Meter	Water Level Chart Recorder	
Flow Start Time	**1200 Mar. 2 1980**	
Drawdown Period	**143** *h*	
Total Test Time	**455** *h*	

show an early time deviation from the chosen match to the line source solution until the specific pressure drawdown reaches about 20 $kPa\text{-}s/m^3$ after which an excellent fit is obtained.

The buildup data match well to the buildup portion of the line **source** solution until a time of 320 hours when the data drop below the theoretical curve indicating interaction with pressure support in the system. Possible constant pressure **sources** are discussed in Test **B1 (§ 7.3.1).**

TABLE 7.12

TEST B9: BR34 RESPONSE TO BR19 DISCHARGE

DRAWDOWN FLOW RATE DATA

35.0	68.0
57.0	
85.0	67.3
103.0	
132.0	66.2

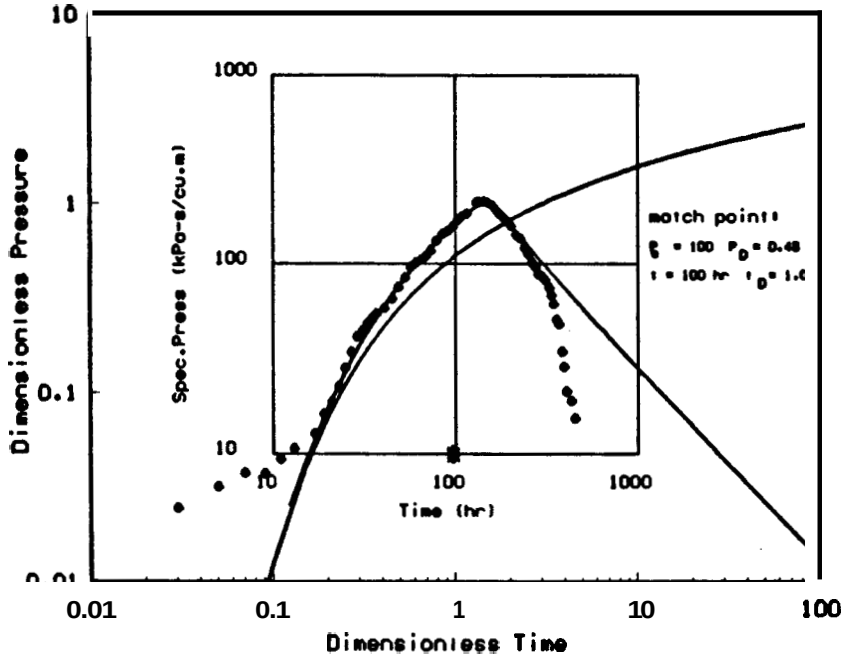

Fig. 7.34 Log-log match of data to *Eipper* type curves for r_2/r_1 =1.5.

The **match points were:**

$$p_s = 10\ kPa\text{-}s/m^3 \quad p_D = 0.048$$

$$t = 100\ h \qquad \frac{t_D}{r_D^2} = 1.00$$

While the match shown in Figure 7.34 appears to be satisfactory a non-uniqueness problem exists with the data. Early time line source behavior is masked by the anomalous behavior of data for specific pressure levels of less than 20 $kPa\text{-}s/m^3$. An alternative match of the data to the *Theis* line source solution alone is shown in Figure 7.34. This match appears equally as plausible. The reason for this is that the resolution of the data is insufficient to distinguish between the line source solution and semi-infinite solutions for r_2/r_1 ratios ≤ 2 (refer §5.2). The buildup data follow the theoretical behavior for only one-half a log cycle providing no additional assistance in defining the match point. Hence the non-uniqueness of the match.

Figure 7.35 shows the match point to the line source solution as:

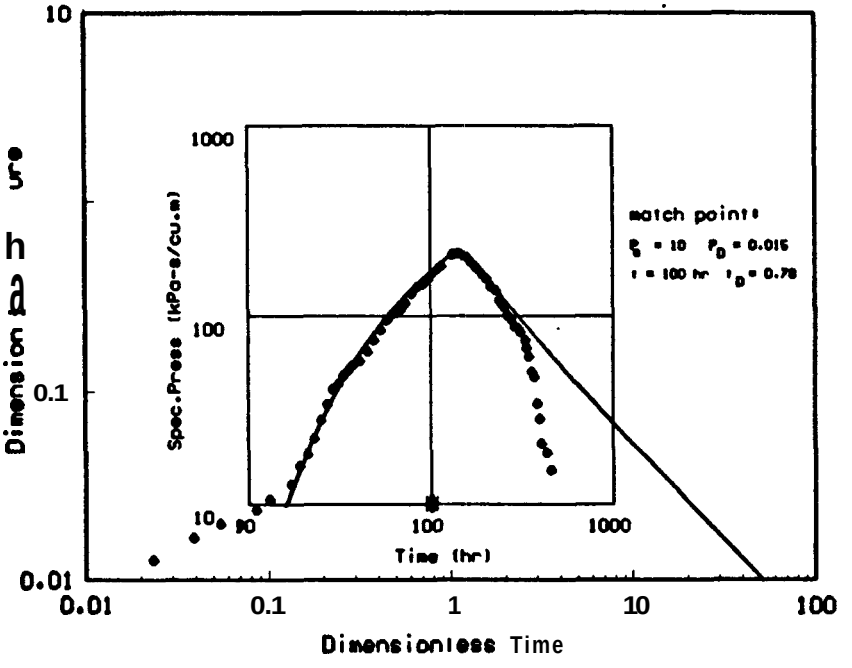

Fig. 7.35 Log-log match of data to line source solution.

$$p_s = 10\ kPa\text{-}s/m^3 \quad p_D = 0.015$$

$$t = 100\ h \qquad \frac{t_D}{r_D^2} = 0.78$$

The permeability ratio between the two matches is three, while the storativity ratio is only 1.25

which demonstrates the greater sensitivity of permeability to the matching process. The storativity derived from this match point which is relatively insensitive to changes in the matched pressure level is presented in Table 8.1 for the match to the curve for $r_2/r_1 = 1.5$.

Both the drawdown and buildup data show oscillations about the theoretical curves which may be the result of earth tides or residual barometric fluctuations.

7.3.8.2. Semi-log Analysis

Semi-log plots for the $r_2/r_1 = 1.5$ match and the line source match are shown in Figures 7.36 and

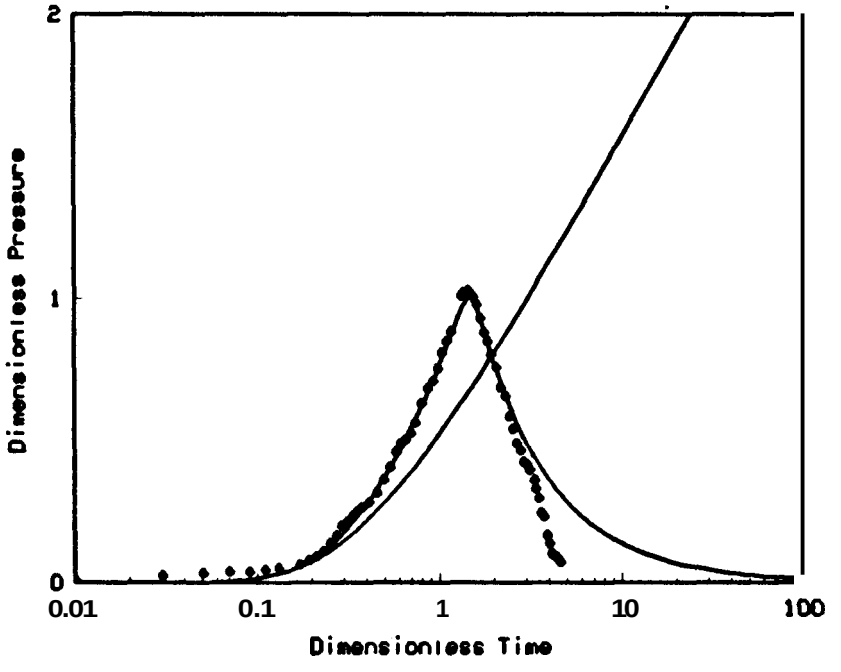

Fig. 7.36 Semi-log match of data to semi-infinite type *curves* for $r_2/r_1 = 1.5$.

7.37 respectively. Both plots show the same quality of fit with the characteristics described for the log-log plots except that the early time data deviation is masked by the semi-log scale.

Drawdown and buildup data again show oscillations about the ,theoretical curves which may be the result of earth tides or residual barometric fluctuations.

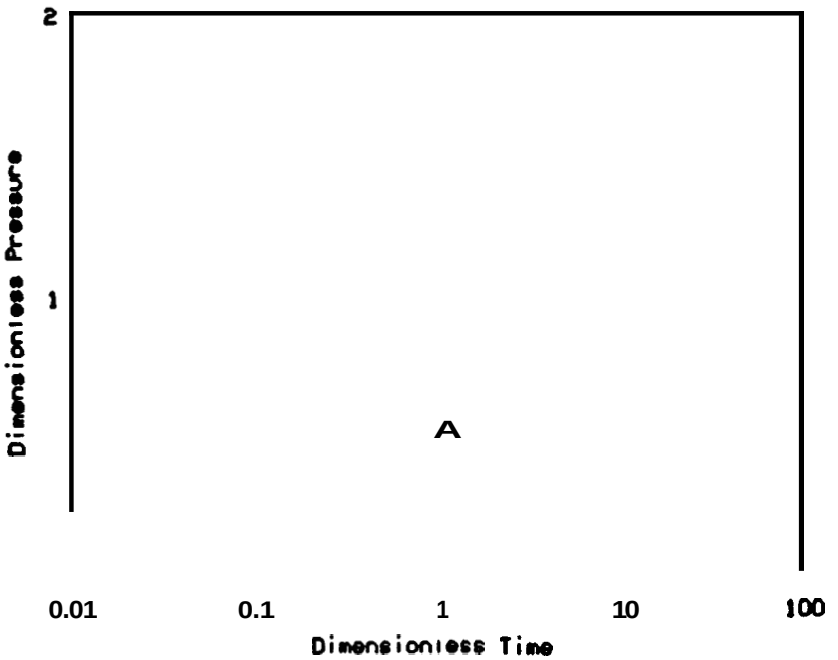

Fig. 7.37 Semi-log match of data to line source solution.

7.3.3. Horner Analysis

The *Horner* plot for $r_2/r_1 = 1.5$ is presented in Figure 7.38 and confirms an excellent match of the early time buildup data with the theoretical solution even though a unique match is not possible. Oscillations in the data are still evident and the effect of pressure support is seen for Horner times ≤ 2. An alternative graph for the line source match (Figure 7.39) shows similar characteristics.

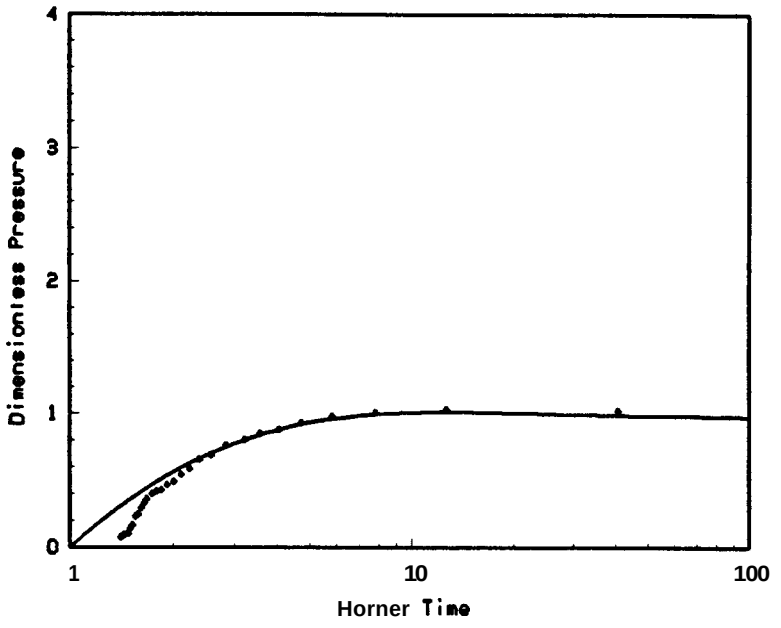

Fig. 7.38 Match of buildup data on a *Horner* graph for $r_2/r_1 = 1.5$.

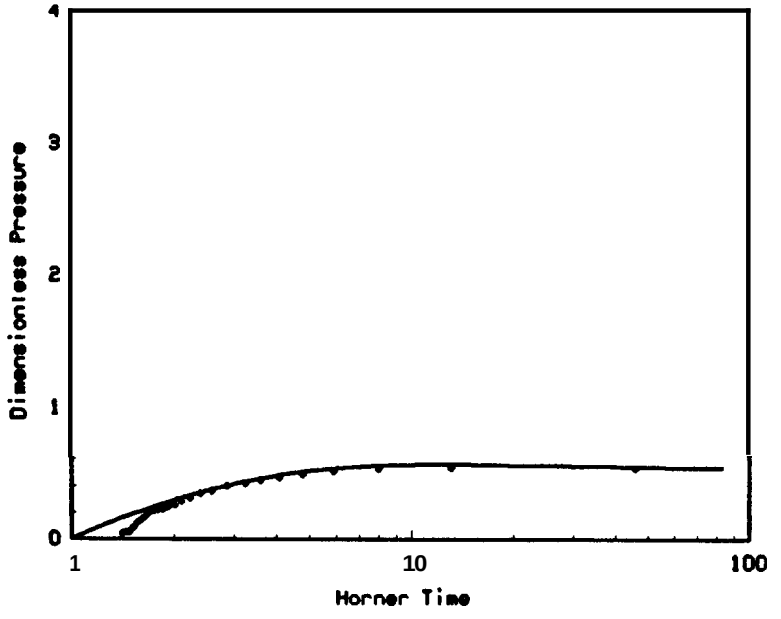

Fig. 7.39 Match of buildup data on a *Horner* graph to line source solution.

7.3.9. TEST B10: BR23 RESPONSE TO BR13 SHUT-IN

Specific pressure verses time data for this test are presented in Table B9 and plotted in cartesian form in Figure 7.40. Test specifications are shown in Table 7.13.

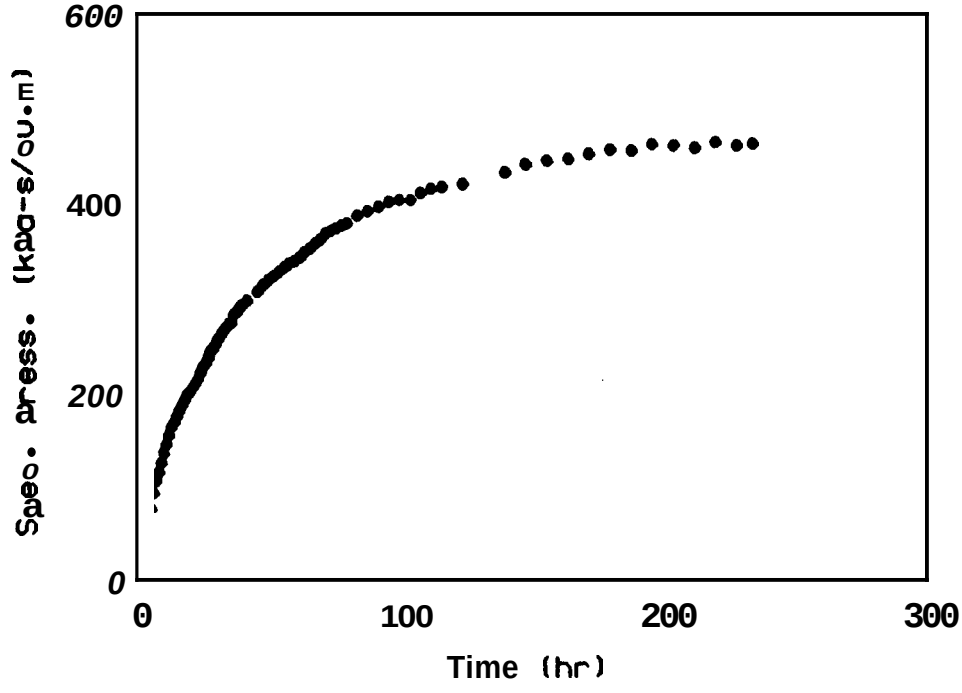

Fig. 7.40 Cartesian graph of the interference data.

This test was originally part of Test B2. Large fluctuations in flow rate at the end of the drawdown period meant that data obtained was not suitable for analysis. After five days of fluctuations, pressures in well BR23 fortuitously reached steady state. The well was then shut and the buildup performance monitored.

For a minimum pressure significance level of 3 *kPa* (refer §3.4) and an average early time flow rate of 52 *l/s* the minimum specific pressure significance level is 58 $kPa\text{-}s/m^3$.

7.3.9.1. Log-log Analysis

A log-log pressure-time graph of the data is drawn and matched on the *Theis* line source solution graph (Figure 7.41). The data give a good match to the line source for all times except for the first data point which is below the minimum specific pressure significance level of *58*

TABLE 7.13

TEST B10: BR23 RESPONSE TO BR13 DISCHARGE

TEST SPECIFICATIONS

	Observation Well	Source Well
Well No.	BR23	BR13
Coordinates *(Broadlands Grid)*	S 78923.12 *ft* W 45215.27 *ft*	S 79705.90 *ft* W 45687.30 *ft*
R.L. (C.H.F.) *(Moturiki Datum)*	291.8 *m*	293.5 *m*
Permeable Depth	1015 - 1055	915 ± 30 *m*
Drilled Depth	1097 *m*	1081 *m*
Open Hole Diam.	194 *mm*	197 *mm*
Interwell Distance	279 *m*	
Discharge Rate	51.9 *l/s* (volumetric average rate during drawdown)	
Discharge Temp.	-	
Discharge Enthalpy	1050 *kJ/kg*	
Recording Meter	Water Level Chart Recorder	
Buildup Start Time	1600 April 21 1980	
Total Test Time	234 *h*	

kPa–s/m^3 and chose after 100 hours of the test where there is a slight indication of a no-flow boundary.

The match points chosen were:

$$p_s = 10\ kPa\text{–}s/m^3 \quad p_D = 0.04$$

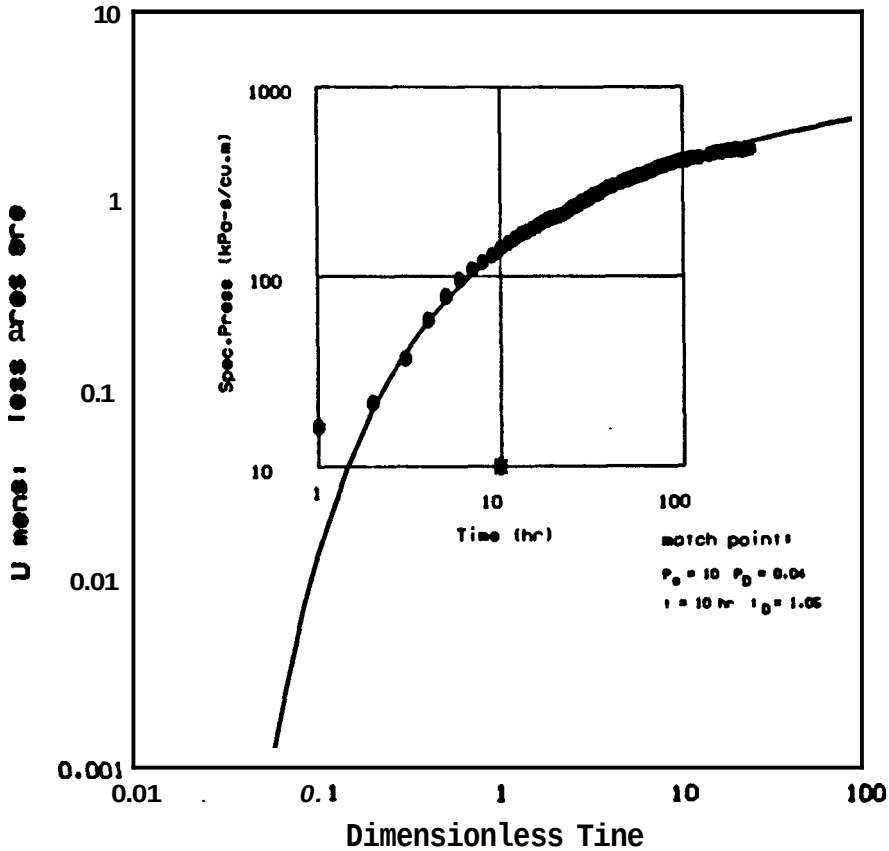

Fig. 7.41 Log-log match of data to *Theis* type curve.

$$t = 10\ h \qquad \frac{t_D}{r_D^2} = 1.05$$

Values of permeability and storativity derived from the match point are presented in Table 8.1.

The data appear to show oscillations about the theoretical curves which may be the result of earth tides or residual barometric fluctuations.

7.3.9.2. Semi-log Analysis

A semi-log graph of the data on the *Theis* line source solution is shown in Figure 7.42. The scale of the semi-log graph gives better definition to the no-flow boundary effect which is shown by the data dropping below the line source solution at $t_D/r_D^2 = 18$ or $t = 170$ hours.

The data show oscillations about the line source curve which may be the result of earth tides or residual barometric fluctuations.

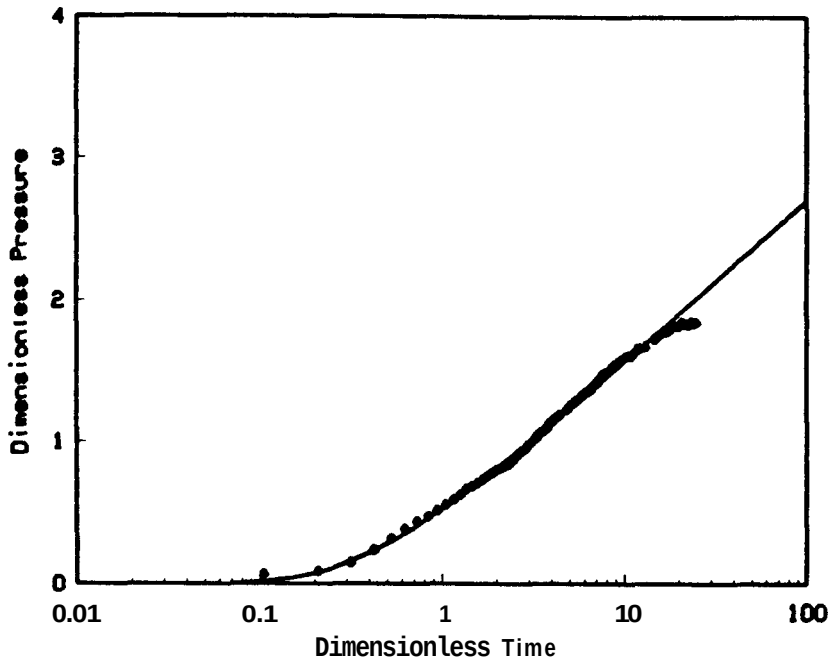

Fig. 7.42 Semi-log match of data to the line source solution.

Better definition can be obtained using the type of *Sugeev* et *al*. [1985]. Figurer 7.43 presents a semi-log match of the dimensionless pressure data to the type Curve presented by *Sugeev* et *al*. [1985]. The pressure match point is:

$$p_D = 0.0 \qquad p_D^* = 2.40$$

Substituting the semi-log pressure match point into Equation 7.5 and solving for the ratio r_2/r_1 yields:

$$r_2/r_1 = \exp\left[(p_D - p_D^*) + ln(100-1) \right] \tag{7.24}$$

$$r_2/r_1 = \exp(0.0 - 2.40 + ln99) = 9.0 \tag{7.17}$$

From the semi-log graph it can be noted that in order to get a unique match, only one semi-log straight line and the transition period are required. The data show that during the drawdown period the first semi-log straight line and the transition developed, but the second semi-log straight line did not.

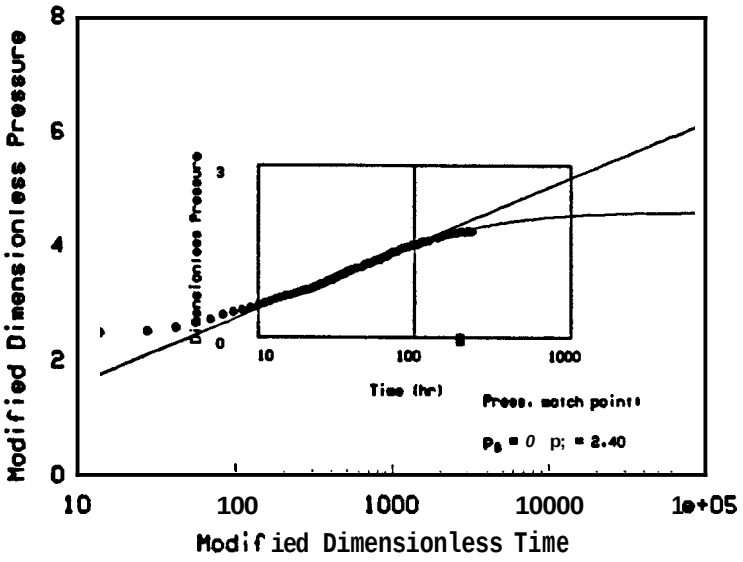

Fig. 7.43 Semi-log match of drawdown data to *Sugeev er al. type curves.*

The corresponding inference ellipse to which the postulated linear boundary is tangent is presented in Figure 7.44.

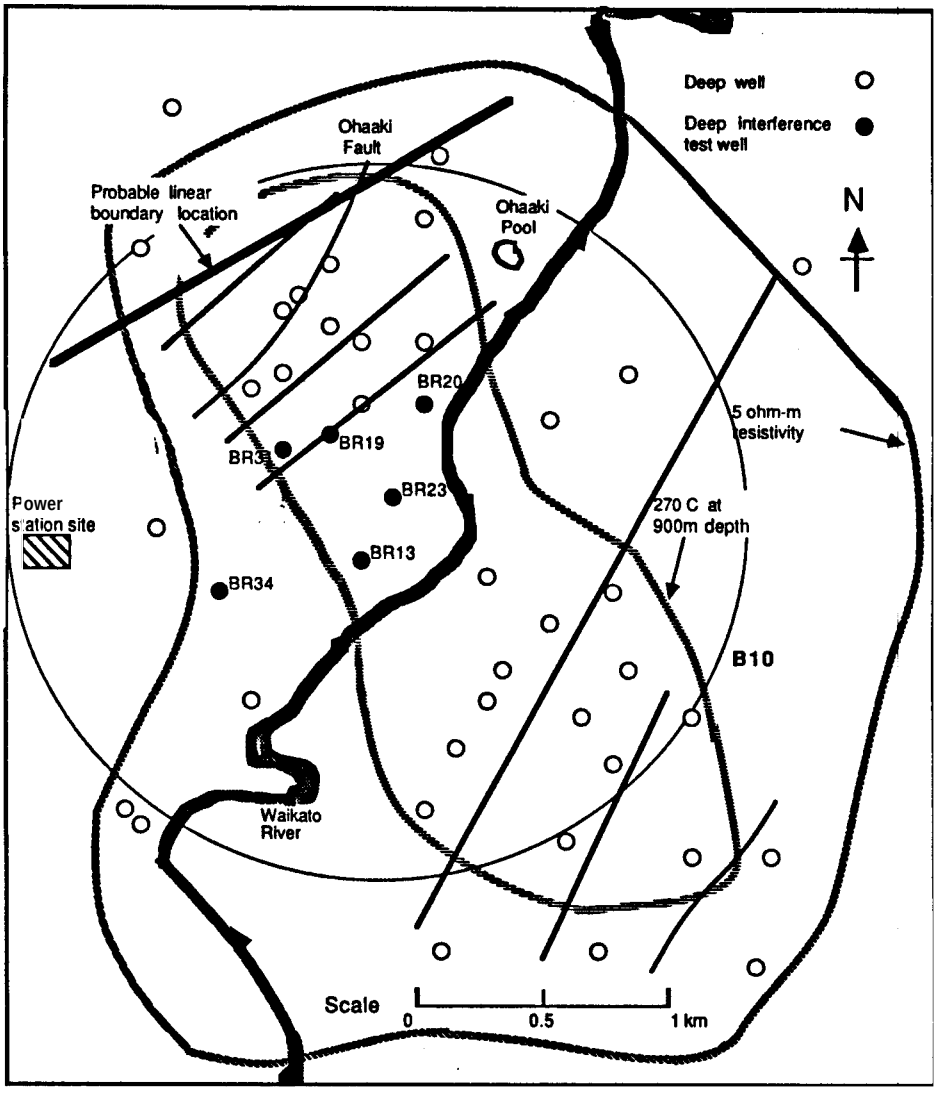

Fig. 7.44 Inference ellipse location.

7.4. DATA FROM QUARTZ CRYSTAL GAUGES

7.4.1. TEST C1: BR13 RESPONSE TO BR20 DISCHARGE

The data for this test are presented in Table B10 and plotted in Cartesian form in Figure 7.45. Test specifications are shown in Table 7.14.

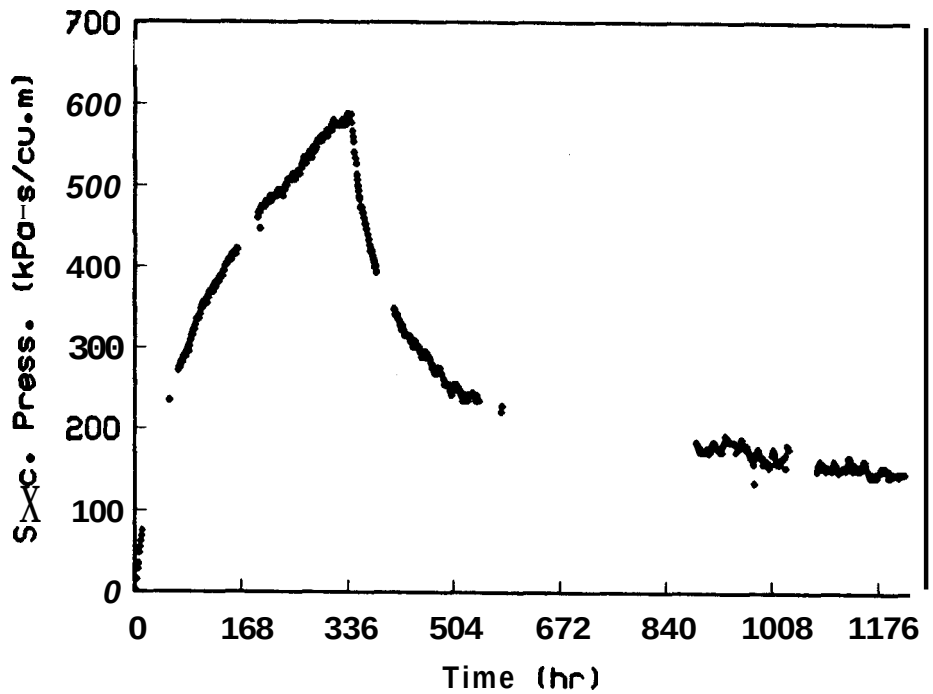

Fig. 7.45 Cartesian graph of the interference data.

Equipment malfunction meant that no data was recorded for the periods 12 to 54 hours, 55 to 69 hours, 163 to 194 hours, 380 to 407 hours, 545 to 578 hours and 580 to 889 hours.

For a minimum pressure significance level of 3 *kPa* (refer §3.4) and an average early time flow rate of 84 *l/s* the minimum specific pressure significance level is 36 $kPa\text{-}s/m^3$.

7.4.1.1. Log-log Analysis

A log-log pressure-time graph of the data is drawn and matched on the Eipper dimensionless pressure-time graph (Figure 7.46). On this graph the lower curve is the *Theis* line source solution while the upper curve is for a no-flow boundary with $r_2/r_1 = 4.0$. Despite the missing data a half log cycle is available for a match with the *Theis* line source solution with the data after

TABLE 7.14

TEST C1: BR13 RESPONSE TO BR20 DISCHARGE

TEST SPECIFICATIONS

	Observation Well	Source Well
Well No.	BR13	BR20
Coordinates (Broadlands Grid)	S 79705.90 *ft* W 45687.30 *ft*	S 77671.30 *ft* W 44714.90 *ft*
R.L. (C.H.F.) (*Moturiki* Datum)	293.5 *m*	291.7 *m*
Permeable Depth	915 ± 30 *m*	815 *m*, 945 *m*, 1045 *m*
Drilled Depth	1081 *m*	
Open Hole Diam.	197 *mm*	
Interwell Distance	687 m	
Discharge Rate	84.0 *l/s*	
Discharge Temp.	260°C	
Discharge Enthalpy	-	
Recording Meter	quartz crystal gauge	
Flow Start Time	1430 May 1 1984	
Drawdown Period	339 *h*	
Total Test Time	1217 *h*	

69 hours showing a good fit to the upper no-flow boundary curve.

The buildup data match to the no-flow boundary curve for $r_2/r_1 = 4.0$ up to 540 hours at which point the data deviate above this curve. If real, this trend would indicate the presence of a second no-flow boundary in the system. No other test was run for a similar length of time so there is no data with which to confirm this trend. The pressure and time match points for r_2/r_1

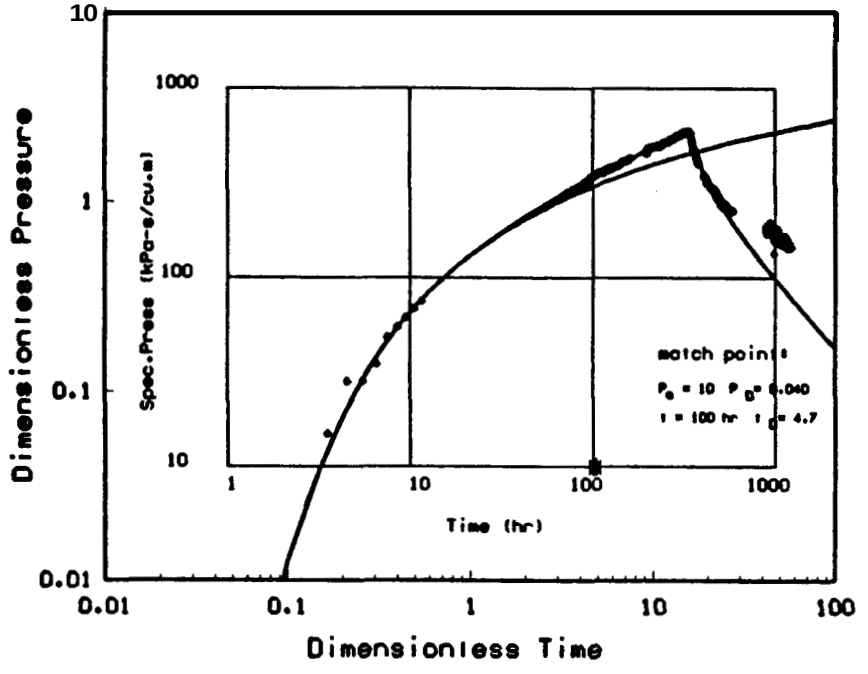

Fig. 7.46 Log-log match of data to *Eipper* type curves.

are:

$$p_s = 10\ kPa\text{-}s/m^3 \quad p_D = 0.040$$

$$t = 100\ h \qquad \frac{t_D}{r_D^2} = 4.7$$

Values of permeability and storativity derived from the match point are presented in Table **8.1.**

The drawdown data show minor oscillations about the theoretical curves which may be the result of earth tides or residual barometric fluctuations.

7.4.1.2. **Semi-log** Analysis

A semi-log graph of the data is shown in Figure **7.47.** The lower curve is the Theis line source solution while the upper curve is the solution for a linear no-flow boundary at $r_2/r_1 = 4.0$. This graph confirms the good fit of the the late time drawdown data and the initial buildup data to the upper no-flow boundary curve.

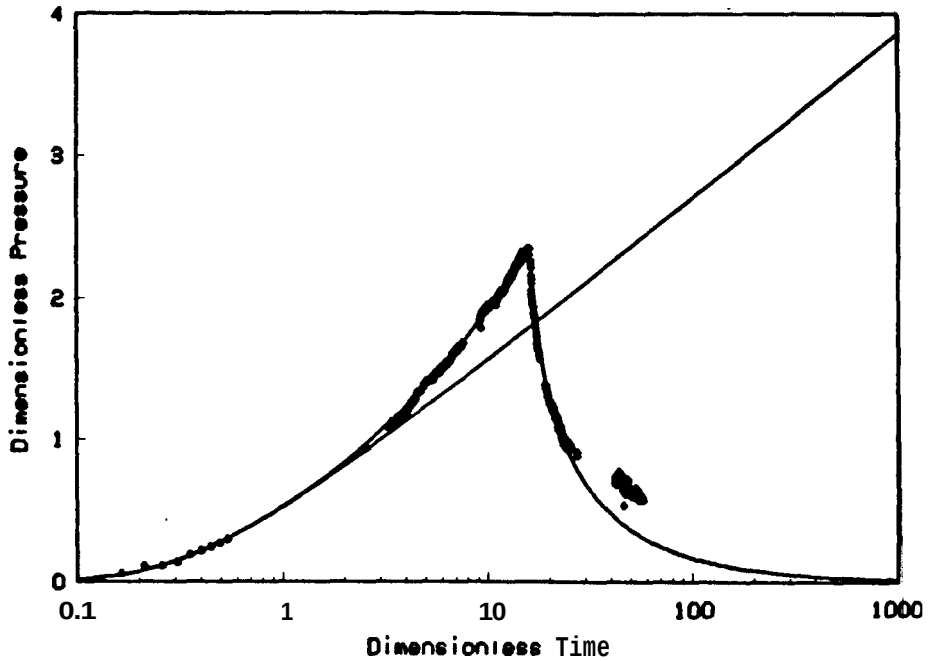

Fig. 7.47 Semi-log match of data to semi-infinite type curves.

Drawdown data again show oscillations about the theoretical curves which may be the result of earth tides or residual barometric fluctuations.

7.4.13. Horner Analysis

The Horner plot for $r_2/r_1 = 4.0$ (Figure 7.48) shows a good match of the early time buildup data with the theoretical curve. The periodic nature of fluctuations about the theoretical curve indicate that this is more likely due to earth tides rather than barometric pressure variations. Deviation of the data above the linear boundary curve for $r_2/r_1 = 4.0$ at Horner times less than three ($t \geq 540$hours) show possible contact with a further no-flow boundary. Since no other test showed a similar trend further analysis of the second no-flow boundary has not been undertaken.

The Horner plot confirms the match obtained form the semi-log and log-log graphs. The distance between the source well and observation well, r_1, is 687 meters. Hence the distance between the observation well and the image well, r_2, is:

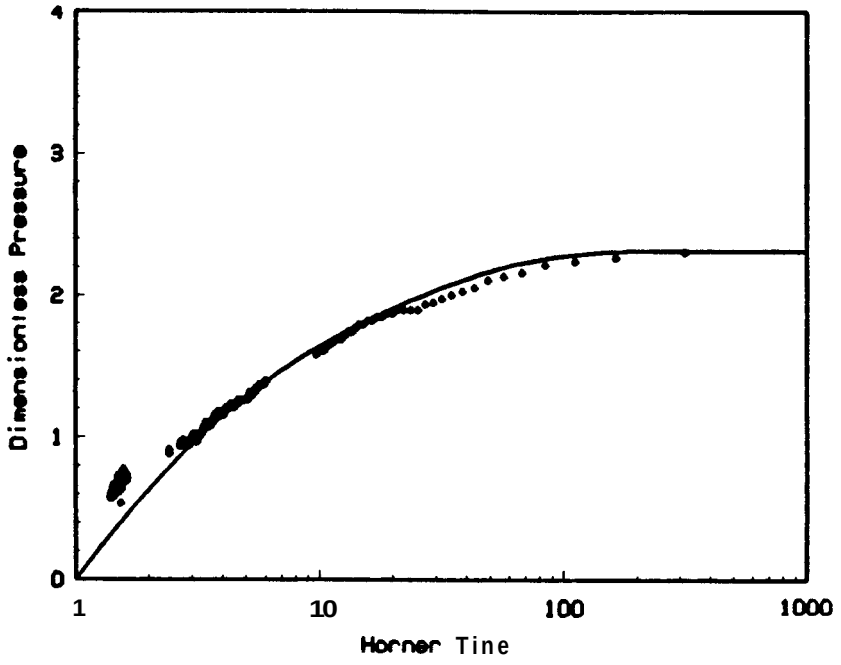

Fig. 7.48 Match of buildup data **on a *Horner* graph.**

$$r_2 = (687)(4.0) = 2748 \text{ meters}$$

The corresponding inference ellipse to which the first postulated linear no-flow boundary is tangent is presented in Figure 7.49.

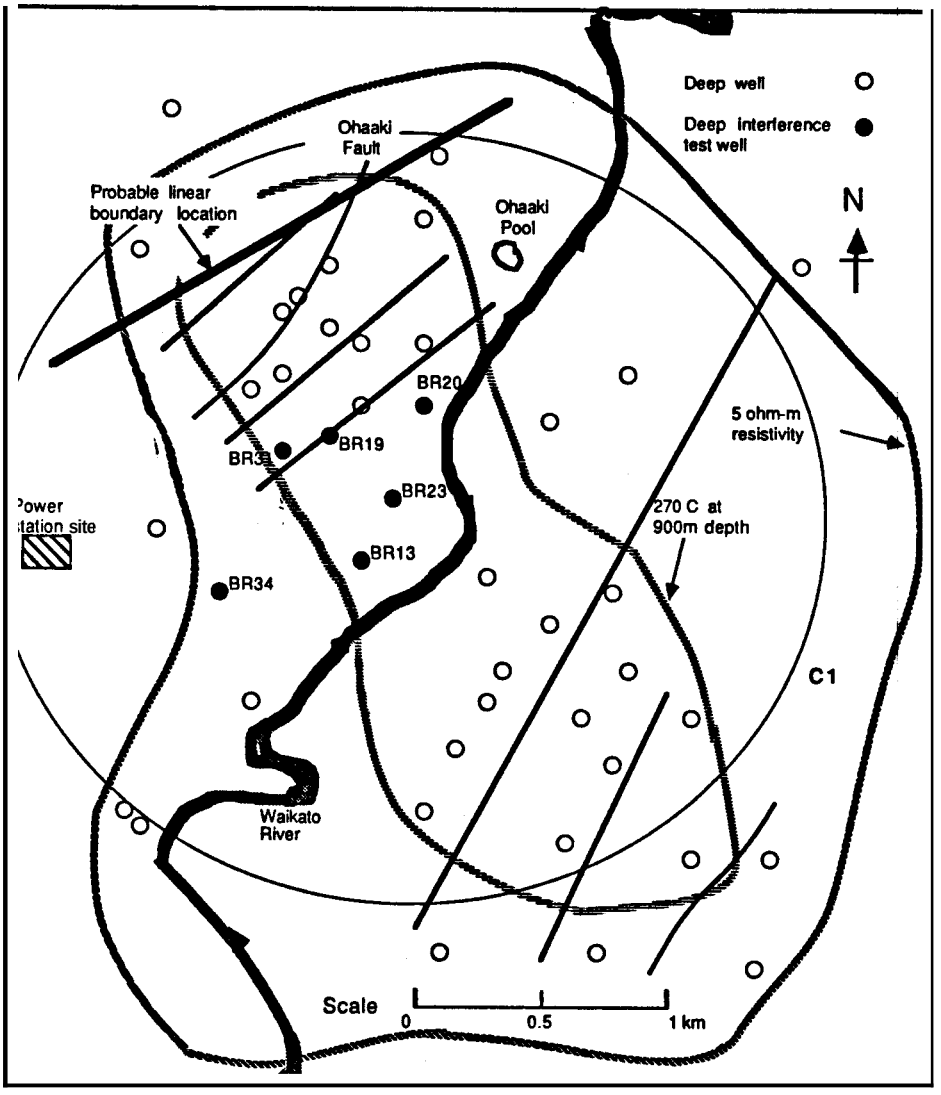

Fig. 7.49 Inference ellipse location.

7.4.2. TEST C2: BR23 RESPONSE TO BR20 DISCHARGE

The data for this test are presented in Table B11 and plotted in Cartesian form in Figure 7.50. Test specifications are shown in Table 7.15.

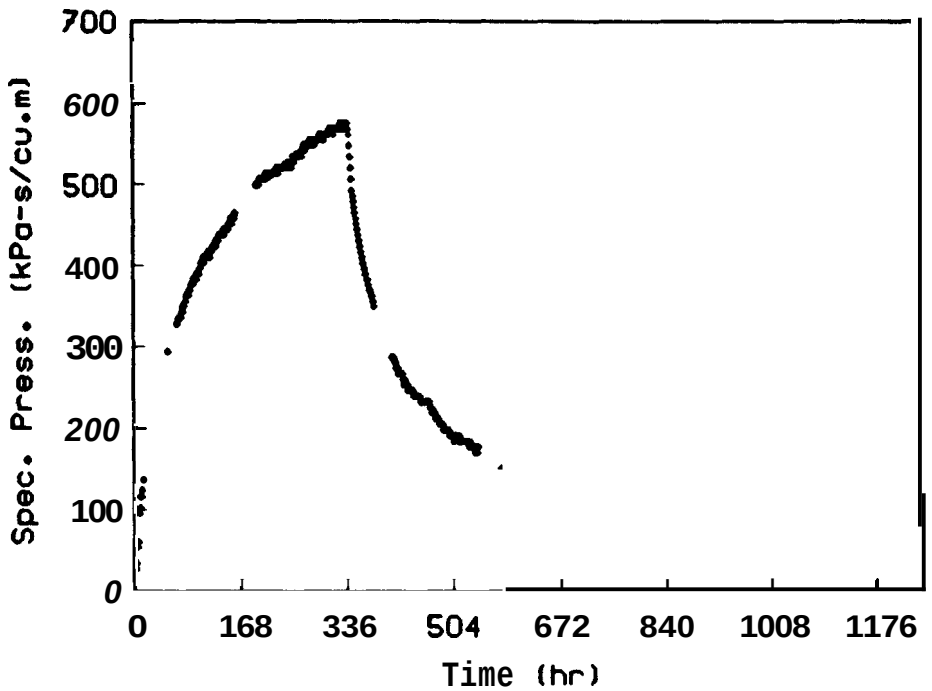

Fig. 7.50 Cartesian graph of the interference data.

Equipment malfunction meant that no data was recorded for the periods 12 to 54 hours, 55 to 69 hours, 163 to 194 hours, 380 to 407 hours and 545 to 578 hours.

For a minimum pressure significance level of 3 *kPa* (refer §3.4) and an average early time flow rate of 84 *l/s* the minimum specific pressure significance level is 36 $kPa\text{-}s/m^3$.

7.4.2.1. Log-log Analysis

A log-log pressure-time graph of the data is drawn and matched on the Eipper dimensionless pressure-time graph (Figure 7.51). On this graph the lower curve is the Theis line source solution while the upper curve is for a no-flow boundary with $r_2/r_1 = 4.0$. Despite the missing data a half log cycle is available for a match with the *Theis* line source solution. With the data after 69 hours showing an excellent fit to the upper no-flow boundary curve.

TABLE 7.15

TEST C2: BR23 RESPONSE TO BR20 DISCHARGE

TEST SPECIFICATIONS

	Observation Well	Source Well
Well No.	BR23	BR20
Coordinates *(Broadlands Grid)*	S 78923.12 *ft* W 45215.27 *ft*	S 77671.30 *ft* W 44714.90 *ft*
R.L. (C.H.F.) *(Moturiki Datum)*	291.8 *m*	291.7 *m*
Permeable Depth	1015 - 1055 *m*	815 *m*, 945 *m*, 1045 *m*
Drilled Depth	1097 *m*	-
Open Hole Diam.	194 mm	-
Interwell Distance	411 *m*	
Discharge Rate	84.0 *l/s*	
Discharge Temp.	260°C	
Discharge Enthalpy	-	
Recording Meter	quartz crystal gauge	
Flow Start Time	1430 May 1 1984	
Drawdown Period	339 *h*	
Total Test Time	579 *h*	

The buildup data show a fair match with the buildup solution for a boundary located at $r_2/r_1 = 4.0$. The pressure and time match points for $r_2/r_1 = 4.0$ are:

$$p_s = 10\ kPa\text{-}s/m^3 \quad p_D = 0.060$$

$$t = 100\ h \qquad \frac{t_D}{t0} = 16.0$$

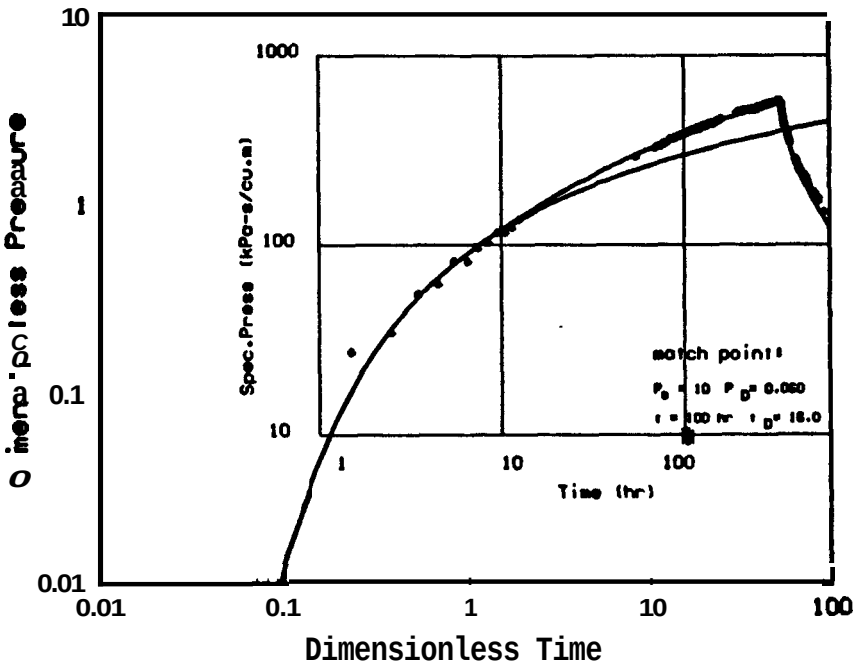

Fig. 7.51 Log-log match of data to *Eipper* type *curves.*

Values of permeability and storativity derived from the match point are presented in Table 8.1.

The drawdown data show minor oscillations about the theoretical curves which may be the result of earth tides or residual baromemc fluctuations.

7.4.2.2. Semi-log Analysis

A semi-log graph of the data is shown in Figure 7.52. The lower curve is the Theis line source solution while the upper curve is the solution for a linear no-flow boundary at $r_2/r_1 = 4.0$. This graph confirms the good fit of the the late time drawdown data and the initial buildup data to the upper no-flow boundary curve.

Drawdown data again show oscillations about the theoretical curves which may be the result of earth tides or residual baromemc fluctuations.

7.4.23. Horner Analysis

The *Homer* plot for $r_2/r_1 = 4.0$ (Figure 7.53) shows a fair match of the early time buildup data with the theoretical curve.

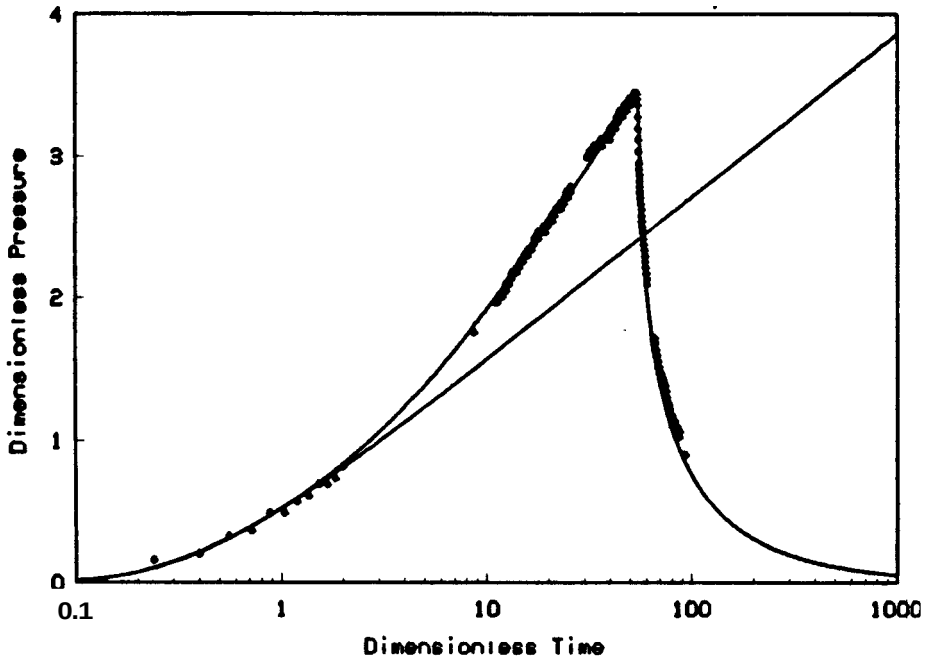

Fig. 7.52 Semi-log match of data to semi-infinite type curves.

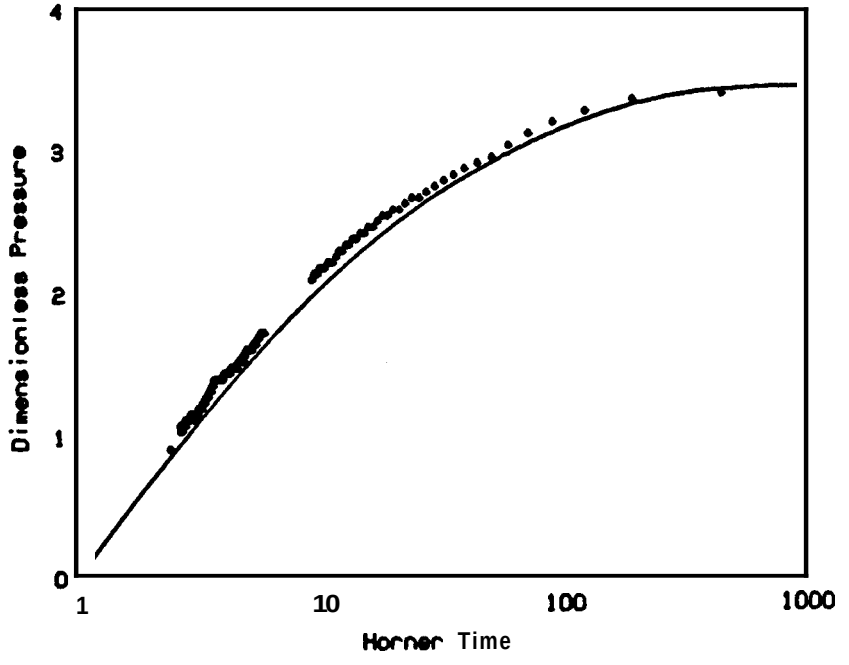

Fig. 7.53 Match of buildup data on a *Horner* graph.

The value of using the ***Homer*** analysis is demonstrated in identifying the slight mismatch. The mismatch of the buildup data on the log-log and semi-log plots was barely discernible. The Homer plot expands the time scale on the initial buildup period making any mismatch of data much more obvious.

The ***Homer*** plot confirms the match obtained form the semi-log and log-log graphs. The distance between the source well and observation well, r_1, is 411 meters. Hence the distance between the observation well and the image well, r_2, is:

$$r_2 = (411)(4.0) = 1644 \text{ meters}$$

The corresponding inference ellipse to which the postulated linear no-flow boundary is tangent is presented in Figure 7.54.

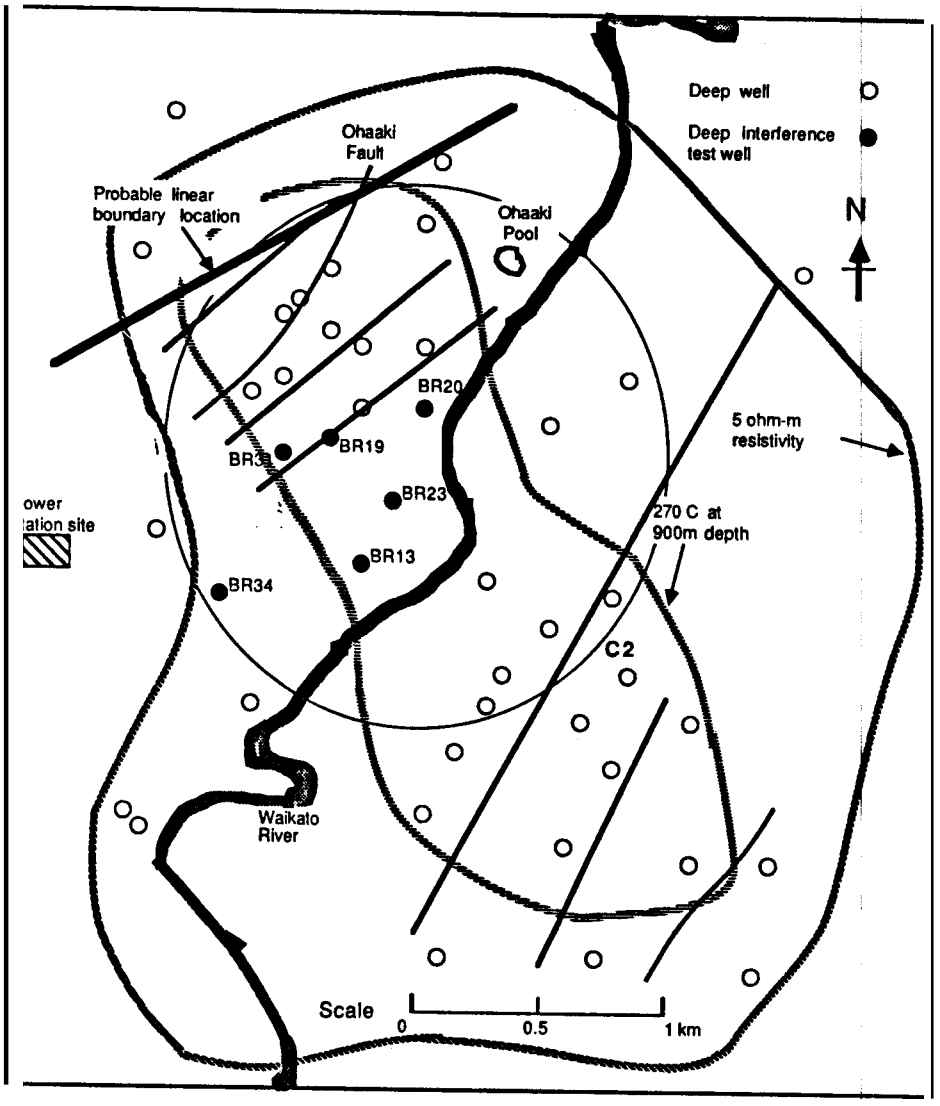

Fig. 7.54 Inference ellipse location.

7.4.3. TEST C3: BR34 RESPONSE TO BR20 DISCHARGE

The data for this test are presented in Table B12 and plotted in cartesian form in Figure 7.55. Test specifications are shown in Table 7.16.

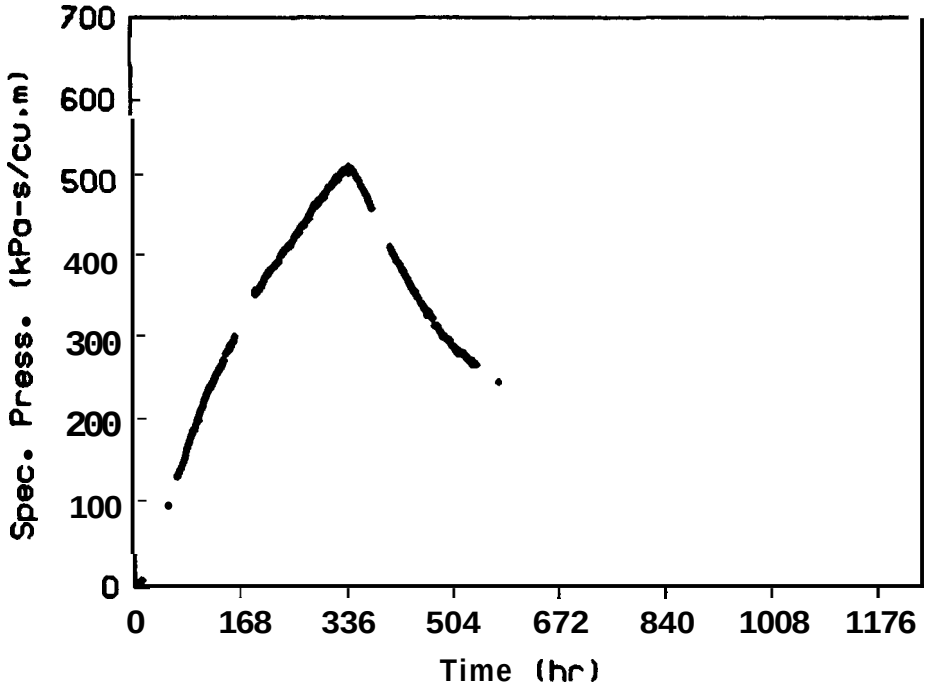

Fig. 7.55 Cartesian graph of the interference data.

Equipment malfunction meant that no data was recorded for the periods 12 to 54 hours, 55 to 69 hours, 163 to 194 hours, 380 to 407 hours and 545 to 578 hours.

For a minimum pressure significance level of 3 *kPa* (refer §3.4) and an average early time flow rate of 84 *Us* the minimum specific pressure significance level is 36 $kPa\text{-}s/m^3$.

7.4.3.1. Log-log Analysis

Log-log pressure-time plots of the data are drawn and matched on the *Eipper* dimensionless pressure-time curves (Figures 7.56, 7.57). Both plots show an excellent match to the data above the critical pressure level of 36 $kPa\text{-}s/m^3$ thereby demonstrating that from the log-log plots alone a unique match is not possible. On Figure 7.56, the lower curve represents the *Theis* line source solution while the upper curve is for a no-flow boundary located at r_2/r_1 =

TABLE 7.16

TEST C3: BR34 RESPONSE TO BR20 DISCHARGE

TEST SPECIFICATIONS

	Observation Well	Source Well
Well No.	BR34	BR20
Coordinates (*Broadlands* Grid)	S 80200.84 *ft* W 47490.01 *ft*	S 77611.308 W 44714.90 *ft*
R.L. (C.H.F.) (*Moturiki Datum*)	308.2 *m*	291.7 *m*
Permeable Depth		815 *m*, 945 *m*, 1045 *m*
Drilled Depth	2587 *m*	
Open Hole Diam.	216 *mm*	
Interwell Distance	1145 m	
Discharge Rate	84.0 *l/s*	
Discharge Temp.	260°C	
Discharge Enthalpy	-	
Recording Meter	quartz crystal gauge	
Flow Start Time	1430 May 1 1984	
Drawdown Period	339 *h*	
Total Test Time	579 *h*	

1.5.

The pressure and time match points are:

$$p_s = 10\ kPa\text{-}s/m^3 \quad p_D = 0.030$$

$$t = 100\ h \qquad \frac{t_D}{r_D^2} = 0.78$$

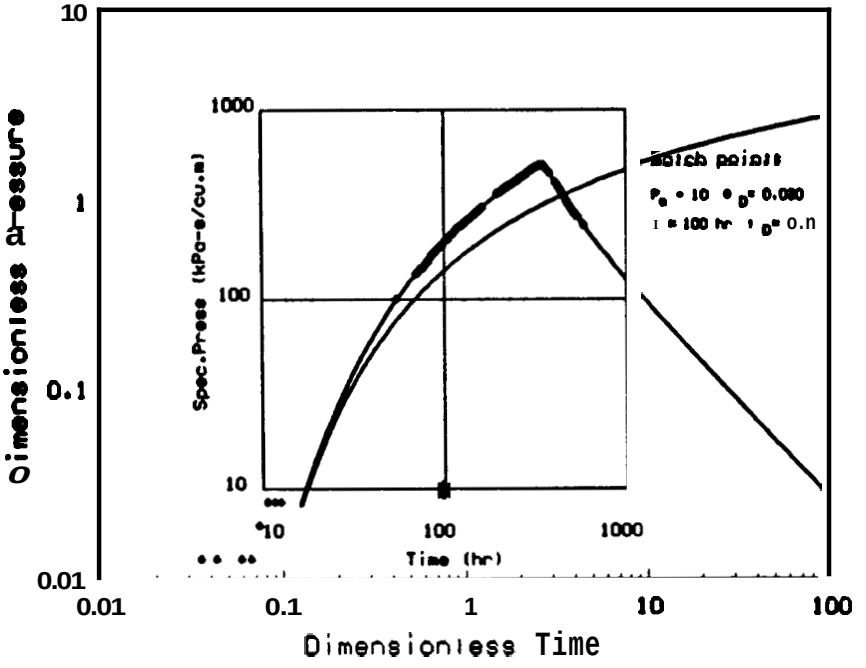

Fig. 7.56 Log-log **match of data to** ***Eipper*** type **curves for** r_2/r_1 **=1.5.**

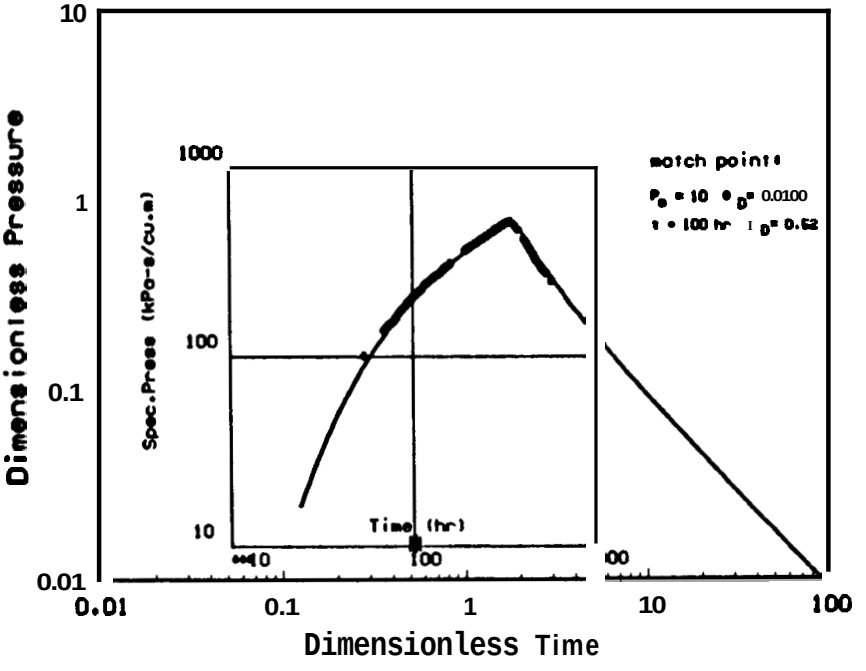

Fig. 7.57 Log-log match of data to line source solution.

Figure 7.57 represents the match of the data to the line source solution. The match points for this graph were:

$$p_s = 10\ kPa\text{-}s/m^3 \quad p_D = 0.015$$

$$t = 100\ h \qquad \frac{t_D}{r_D^2} = 0.52$$

This interference test poses singularly difficult problems which make a unique match to the data impossible. The specific issue of non-uniqueness is covered in detail in §5.

The observation well BR34 is in a non-productive part of the field and could therefore be expected to be close to a hydrological boundary. The distance between the source well, BR20, and BR34 is 1145 meters which is nearly twice as large as any of the other tests. A combination of both these two factors means that a boundary if present could have an r_2/r_1 ratio of close to unity. If this is the case then the *Theis* line source behavior may not be detectable during the drawdown period as it will occur at pressure levels well below the critical level of 36 $kPa\text{-}s/m^3$. Test B9 (0 7.3.8) illustrated this point. Inspection of Figures 7.56, 7.57 confirms:

(i) That there can be no match to the line source since the data that do exist in the early time region ($t_D/r_D^2 \leq 0.5$) are below the critical significance level of 36 $kPa\text{-}s/m^3$.

(ii) That there is less than one-third of a log cycle of buildup data which is insufficient to obtain a unique match of the data to a buildup curve for a given boundary location.

(iii) The drawdown data above the critical specific pressure level lie entirely within the transition flow region.

The net result of these observations is that a unique match cannot be made from the log-log graph. The value of storativity which is relatively insensitive to the matched pressure level is presented in Table 8.1.

7.4.3.2. Semi-log Analysis

Semi-log plots of the data are shown in Figures 7.58, 7.59. On Figure 7.58 the lower curve

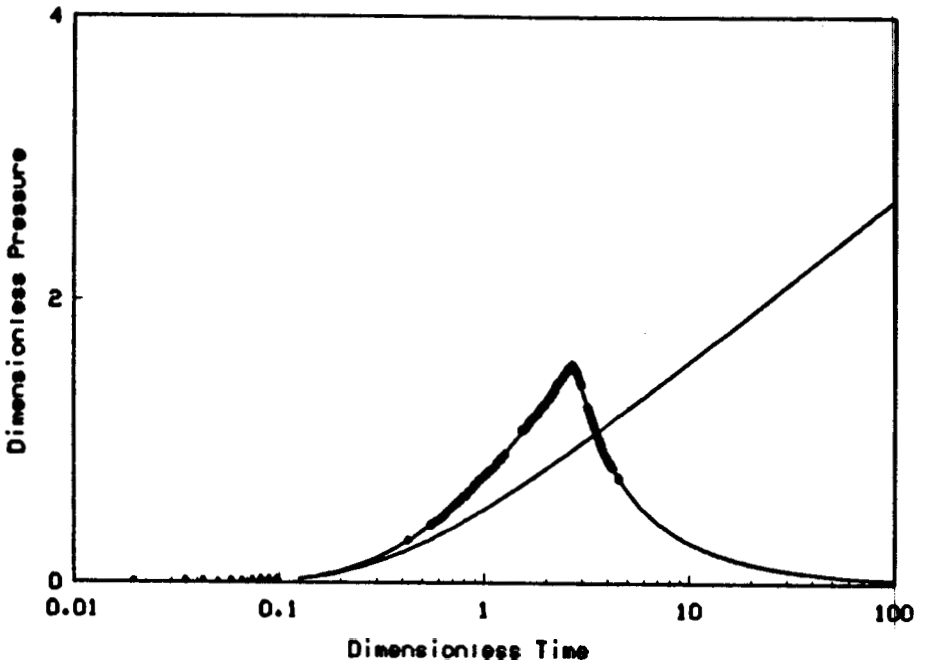

Fig. 7.58 Semi-log match of data to semi-infinite type *curves* for r_2/r_1 =1.5.

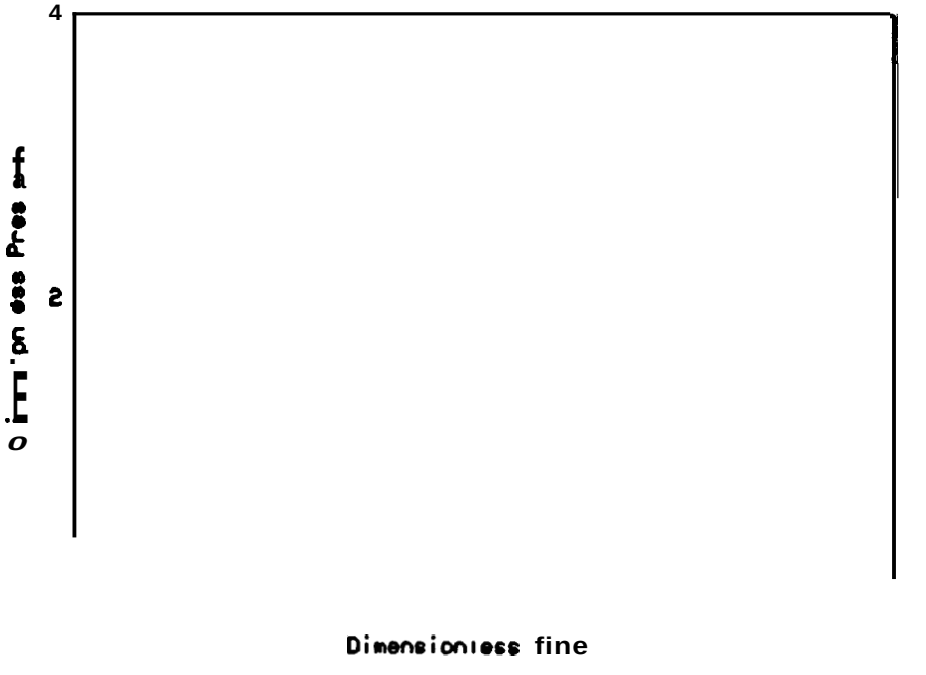

Fig. 7.59 Semi-log match of data to line source solution.

represents the Theis line source solution while the upper curve is the solution for a linear no-flow boundary at $r_2/r_1 = 1.5$. On Figure 7.59 the data is matched to the line source solution alone. The excellent fits of data at all times on both plots adds no additional definition to the boundary location.

7.4.3.3. Horner Analysis

Horner plots for $r_2/r_1 = 1.5$ and for the Theis line source solution are presented in Figures 7.60 and 7.61 respectively.

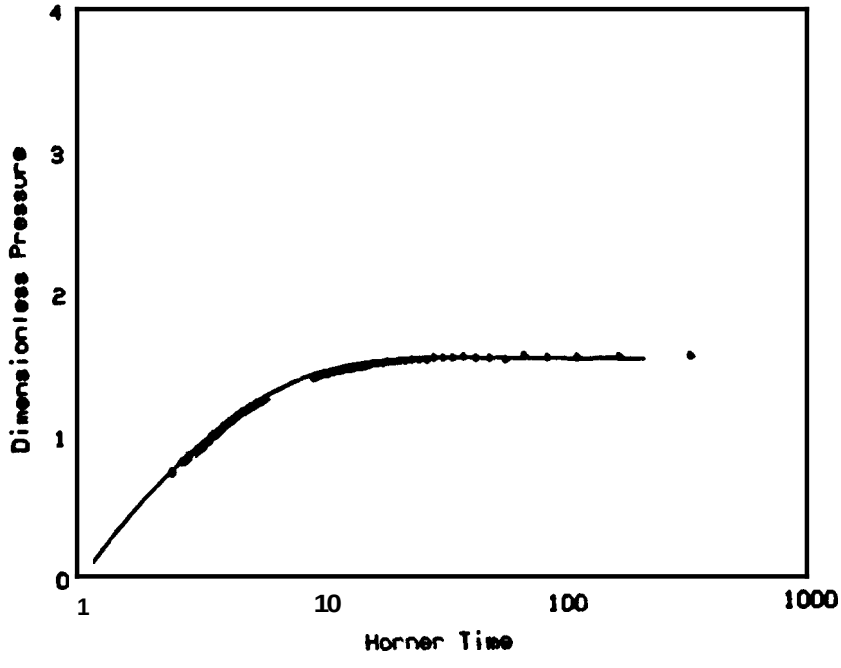

Fig. 7.60 Match of buildup data on a Horner graph for $r_2/r_1 = 1.5$.

The Horner plot expands the time scale on the initial buildup period making any mismatch of data much more obvious. Unfortunately the missing data along with the difficulty of obtaining a unique match for the low r_2/r_1 ratio mean that the location of the inference ellipse cannot be determined.

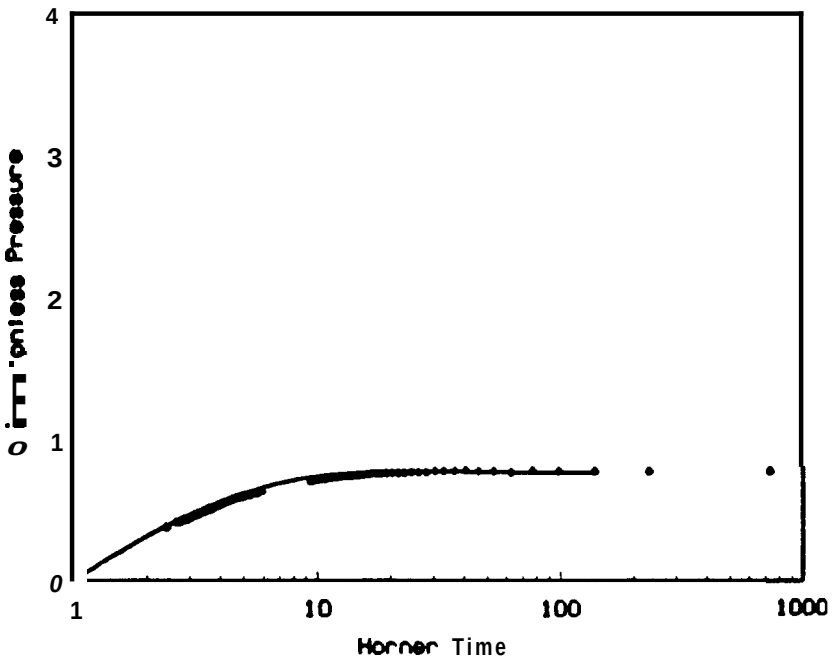

Fig. 7.61 Match of buildup data on a *Horner* graph to line source.

8. RESULTS

8.1. TRANSMISSIVITIES AND STORATIVITIES

Transmissivities and storativities are calculated using Equations 2.13 and 2.14. Results are shown in Table 8.1.

TABLE 8.1

TRANSMISSIVITIES AND STORATIVITIES

EST	OBS. WELL	SOURCE WELL	INTERWELL DISTANCE (m)	r_2/r_1	kh (d–m)	$\phi c_t h$ ($m/kPa \times 10^4$)
B1	23	13	279	9.25	94	0.65
B2	23	13	279			2.50
B3	23	19	357	2.80	115	4.40
B4	23	13	279			
B6	23	20	411			
B7	34	31	564	1.80	49	15.00
B8	34	23	795			40.00
B9	34	19	727			5.20
B10	23	13	279	9.25	64	2.80
C1	13	20	687	4.00	64	1.00
C2	23	20	411	4.00	96	1.30
C3	34	20	1145			1.70

Transmissivities range from 49 d–m in Test B7 to 115 d–m in Test B3. The average is 80 d–m. Test B7 was performed between wells BR34 and BR31 which are closer to the resistivity

boundary of the field than any of the other well pairs for which transmissivities were obtained. The lower permeability recorded for this test may be a reflection of lower permeability in this part of the field. The remaining well tests show relatively uniform values of transmissivity values with the average of these being 82 *d–m* and the range being 140% to 60% of this value.

An approximate value of horizontal permeability can be calculated by assuming a reservoir thickness of 700 meters (Figure 6.3):

$$k = \frac{80\times10^{3}}{700}$$

$$k = 114\ md$$

Storativites show a much greater range than the transmissivities possibly reflecting the formation of small two phase zones during drawdown in those regions where the permeability is likely to be low. Tests B7, B8, B9, C3 for which pressures were measured at Bk34 could be expected to fall into this category. Tests B7 and B8 show significantly larger storativities than any of the other tests. Test B9 has a large storativity and Test C3 shows a near average storativity. Flow rates in these tests ranged from about 66 *l/s* to 84 *l/s*. While there could be expected to be some significance in the trend of storativities with the location of the doublet in the field it does not show conclusively in the results. Excluding the anomalously high storativities for Tests B7 and B8 the average is 2.4×10^{-4} *m/kPa* with the range varying from 158% to 30% of this value. An estimate of the compressibility of the system can be made assuming that the porosity in the reservoir is 20% and the reservoir thickness is 700 meters.

$$\phi c_t h = 2.4\times10^{-4}\ m/kPa$$

$$c_t = \frac{2.4\times10^{-4}}{0.2\times700} = 1.7\times10^{-6}\ kPa^{-1}$$

From *Bixley* [1982] (Figure 6.4) the average reservoir pressure in the productive region of the reservoir at the average depth of 800 meters is 7 *MPa*. The average enthalpy per test of discharged fluid was 1152 *kJ/kg* which corresponds to a brine temperature of 263°C. The compressibility of 263°C fluid at a pressure of 7 *MPa* is $1.7\times10^{-6}\ kPa^{-1}$. The fact that this value

is close to that calculated using the assumed reservoir properties probably indicates that there are no permanent *two* phase zones present within the sphere of influence of these tests. This sphere of influence is assumed not to include that portion of the field covered by the data which showed both pressure support and no-flow boundary trends in Tests B1, B2, B9 and C3 but does cover an area roughly approximating that contained within the *5 ohm-m* resistivity boundary of the field.

8.2. LINEAR BOUNDARY LOCATION

The location of the principal no-flow boundary is shown in Figure 8.1. The superposition of the inference ellipses for Tests B1, B3, B7, B10, (31, C2 can be interpreted to show a NE-SW trending hydrological barrier near the resistivity boundary in the northern part of the field. The NE-SW trend of faults located from geological interpretation support the locatibn of the no-flow boundary (Figure *6.5).* The location is also supported by the fact that the northern boundary of those wells defined by *Bixley* [1982] as having the "lowest" pressure gradient (Figure *6.5)* coincides closely in direction and location with the located no-flow boundary.

If Test B3 is excluded from the analysis it is possible that the no-flow boundary could be located in a N-S direction under the power station site. This location is supported by surface geology which shows a fault scarp at about the same location in this direction./However the weight of evidence points strongly *to* the first located position. Other possible locations of barriers to the south and east of the field cannot be convincingly supported by the location of the inference ellipses.

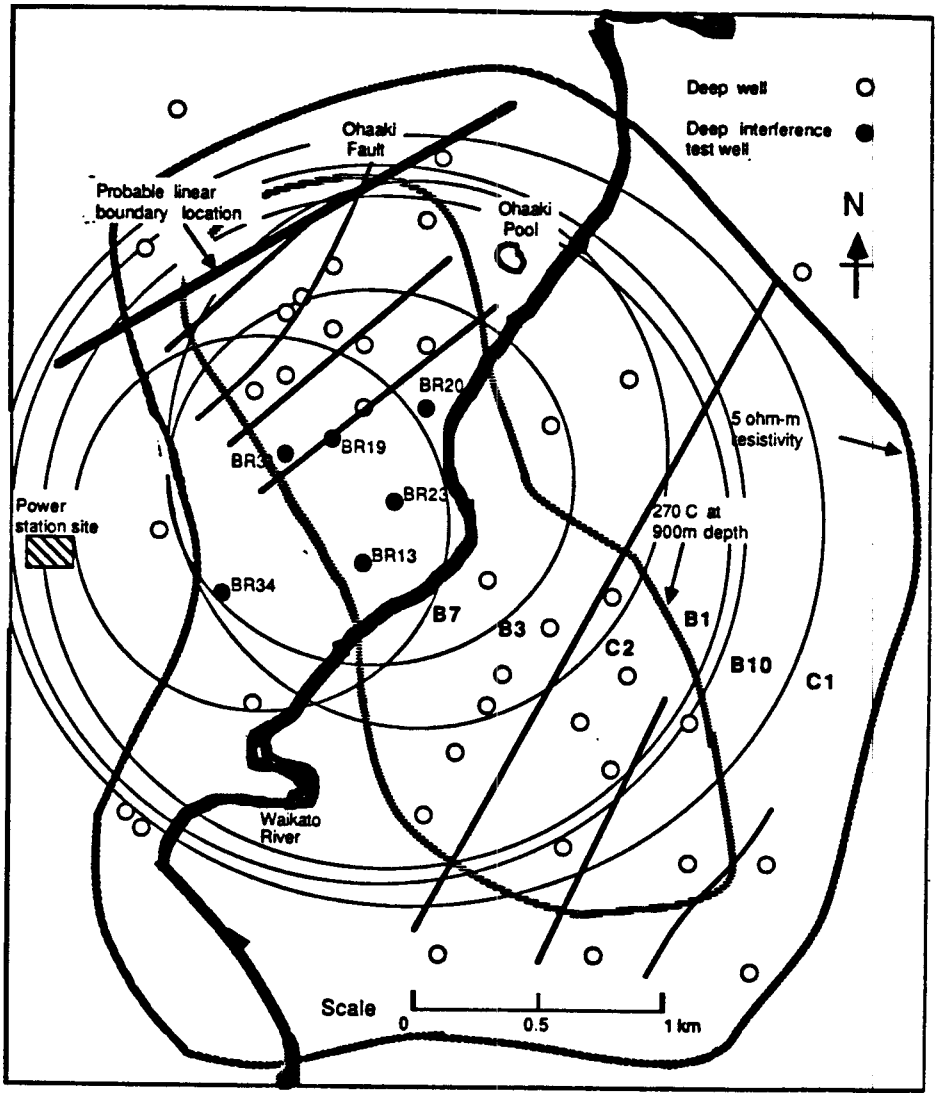

Fig. 8.1 Inference ellipse locations for Tests B1, B3, B7, B10, C1, C2.

9. DISCUSSION

9.1. GENERAL (*Sageev et al.* 1986)

The main advantage of interference testing over source well testing for detecting reservoir limits is the increased characteristic length scale. When analyzing source well pressure data, the characteristic length scale is the diameter of the wellbore, that is typically on the order of a few inches. In interference testing, the characteristic length scale is the distance between the observation well and the source well, that is on the order of tens or hundreds of meters. Also, some near wellbore effects such as wellbore skin in a source well of a constant rate test are not significant in interference testing.

The main disadvantage of interference testing is the decreased amplitudes of the pressure changes. As the observation well is located further form the source well, the space resolution increases but the magnitude of the pressure changes decreases. These are competing effects that have to be addressed during the design stages of a test. When the early time pressure changes are small, the effects of earth tides and barometric pressure may be significant, and might lead to large uncertainties in the estimation of reservoir parameters.

In the case of interference testing for linear boundary detection, there is an added problem that is purely geometrical. For distance ratios smaller than 2, it is very difficult to detect the presence of an impermeable linear boundary regardless of the actual distance between the observation well and the source well.

9.2. ANALYSIS TECHNIQUES

The use of a variety of type curves assists in obtaining the correct match. The log-log Stallman type curves (Figure 2.2) for drawdown are useful in matching the early time data to the line source solution. Once a match of the early time data has been obtained semi-log plots of the *Stallman* type curves (Figure 2.4) can be used to match the late time drawdown data. The Eipper type curves (Figure 2.3) are useful for obtaining both the early time data match and

where applicable a preliminary match of the buildup data. Once a preliminary match has been made a *Horner* plot can confirm the match of the drawdown data. For $r_2/r_1 \geq 10$ in drawdown tests the *Sageev* et *al.* type curves (Figure 2.5) can be used to determine the r_2/r_1 ratio with the Fox type curve (Figure 2.6) used to confirm this ratio on the buildup data. Determination of the inference ellipse from the r_2/r_1 ratio is performed using *Vela's* technique (Equation 2.12).

93. DATA MATCHING

Analysis of the test results showed that early time data up to the minimum significant pressure level of 3 *kPa* (§ 3.4) failed to match the theoretical curves due to the effect of earth tides, Clipping techniques often exclude data which fall when the overall trend is a rise and hence earth tide oscillations are either filtered out or occur below the resolution of the gauge. Tests B3, B6, B7, B9, B10, C3 exhibited this characteristic at early time.

Interaction with more than one hydrological heterogeneity was indicated in Tests B1, B2, B9, C1 due to the deviation of data at late dimensionless time from the initial matched curve. Tests B1 and B9 showed pressure support effects while tests B2 and C1 indicated contact with second no-flow boundaries. The lack of consistency in these late time trends precluded further analysis. All the trends with the exception of Test B2 appear to be credible. Test B2 is less credible because the appearance of the two no-flow boundaries was not confirmed in Test B10 which was performed immediately following Test B2. It is possible that the pressure support seen in Tests B1 and B9 was due to a two phase zone which later collapsed add therefore did not appear in Test C1.

The interference response of Test B4 was affected by gravity segregation, thermal, moving front and deposition effects associated with the injection of colder separated brine into the reservoir. It may be possible to analyze all these effects with the aid of a thermal simulator but this has not been attempted in this study.

Non-uniqueness problems in Tests B6, B8, B9, C3 meant that values of permeabilities were not obtained for these tests but values of storativity which are less affected by the non-

uniqueness problems were retained in Tests B8, B9, C3. Test B6 was too shdrt for a match. Tests B6 , B9 and C3 were expected to show no-flow boundaries but the boundaries if present occurred at r_2/r_1 ratio's of less than about two making detection improbable (§ 5.2).

9.4. RESERVOIR PARAMETERS

The principal results obtained were that the average test transmissivity was 80 *d-m* and tha average storativity was 2.4×10^{-4} *m/kPa* with both values having a range of about ±50% if tha two high storativity values from Tests B7 and B8 are excluded. For a porosity of 20% and reservoir thickness of 700 meters the average test compressibility is 1.7×10^{-6} kPa^{-1} and the average test permeability is 114 *md.* The estimated compressibility agrees with that for brine at the average production temperature 263°C indicating that there are no resident *two* phase zones in the field. Interpretation of the superposed inference ellipses indicates that there is a NE-SW trending no-flow boundary near the extreme northern end of the productive area of the field (Figure 8.1).

9.5. OPTIMIZING TEST PARAMETERS

Interference tests benefit from the following features:

(i) Atmospheric earth tide and barometric pressure measurements measured to 1 Pa which allow resolution and deconvolution of earth tide components.

(ii) Downhole gauge resolution better than 100 Pa to allow correction of primary interference/test data for earth tide effects and also allow the deconvoluted earth tide data to be used to determine reservoir parameters.

(iii) Flow rates large enough to produce early time data that can be matched to the line source solution. Large flow rates may produce two phase effects in the field due to drawdown, during production.

(iv) Doublets chosen to produce r_2/r_1 ratios in the range 3 to 8 on the best information available to the designer prior to the start of the test.

(v) Cautious use of interference tests with injected fluid as complex analysis is required to determine in-situ reservoir parameters.

10. CONCLUSIONS

(i) Careful interpretation is required to obtain the correct reservoir properties from interference tests.

(ii) Assuming a reservoir thickness of 700*m* the average permeability for the productive Ohaaki reservoir is 110 *md.*

(iii) The average compressibility of $1.7\times10^{-6} kPa^{-1}$ derived from the interference tests indicates that there are no mobile two phase zones in the Ohaaki reservoir within the sphere of influence of the test.

(iv) A no-flow boundary was located utilizing the inference ellipses deduced from 6 of the 12 tests analyzed.

(v) Tests B1 and B9 showed evidence of late time pressure support which may have been due to a two phase zone in the reservoir which later collapsed, while Test C1 showed evidence of a second no-flow boundary.

NOTATION

B_w formation volume factor for brine

B_g formation volume factor for gas

c_f formation compressibility (kPa^{-1})

c_g vapour compressibility (kPa^{-1})

c_{ph} compressibility due to phase change (kPa^{-1})

c_t total compressibility (kPa^{-1})

c_w brine compressibility (kPa^{-1})

d well depth (m)

d_D dimensionless distance between source well and boundary

d_{pz} permeable zone depth (m)

d_{wl} depth of water surface (m)

G_m mamx shear modulus

h formation thickness (m)

h_{fg} latent heat (kJ/kg)

h_w height of water surface above permeable zone (m)

k permeability ($darcy$)

P pressure (kPa)

p_{atm} atmospheric pressure (kPa)

P_C overburden pressure at average reservoir depth (kPa)

P_i initial pressure (kPa)

p_s specific pressure (kPa–s/m^3)

p_{sat} saturation pressure (kPa)

p_D dimensionless pressure

p_D^* modified dimensionless pressure

p_{DH}^* modified *Horner* dimensionless pressure

p_{pz} permeable zone pressure at the well (kPa)

p_{sat} saturation pressure (kPa)

q volumetric flow rate (m^3/s)

r distance between pressure point and source well (m)

r_1 distance between source well and observation well (m)

r_2 distance between observation well and the image well (m)

r_w source well radius (m)

S^* storage coefficient

S_g vapor saturation

S_w water saturation

t time (s)

t_D dimensionless time

t_D^* modified dimensionless time

t_{DH} dimensionless *Horner* time

t_{DH}^* modified dimensionless *Horner* time

t_{pD} dimensionless production time

μ dynamic viscosity ($kPa-s$)

ω earth tide frequency

ϕ porosity

ρ_f formation density (kg/m^3)

ρ_g vapor density (kg/m^3)

ρ_w brine density (kg/m^3)

REFERENCES

Arditty P : "The Earth Tide Effects on Petroleum Reservoirs," *M.S. thesis, Stanford University*. Stanford Geothermal Programme Report SGP-TR-34 (1979).

Barenblatt G I, Zheltov Y P : "Fundamental Equations of Homogeneous Liquids in Fissured Rocks," *Dokl. Akad. Nauk*. U.S.S.R. (June 1960), pp 545-548.

Barenblatt G I, Zheltov Y P, Kochina I N : "Basic Concepts in the *Theory* of Seepage of Homogeneous Liquids in Fissured Rocks (Strata)," J. *Appl. Math. Mech.*, U.S.S.R. (1960), pp 1286-1303.

Bixley P F : "Broadlands Geothermal Area: Underground Temperatures and some Thoughts on the Reservoir and Future Drilling," *Ministry of* Works *and Development*, Wairakei (1976), Geothermal Circular PFB 1.

Bixley P F : "Hydrology of the Western Broadlands Reservoir," *Ministry of Works and Development*, Wairakei (Feb. 1982), file 27/35.

Bixley P F, Grant M A : "Reinjection Testing at Broadlands," *Proc.* 6th *Stanford Geothermal Workshop* (1980).

Blakely M R, O'Sullivan M J, Bodvarsson G S: "A Simple Model of the Ohaaki Geothermal Reservoir," Proc., *5th N.Z. Geothermal Workshop* (1983), pp 11-15.

Bodvarsson G : "Confined Fluids as Strain Meters," J. *Geophys. Research (1970)*, 75(14), pp 2711-2718.

Braithwaite R L : "Petrological Report: Broadlands Drillhole Br34," *Geological Survey, D.S.I.R.*, Lower Hutt, N.Z. (June 1979).

Bredehoeft J D : "Response of Well-Aquifer System to Earth Tides," J. *Geophys.*, 72(12) (1967), pp 3075-3087.

Browne P R L : "The Geology, Mineralogy and Geothermometry of the Broadlands Geothermal Field, Taupo Volcanic Zone, New Zealand," *Ph.D. dissertation, Victoria University,* Wellington (1973).

Davis G E, Hawkins M F : "Linear Fluid-Barrier Detection by Well Pressure Measurements," *J. Pet. Tech.* (Oct. 1963), pp 1077-1079.

Deruyck B G, Bourdet D P, DaPratt G, Ramey H J Jr.: "Interpretation of Interference Tests in Reservoirs With Double Porosity Behaviour--Theory and Field Examples," *SPE 57th Annual Conference,* New Orleans (Sept. 1982), SPE paper 11025.

Earlougher R C, Ramey H J Jr.: "Interference Analysis in Bounded Systems," J. *Can. Pet. Tech.* (Oct.-Dec. 1973), pp 33-45.

Eipper M E : "Computer Generation of Type Curves," *M.S.thesis, Stanford University.* Stanford Geothermal Programme Report SGP-TR-86 (1985).

Ellis A J, Mahon W A J : *Chemistry and Geothermal System,* Academic Press, New York (1977).

Ferris J G, Knowles D B, Brown R H, Stallman R W :"Theory of Aquifer Tests", *U.S.Geol Survey, Water Supply,* paper 1536-E (1962).

Fox G : "Linear Boundary Detection using Pressure Buildup Tests," *M.S. thesis, Stanford University.* Stanford Geothermal Programme Report SGP-TR-83 (1984).

Grant M A : "Broadlands Geothermal Field, Interference Tests at Br13, 19 and 23," *Applied Mathematics Division, D.S.I.R.,* Wellington, New Zealand (1980), Report AMD 98.

Grant M A : "Broadlands a Gas Dominated Reservoir," *Geothermics*, Vol. *6* (1977), pp 9-29.

Grant M A : "Changes in Fluid Distribution at Ohaki," Proc., *2nd NZ. Geothermal Workshop* (1980), pp 69-74.

Grant M A : "A Heat Balance on the Ohaaki Reservoir," *Applied Mathematics Division, D.S.I.R.,* Wellington, New Zealand (1982), Report MAG35.

Grant M A : "The Interaction of the Ohaaki Reservoir with Surrounding Fluid" *Applied Mathematics Division, D.S.I.R.,* Wellington, New Zealand (1982), Report MAG37.

Grant M A : "Broadlands Reservoir Structure," *Applied Mathematics Division, D.S.I.R.,* Wellington, New Zealand (Nov. 1983).

Grant M A, Donaldson I G, Bixley P F : *Geothermal Reservoir Engineering,* Academic Press, New York (1982).

Grant M A, Iles D W : "A Simple Model of the Connection Between Eastern and Western Sections of Broadlands Geothermal Field," *Applied Mathematics Division, D.S.I.R.,* Wellington, New Zealand (1982), Report MAG34.

Grant M A, Sorey M L : "The Compressibility and Hydraulic Diffusivity of a Steam-Water Mixture," *Water Resources Research* (1979), pp 684-686.

Grindley G W, Browne P R L : "The Subsurface Geology of the Broadlands Geothermal Field," *N.Z. Geological Survey* (1968), Report 34.

Hall H N : "Compressibility of Reservoir Rocks," *Trans.,* AIME, **198** (1953), pp 309-311.

Henley R W, Harper R T : "Water-Rock Interactions During Injection of Flashed BR2 Water at BR34 - Preliminary Interpretations and Some Implications," *Chemistry Division, D.S.I.R.,* New Zealand (1979).

Hitchcock G W, Bixley P F : "Observations of the Effect of a Three Year Shutdown at Broadlands Geothermal Field," Proc., *2nd U.N. Conference on the Development and Use of Geothermal Resources* (1975), pp 1657-1661.

Hedenquist J W : "Characteristics of Broadlands-Ohaaki Water Chemistry and Changes Subject to Initial Production," *Proc., 5th N.Z. Geothermal Workshop* (1983), pp 139-144.

Hedenquist J W, Stewart M K : "Natural CO_2-Rich Steam-Heated Waters in the Broadlands-Ohaaki Geothermal System, New Zealand: Their Chemistry, Distribution and Corrosive Nature," *Trans.,* Geothermal Resources Council, Vol. 9, Part 2 (Aug. 1985), pp 245-250.

Horne R N : "Geothermal Reservoir Engineering Course Notes," *Japan Geothermal Energy Development Centre,* Tokyo (1980).

Horner D R : "Pressure Build-Up in Wells," *Proc. Third World Pet. Congress, Section 11,* E. J. Leiden, Netherlands (1951).

Hunt T M : "Recharge at Broadlands (Ohaaki) Geothermal Field 1967-1983 Determined from Repeat Gravity Measurements," *Proc., 6th N.Z. Geothermal Workshop* (1984), pp 195 200.

Hunt T M, Hicks S R : "Repeat Gravity Measurements at Broadlands Geothermal Field 1967 1974," *Geophysics Division, D.S.I.R.,* Wellington, New Zealand (1975), Report No. 113.

Hurst W : "Interference Between Oilfields," *Trans., AIME,* 219 (1960), pp 175-192.

Jacob C E : "Coefficients of Storage and Transmissibility Obtained from Pumping Tests in the Houston District, Texas," *Trans.,* Amer. Geophysical Union (1941), pp 744-756.

Jacob C E : "Correlation of Ground-water Levels and Precipitation on Long Island New York, *Trans.,* Amer. Geophysical Union, Part 2 (1944), pp 564-573.

Jargon J R : "Effect of Wellbore Storage and Well Damage at the Active Well on Interference Test Analysis," **J. *Pet. Tech.*** (Aug. 1976), pp 851-858.

Kazemi H, Memll L S, Jargon J R : "Problems in Interpretation of Pressure Fall-off Tests in Reservoirs With and Without Fluid Banks," **J. *Pet. Tech.*** (Sept. 1972), pp 1147-1156.

Kazemi H, Seth M S, Thomas G W : "The Interpretation of Interference Tests in Naturally Fractured Reservoirs With Uniform Fracture Distribution," ***Soc. Pet. Eng. J.*** (Dec. 1969), pp 463-472.

Kazmann R G : "Notes on Determining the Effective Distance to a Line of Recharge", ***Trans.***, Amer. Geophysical Union, Part 2 (Dec. 1946), p 854.

Khurana A K : "Influence of Tidal Phenomena on Interpretation of Pressure Buildup and Pulse Tests," ***Australian Pet. Exploration Assn. J.***, 16(1) (1976), pp 99-105.

Koefoed O : "Simultaneous Observation of Drawdown Data from Several Observation Wells by Means of a Modification of the Walton Method," **J. *Hydrology,* 21(4)** (April 1974), pp 315-319.

LaRocque G A Jr.: "Fluctuations of Water Levels in Wells in the Los Angeles Basin During Five Strong Earthquakes 1933-1940," ***Trans.***, American Geophys. Union, Part 2 (1941), pp 374-386.

Leaver J D, Sageev A, Ramey H J Jr.: "Linear Boundary Detection In a Single Interference, Test," Proc., ***7th NZ. Geothermal Workshop*** (1985).

Leaver J D, Sageev A, Ramey H J Jr.: "Multiple Well Interference Testing in the Ohaaki Geothermal Field," ***SPE Regional Calif. Conf.***, Oakland, April 2-4, paper 15122 (1986).

Martin J C : "Simplified Equations of Flow in Gas Drive Reservoirs and the Theoretical Foundation of Multiphase Pressure Buildup Analyses," ***Trans.***, AIME 216 (1959), pp 309.

McGuinness M J : "Interference Testing of the Rhyolites Overlying the Ohaaki Geothermal Reservoir," ***Trans.,*** Geothermal Resources Council, Vol. 9, Part 2 (Aug. 1985), pp 541-545.

Mueller T D, Witherspoon P A : "Pressure Interference Effects Within Reservoirs 4 Aquifers," ***J. Pet. Tech.*** (April 1965), pp 471-474.

API

(1956), pp 482-509.

Ramey H J Jr.: "Rapid Methods for Estimating Reservoir Compressibilities," ***J. Pet. Tech.*** (April 1964), pp 447-454.

Ramey H J Jr.: "Approximate Solutions for Unsteady Liquid Flow in Composite Reservoirs," ***J. Canadian Pet. Tech.*** (Jan. 1970), pp 32-37.

Ramey H J Jr., Kumar A, Gulati M S : ***Gas Well Test Analysis Under Water Drive Conditions***, Amer. Gas Assn., Arlington, VA.(1973).

Robinson T W : "Earth Tides Shown by Fluctuations of Water Levels in Wells in New Mexico and Iowa," ***Trans.,*** American Geophys. Union, Part 4 (1939), pp 656-666.

Sageev A : "Interference Testing Near a Steam Cap," ***Trans.,*** Geothermal Resources Council

Vol. 9, Part 2 (Aug. 1985), pp 569-572.

Sageev A, Home R N, Ramey H J Jr.: "Detection of Linear Boundaries by Drawdown Tests; A Semilog Curve Matching Approach," *Water Resources Research.*, Vol. 21, no.3 (1985), pp 305-310.

Sageev A, Leaver J D, Ramey H J Jr.: "The Significance of Early Time Data In Interference Testing For Linear Boundary Detection," *Proc. 11th Stanford Geothermal Workshop* (1986).

Stallman R W : "Nonequilibrium Type Curves Modified for Two-well Systems," *Geological Survey Groundwater Note 3*, U.S. Dept. of Int., Washington D.C. (1952).

Standing M B : *Volumetric and Phase Behavior of Oil Field Hydrocarbon Systems*, Reinhold Pub. Co., New York (1952).

Strobel C J, Gulati M S, Ramey H J Jr.: "Reservoir Limit Tests in a Naturally Fractured Reservoir--A Field Case Study Using Type Curves," *J. Pet. Tech.* (Sept. 1976), pp 1097-1106.

Theis C V : "Relation Between the Lowering of the Piezometric Surface and the Rate and Duration of Discharge of a Well Using Ground-Water Storage," Eos *Trans. AGU*, 16(2) (1935), pp 519-524.

Thorsteinsson T, Eliasson J : "Geohydrology of the Laugarnes Hydrotherinal System in Reykjavik, Iceland," *U.N. Sympos. on the Devel. and Use of Geothermal Resources, Vol. 3* (1970), pp 1191-1204.

van Everdingen A F, Hurst W : "The Application of the Laplace Transformation to Flow Problems in Porous Media," *AIME*, 186 (1949), pp 305-324

Vela S : "Effect of a Linear Boundary on Interference and Pulse tests - The Elliptical Inference

Area," *J. Pet. Tech.* (Aug. 1977), pp 947-950.

Warren J E, Root P J : "The Behaviour of Naturally Fractured Reservoirs," *SPE J.* (Sept. 1963), pp 245-255.

Young A : "Tidal Phenomena at Inland Boreholes Near Cradock," Trans., Royal Soc. South Africa, Vol. 3, Part 1 (1913), pp 61-105.

--------- : "Broadlands Geothermal Field Investigation Report," *Power Division, Ministry of Works and Development,* Wellington, New Zealand (1977).

APPENDIX A

LINE SOURCE TYPE CURVE

(Eipper 1985)

```
C
c This program calculates PD vs tD/rD**2 for the line source solution curve.
C
c Variables used:
c mmdei=imsl routine for exponential integral solution
c pd=dimensionless pressure
c td=dimensionless time divided by dimensionless radius squared
C
C
c These loops generate tD/rD**2 values between 0.1 and 10000 and calculate,
c corresponding PD values.
C
      implicit real*8(a-h,o-z)
      dimension td(1000),pd(1000)
      double precision mmdei
      iopt=1
      n=0
      do 10 i=1,6
        do 20 j=1,20
          tdlog=-2.+i+(j-1)/20.
          tdd=10.**tdlog
          if(tdd.gt.10000.)go to 10
          n=n+1
          td(n)=tdd
          arg=-1./(4.*td(n))
          pd(n)=-0.5*mmdei(iopt,arg,ier)
   20   continue
   10 continue
C
c This loop outputs the values for plotting.
C
      write(6,1000)n
 1000 format(i3)
      do 30 i=1,n
        write(6,2000)td(i),pd(i)
 2000   format(e10.5,5x,e15.7)
   30 continue
      stop
      end
```

APPENDIX B

SPECIFIC PRESSURE vs TIME DATA

TABLE B1

TEST B1: BR13 **RESPONSE** TO BR23 DISCHARGE

BR13 Reswnse to BR23 **Discharge**	
Time (h)	Specific Pressure ($kPa-s/m^3$)
0.50000e+00	0.28053e+02
0.15000e+01	0.87023e+02
0.25000e+01	0.12347e+03
0.35000e+01	0.14866e+03
0.45000e+01	0.16832e+03
0.55000e+01	0.18244e+03
0.65000e+01	0.19580e+03
0.75000e+01	0.20649e+03
0.85000e+01	0.21718e+03
0.95000e+01	0.22805e+03
0.10500e+02	0.23588e+03
0.11500e+02	0.24370e+03
0.12500e+02	0.24924e+03
0.13500e+02	0.25763e+03
0.14500e+02	0.26622e+03
0.15500e+02	0.27176e+03
0.16500e+02	0.27729e+03
0.17500e+02	0.28302e+03
0.18500e+02	0.28855e+03
0.19500e+02	0.29427e+03
0.20500e+02	0.30267e+03
0.21500e+02	0.30878e+03
0.22500e+02	0.30935e+03
0.23500e+02	0.31546e+03
0.24500e+02	0.32118e+03
0.25500e+02	0.32385e+03
0.26500e+02	0.32958e+03
0.27500e+02	0.33225e+03
0.28500e+02	0.33798e+03
0.29500e+02	0.34084e+03
0.30500e+02	0.34676e+03
0.31500e+02	0.35019e+03

BR13 Response to BR23 Discharge	
Time (*h*)	Specific Pressure ($kPa-s/m^3$)
0.32500e+02	0.35630e+03
0.33500e+02	0.35859e+03
0.34500e+02	0.36126e+03
0.35500e+02	0.36603e+03
0.36500e+02	0.36889e+03
0.37500e+02	0.37156e+03
0.38500e+02	0.37156e+03
0.39500e+02	0.37729e+03
0.40500e+02	0.37996e+03
0.41500e+02	0.38569e+03
0.42500e+02	0.38798e+03
0.43500e+02	0.39294e+03
0.44500e+02	0.39790e+03
0.45500e+02	0.40019e+03
0.46500e+02	0.40248e+03
0.47500e+02	0.40496e+03
0.48500e+02	0.40763e+03
0.49500e+02	0.39656e+03
0.50500e+02	0.33473e+03
0.51500e+02	0.28989e+03
0.52500e+02	0.26374e+03
0.53500e+02	0.24504e+03
0.54500e+02	0.22996e+03
0.55500e+02	0.21889e+03
0.56500e+02	0.21508e+03
0.57500e+02	0.20191e+03
0.58500e+02	0.18893e+03
0.59500e+02	0.18149e+03
0.60500e+02	0.17233e+03
0.62500e+02	0.16011e+03
0.64500e+02	0.14771e+03
0.66500e+02	0.14046e+03
0.68500e+02	0.13282e+03
0.70500e+02	0.12233e+03
0.72500e+02	0.11279e+03
0.74500e+02	0.10439e+03
0.77500e+02	0.95992e+02
0.80500e+02	0.89885e+02
0.83500e+02	0.85305e+02
0.86500e+02	0.76908e+02
0.89500e+02	0.72328e+02
0.92500e+02	0.66412e+02
0.95500e+02	0.62023e+02
0.98500e+02	0.55153e+02
0.10150e+03	0.51336e+02
0.10450e+03	0.46756e+02
0.10750e+03	0.43511e+02
0.11050e+03	0.37977e+02
0.11350e+03	0.35115e+02
0.11650e+03	0.32443e+02
0.11950e+03	0.29962e+02

Time (h)	Specific Pressure ($kPa-s/m^3$)
0.12250e+03	0.23282e+02
0.12550e+03	0.17557e+02
0.12850e+03	0.17557e+02
0.13150e+03	0.15840e+02
0.13450e+03	0.13550e+02
0.13750e+03	0.78244e+01
0.14250e+03	0.11450e+01

TABLE B2

TEST B2: BR23 RESPONSE TO BR13 DISCHARGE

BR23 Response *to* BR13 Discharge	
Time (*h*)	Specific Pressure ($kPa-s/m^3$)
0.10000e+01	0.67500e+01
0.20000e+01	0.14430e+02
0.30000e+01	0.38480e+02
0.40000e+01	0.57990e+02
0.50000e+01	0.78760e+02
0.60000e+01	0.94040e+02
0.70000e+01	0.10478e+03
0.80000e+01	0.12244e+03
0.90000e+01	0.13221e+03
0.10000e+02	0.14379e+03
0.11000e+02	0.15346e+03
0.12000e+02	0.16326e+03
0.13000e+02	0.17114e+03
0.14000e+02	0.17954e+03
0.15000e+02	0.18821e+03
0.16000e+02	0.19870e+03
0.17000e+02	0.20556e+03
0.18000e+02	0.21229e+03
0.19000e+02	0.21825e+03
0.20000e+02	0.22421e+03
0.21000e+02	0.23017e+03
0.22000e+02	0.23613e+03
0.23000e+02	0.24026e+03
0.24000e+02	0.24543e+03
0.25000e+02	0.25336e+03
0.26000e+02	0.25932e+03
0.28000e+02	0.26732e+03
0.30000e+02	0.27741e+03
0.32000e+02	0.29014e+03
0.34000e+02	0.29630e+03
0.36000e+02	0.30640e+03
0.38000e+02	0.31255e+03
0.40000e+02	0.31869e+03
0.42000e+02	0.32879e+03
0.44000e+02	0.33679e+03
0.46000e+02	0.34332e+03
0.48000e+02	0.35277e+03
0.50000e+02	0.36064e+03
0.52000e+02	0.36545e+03
0.54000e+02	0.37278e+03
0.56000e+02	0.37998e+03
0.58000e+02	0.38731e+03
0.60000e+02	0.39624e+03
0.62000e+02	0.40317e+03
0.64000e+02	0.40704e+03

BR23 Response to BR13 Discharge	
Time (h)	Specific Pressure ($kPa-s/m^3$)
0.66000e+02	**0.41678e+03**
0.68000e+02	0.42185e+03
0.70000e+02	0.42611e+03
0.72000e+02	0.42690e+03
0.74000e+02	0.42929e+03
0.76000e+02	0.43635e+03
0.78000e+02	**0.43820e+03**
0.80000e+02	0.44915e+03
0.82000e+02	**0.45408e+03**
0.86000e+02	**0.46325e+03**
0.90000e+02	0.47525e+03
0.94000e+02	0.48012e+03
0.98000e+02	**0.48768e+03**
0.10200e+03	0.49886e+03
0.10600e+03	**0.51275e+03**
0.11000e+03	**0.52003e+03**
0.11400e+03	**0.52974e+03**
0.11800e+03	**0.53553e+03**
0.12200e+03	**0.54294e+03**
0.12600e+03	0.55386e+03
0.13000e+03	**0.56357e+03**
0.13400e+03	0.57111e+03
0.13800e+03	**0.58001e+03**
0.14200e+03	0.58687e+03
0.14600e+03	**0.59549e+03**
0.15000e+03	**0.60385e+03**
0.16600e+03	**0.63523e+03**
0.17800e+03	0.66016e+03
0.19000e+03	0.68114e+03
0.20200e+03	0.70281e+03
0.21400e+03	**0.72530e+03**
0.22600e+03	0.74628e+03
0.23800e+03	0.76755e+03
0.25000e+03	**0.78730e+03**
0.26200e+03	**0.83230e+03**
0.27400e+03	0.85148e+03
0.28600e+03	0.86869e+03
0.29800e+03	0.88872e+03
0.31000e+03	**0.90705e+03**
0.33200e+03	0.92623e+03
0.33100e+03	**0.94048e+03**
0.33400e+03	**0.10543e+04**
0.34600e+03	**0.10589e+04**
0.35800e+03	**0.10663e+04**
0.38200e+03	0.11512e+04

TABLE B3

TEST B3: BR23 RESPONSE TO BR19 DISCHARGE

BR23 Response to BR19 Discharge	
Time (h)	Specific Pressure ($kPa\text{-}s/m^3$)
0.10000e+01	0.34856e+01
0.20000e+01	0.10577e+02
0.30000e+01	0.15865e+02
0.40000e+01	0.24760e+02
0.50000e+01	0.29567e+02
0.60000e+01	0.36538e+02
0.70000e+01	0.43630e+02
0.80000e+01	0.47236e+02
0.90000e+01	0.52524e+02
0.10000e+02	0.59615e+02
0.11000e+02	0.64904e+02
0.12000e+02	0.68389e+02
0.13000e+02	0.73678e+02
0.14000e+02	0.77284e+02
0.15000e+02	0.81490e+02
0.16000e+02	0.86779e+02
0.17000e+02	0.89784e+02
0.18000e+02	0.92909e+02
0.19000e+02	0.95192e+02
0.20000e+02	0.96875e+02
0.21000e+02	0.99639e+02
0.22000e+02	0.10144e+03
0.23000e+02	0.10553e+03
0.24000e+02	0.10721e+03
0.25000e+02	0.11082e+03
0.26000e+02	0.11430e+03
0.27000e+02	0.11563e+03
0.28000e+02	0.11911e+03
0.29000e+02	0.12392e+03
0.30000e+02	0.12740e+03
0.31000e+02	0.12921e+03
0.32000e+02	0.13269e+03
0.33000e+02	0.13630e+03
0.34000e+02	0.13810e+03
0.35000e+02	0.14159e+03
0.36000e+02	0.14507e+03
0.37000e+02	0.14688e+03
0.37000e+02	0.14688e+03
0.38000e+02	0.14844e+03
0.39000e+02	0.15349e+03
0.40000e+02	0.15493e+03
0.41000e+02	0.15673e+03
0.42000e+02	0.16022e+03
0.43000e+02	0.16202e+03
0.44000e+02	0.16755e+03

BR23 Response to BR19 Discharge	
Time (*h*)	Specific Pressure ($kPa-s/m^3$)
0.45000e+02	0.17344e+03
0.46000e+02	0.17536e+03
0.47000e+02	0.17764e+03
0.48000e+02	0.17969e+03
0.49000e+02	0.18173e+03
0.50000e+02	0.18401e+03
0.51000e+02	0.18522e+03
0.52000e+02	0.19026e+03
0.55000e+02	0.19303e+03
0.57000e+02	0.19639e+03
0.59000e+02	0.20216e+03
0.61000e+02	0.20625e+03
0.63000e+02	0.20877e+03
0.65000e+02	0.21298e+03
0.67000e+02	0.21827e+03
0.69000e+02	0.21827e+03
0.71000e+02	0.22055e+03
0.73000e+02	0.22236e+03
0.75000e+02	0.22536e+03
0.77000e+02	0.22813e+03
0.79000e+02	0.23317e+03
0.81000e+02	0.23498e+03
0.89000e+02	0.24736e+03
0.93000e+02	0.25132e+03
0.97000e+02	0.25656e+03
0.10100e+03	0.26502e+03
0.10500e+03	0.26851e+03
0.10900e+03	0.27308e+03
0.11300e+03	0.28017e+03
0.11700e+03	0.28245e+03
0.12100e+03	0.28678e+03
0.12500e+03	0.29435e+03
0.12900e+03	0.29784e+03
0.13700e+03	0.30925e+03
0.18900e+03	0.33425e+03

TABLE B4

TEST **B4: BR23** RESPONSE TO BR13 INJECTION

BR23 Response to BR13 Discharge	
Time (*h*)	Specific Pressure (*kPa-s/m*^{3})
0.10000e+01	0.14878e+02
0.20000e+01	0.51789e+02
0.30000e+01	0.67420e+02
0.40000e+01	0.83051e+02
0.50000e+01	0.10979e+03
0.60000e+01	0.12825e+03
0.70000e+01	0.14670e+03
0.80000e+01	0.16422e+03
0.90000e+01	0.17910e+03
0.10000e+02	0.19379e+03
0.11000e+02	0.20866e+03
0.12000e+02	0.22147e+03
0.13000e+02	0.23352e+03
0.14000e+02	0.24557e+03
0.15000e+02	0.25480e+03
0.16000e+02	0.26478e+03
0.17000e+02	0.27213e+03
0.18000e+02	0.28493e+03
0.19000e+02	0.29736e+03
0.20000e+02	0.30377e+03
0.21000e+02	0.31299e+03
0.22000e+02	0.32185e+03
0.23000e+02	0.32467e+03
0.24000e+02	0.33672e+03
0.25000e+02	0.35141e+03
0.26000e+02	0.36347e+03
0.27000e+02	0.37175e+03
0.28000e+02	0.37815e+03
0.29000e+02	0.38832e+03
0.30000e+02	0.39473e+03
0.31000e+02	0.40113e+03
0.32000e+02	0.40753e+03
0.33000e+02	0.41431e+03
0.34000e+02	0.42072e+03
0.35000e+02	0.42712e+03
0.36000e+02	0.43635e+03
0.37000e+02	0.43992e+03
0.38000e+02	0.44633e+03
0.39000e+02	0.45273e+03
0.40000e+02	0.45631e+03
0.41000e+02	0.46271e+03
0.42000e+02	0.46667e+03
0.43000e+02	0.47382e+03
0.44000e+02	0.48060e+03
0.45000e+02	0.48418e+03

Time (h)	Specific Pressure ($kPa-s/m^3$)
0.46000e+02	0.48776e+03
0.47000e+02	0.49134e+03
0.69000e+02	0.56798e+03
0.10000e+03	0.64821e+03
0.10600e+03	0.66252e+03
0.11800e+03	0.68983e+03
0.13000e+03	0.71770e+03
0.14200e+03	0.77985e+03
0.15400e+03	0.79699e+03
0.17800e+03	0.81525e+03
0.19200e+03	0.83503e+03
0.21600e+03	0.85669e+03
0.24000e+03	0.87702e+03
0.26400e+03	0.89134e+03
0.40200e+03	0.93089e+03

TABLE B5

TEST B6: BR23 RESPONSE TO BR20 DISCHARGE

BR23 Response to BR20 Discharge	
Time (h)	Specific Pressure ($kPa-s/m^3$)
0.10000e+01	**0.27559e+01**
0.15000e+01	0.73228e+01
0.22500e+01	0.12913e+02
0.55000e+01	0.2 1181e+02
0.65000e+01	**0.20079e+02**
0.75000e+01	**0.18268e+02**
0.85000e+01	**0.16299e+02**
0.95000e+01	**0.15827e+02**
0.10500e+02	**0.14961e+02**
0.11500e+02	**0.14331e+02**
0.12500e+02	**0.14252e+02**
0.13500e+02	0.13780e+02
0.14500e+02	0.13386e+02
0.15500e+02	0.13**150e+02**
0.16500e+02	**0.12913e+02**
0.18500e+02	0.12441e+02
0.19500e+02	0.11654e+02
0.20500e+02	**0.11024e+02**
0.21500e+02	**0.10079e+02**

TABLE B6

TEST B7: BR34 RESPONSE TO BR31 DISCHARGE

BR34 Response to BR31 Discharge	
Time (*h*)	Specific Pressure ($kPa-s/m^3$)
0.60000e+01	0.25000e+00
0.70000e+01	0.80000e+00
0.75000e+01	0.13500e+01
0.17500e+02	0.31700e+01
0.24500e+02	0.54400e+01
0.30500e+02	0.77100e+01
0.33500e+02	0.10000e+02
0.41000e+02	0.13950e+02
0.49000e+02	0.20190e+02
0.61000e+02	0.28470e+02
0.73000e+02	0.42680e+02
0.85000e+02	0.58180e+02
0.97000e+02	0.70230e+02
0.10900e+03	0.79050e+02
0.12100e+03	0.89230e+02
0.13300e+03	0.97820e+02
0.14500e+03	0.10992e+03
0.15700e+03	0.11950e+03
0.16900e+03	0.12843e+03
0.18100e+03	0.13791e+03
0.20500e+03	0.15938e+03
0.22900e+03	0.17869e+03
0.25300e+03	0.19884e+03
0.27700e+03	0.21722e+03
0.29300e+03	0.22750e+03

TABLE B7

TEST B8: BR34 RESPONSE TO BR23 DISCHARGE

BR34 Response to BR23 Discharge	
Time (h)	Specific Pressure ($kPa-s/m^3$)
0.19000e+02	0.45200e+01
0.31000e+02	0.16310e+02
0.43000e+02	0.35390e+02
0.55000e+02	0.52840e+02
0.67000e+02	0.72240e+02
0.79000e+02	0.92930e+02
0.91000e+02	0.11371e+03
0.10300e+03	0.13071e+03
0.11500e+03	0.14873e+03
0.12700e+03	0.16591e+03
0.13900e+03	0.18527e+03
0.15100e+03	0.20056e+03
0.16300e+03	0.21139e+03
0.18500e+03	0.22544e+03
0.19700e+03	0.23996e+03
0.20900e+03	0.25244e+03
0.22100e+03	0.26654e+03
0.22300e+03	0.26898e+03

TABLE B8

TEST B9: BR34 RESPONSE TO BR19 DISCHARGE

BR34 Response *to* BR19 Discharge	
Time (*h*)	Specific Pressure ($kPa-s/m^3$)
0.10000e+01	0.15487e+02
0.30000e+01	0.70099e+02
0.50000e+01	0.92554e+02
0.70000e+01	0.11047e+03
0.90000e+01	0.11001e+03
0.11000e+02	0.13213e+03
0.13000e+02	0.15151e+03
0.17000e+02	0.18202e+03
0.19000e+02	0.23086e+03
0.21000e+02	0.26784e+03
0.23000e+02	0.32462e+03
0.25000e+02	0.40577e+03
0.27000e+02	0.49367e+03
0.29000e+02	0.59208e+03
0.31000e+02	0.63445e+03
0.33000e+02	0.69849e+03
0.35000e+02	0.74465e+03
0.37000e+02	0.79015e+03
0.41000e+02	0.84681e+03
0.45000e+02	0.95336e+03
0.49000e+02	0.10936e+04
0.53000e+02	0.12374e+04
0.57000e+02	0.14010e+04
0.61000e+02	0.14884e+04
0.65000e+02	0.15358e+04
0.69000e+02	0.16142e+04
0.73000e+02	0.17259e+04
0.79000e+02	0.19476e+04
0.85000e+02	0.21123e+04
0.91000e+02	0.21975e+04
0.97000e+02	0.23399e+04
0.10300e+03	0.25157e+04
0.10900e+03	0.26475e+04
0.11500e+03	0.27496e+04
0.13100e+03	0.31562e+04
0.13300e+03	0.31881e+04
0.13500e+03	0.31929e+04
0.14300e+03	0.32198e+04
0.15100e+03	0.31626e+04
0.15900e+03	0.30778e+04
0.16700e+03	0.29246e+04
0.17500e+03	0.27724e+04
0.18300e+03	0.26817e+04
0.19100e+03	0.25317e+04
0.20300e+03	0.24006e+04

BR34 Response to BR19 Discharge	
Time ***(h)***	Specific **Pressure** ***(kPa-s/m^3)***
0.21500e+03	**0.21762e+04**
0.22700e+03	**0.20773e+04**
0.23900e+03	**0.18514e+04**
0.25100e+03	0.17**165e+04**
0.26300e+03	**0.15520e+04**
0.27500e+03	0.14784e+04
0.28700e+03	**0.13522e+04**
0.29900e+03	**0.13235e+04**
0.31100e+03	**0.12613e+04**
0.32800e+03	0.11**515e+04**
0.33500e+03	**0.10475e+04**
0.34700e+03	0.94134e+03
0.35900e+03	0.78263e+03
0.37100e+03	0.73768e+03
0.38300e+03	0.53281e+03
0.39500e+03	0.44185e+03
0.40700e+03	0.32771e+03
0.43100e+03	0.29385e+03
0.45500e+03	0.23693e+03

TABLE B9

TEST B10: BR23 RESPONSE TO BR13 SHUT-IN

BR23 Response to BR13 Shut-in	
Time (*h*)	Specific Pressure ($kPa-s/cu.m^3$)
0.10000e+01	0.16044e+02
0.20000e+01	0.21495e+02
0.30000e+01	0.36604e+02
0.40000e+01	0.58567e+02
0.50000e+01	0.77882e+02
0.60000e+01	0.95327e+02
0.70000e+01	0.10763e+03
0.80000e+01	0.11682e+03
0.90000e+01	0.12679e+03
0.10000e+02	0.13738e+03
0.11000e+02	0.14657e+03
0.12000e+02	0.15576e+03
0.13000e+02	0.16433e+03
0.14000e+02	0.16947e+03
0.15000e+02	0.17586e+03
0.16000e+02	0.18178e+03
0.17000e+02	0.18769e+03
0.18000e+02	0.19299e+03
0.19000e+02	0.19829e+03
0.20000e+02	0.20187e+03
0.21000e+02	0.20514e+03
0.22000e+02	0.20888e+03
0.23000e+02	0.21464e+03
0.24000e+02	0.22103e+03
0.25000e+02	0.22710e+03
0.26000e+02	0.23131e+03
0.27000e+02	0.23629e+03
0.28000e+02	0.24299e+03
0.29000e+02	0.24673e+03
0.30000e+02	0.25093e+03
0.31000e+02	0.25607e+03
0.32000e+02	0.26121e+03
0.33000e+02	0.26526e+03
0.34000e+02	0.26838e+03
0.35000e+02	0.27243e+03
0.36000e+02	0.27383e+03
0.37000e+02	0.28209e+03
0.38000e+02	0.28474e+03
0.39000e+02	0.28910e+03
0.40000e+02	0.29174e+03
0.42000e+02	0.29688e+03
0.46000e+02	0.30639e+03
0.48000e+02	0.31324e+03
0.50000e+02	0.31822e+03
0.52000e+02	0.32243e+03

BR23 Reswnse *to* BR13 Shut-in	
Time (*h*)	Specific Pressure (*kPa–s/cu.m*^{3})
0.54000e+02	0.32695e+03
0.56000e+02	0.33162e+03
0.58000e+02	0.33598e+03
0.60000e+02	0.33801e+03
0.62000e+02	0.34174e+03
0.64000e+02	0.34735e+03
0.66000e+02	0.35125e+03
0.68000e+02	0.35639e+03
0.70000e+02	0.36059e+03
0.72000e+02	0.36698e+03
0.74000e+02	0.36994e+03
0.76000e+02	0.37243e+03
0.78000e+02	0.37492e+03
0.80000e+02	0.37804e+03
0.84000e+02	0.38551e+03
0.88000e+02	0.39050e+03
0.92000e+02	0.39533e+03
0.96000e+02	0.39984e+03
0.10000e+03	0.40156e+03
0.10400e+03	0.40187e+03
0.10800e+03	0.40888e+03
0.11200e+03	0.41402e+03
0.11600e+03	0.41542e+03
0.12400e+03	0.41916e+03
0.14000e+03	0.43100e+03
0.14800e+03	0.43941e+03
0.15600e+03	0.44377e+03
0.16400e+03	0.44579e+03
0.17200e+03	0.45062e+03
0.18000e+03	0.45530e+03
0.18800e+03	0.45421e+03
0.19600e+03	0.46121e+03
0.20400e+03	0.45950e+03
0.21200e+03	0.45701e+03
0.22000e+03	0.46308e+03
0.22800e+03	0.45981e+03
0.23400e+03	0.46199e+03

TABLE B10

TEST C1: BR13 RESPONSE TO BR20 DISCHARGE

BR13 Response to BR20 Discharge	
Time (h)	Specific Pressure ($kPa-s/m^3$)
0.500000e+00	0.154768e+01
0.150000e+01	0.154768e+01
0.250000e+01	0.154768e+01
0.350000e+01	0.148810e+02
0.450000e+01	0.282142e+02
0.550000e+01	0.282142e+02
0.650000e+01	0.348809e+02
0.750000e+01	0.482143e+02
0.850000e+01	0.548810e+02
0.950000e+01	0.615476e+02
0.105000e+02	0.682142e+02
0.115000e+02	0.748809e+02
0.545000e+02	0.234762e+03
0.695000e+02	0.271429e+03
0.705000e+02	0.274762e+03
0.715000e+02	0.274762e+03
0.725000e+02	0.281429e+03
0.735000e+02	0.281429e+03
0.745000e+02	0.281429e+03
0.755000e+02	0.281429e+03
0.765000e+02	0.288095e+03
0.775000e+02	0.288095e+03
0.785000e+02	0.288095e+03
0.795000e+02	0.288095e+03
0.805000e+02	0.288095e+03
0.815000e+02	0.294762e+03
0.825000e+02	0.294762e+03
0.835000e+02	0.298095e+03
0.845000e+02	0.301429e+03
0.855000e+02	0.294762e+03
0.865000e+02	0.301429e+03
0.875000e+02	0.308095e+03
0.885000e+02	0.308095e+03
0.895000e+02	0.314762e+03
0.905000e+02	0.314762e+03
0.915000e+02	0.314762e+03
0.925000e+02	0.321429e+03
0.935000e+02	0.321429e+03
0.945000e+02	0.321429e+03
0.955000e+02	0.328095e+03
0.965000e+02	0.334762e+03
0.975000e+02	0.334762e+03
0.985000e+02	0.334762e+03
0.995000e+02	0.334762e+03
0.100500e+03	0.334762e+03

BR13 Response to BR20 Discharge	
Time (h)	specific Pressure ($kPa-s/m^3$)
0.101500e+03	0.341428e+03
0.102500e+03	0.341428e+03
0.103500e+03	0.348095e+03
0.104500e+03	0.348095e+03
0.105500e+03	0.348095e+03
0.106500e+03	0.351429e+03
0.107500e+03	0.354762e+03
0.108500e+03	0.354762e+03
0.109500e+03	0.354762e+03
0.110500e+03	0.354762e+03
0.111500e+03	0.354762e+03
0.112500e+03	0.354762e+03
0.113500e+03	0.361429e+03
0.114500e+03	0.354762e+03
0.115500e+03	0.354762e+03
0.116500e+03	0.361429e+03
0.117500e+03	0.368095e+03
0.118500e+03	0.368095e+03
0.119500e+03	0.368095e+03
0.120500e+03	0.368095e+03
0.121500e+03	0.368095e+03
0.122500e+03	0.374762e+03
0.123500e+03	0.368095e+03
0.124500e+03	0.374762e+03
0.125500e+03	0.378095e+03
0.126500e+03	0.374762e+03
0.127500e+03	0.374762e+03
0.128500e+03	0.381428e+03
0.129500e+03	0.381428e+03
0.130500e+03	0.381428e+03
0.131500e+03	0.381428e+03
0.132500e+03	0.381428e+03
0.133500e+03	0.388095e+03
0.134500e+03	0.388095e+03
0.135500e+03	0.388095e+03
0.136500e+03	0.388095e+03
0.137500e+03	0.388095e+03
0.138500e+03	0.388095e+03
0.139500e+03	0.394762e+03
0.140500e+03	0.394762e+03
0.141500e+03	0.394762e+03
0.142500e+03	0.401429e+03
0.143500e+03	0.401429e+03
0.144500e+03	0.401429e+03
0.145500e+03	0.404762e+03
0.146500e+03	0.408095e+03
0.147500e+03	0.408095e+03
0.148500e+03	0.408095e+03
0.149500e+03	0.408095e+03
0.150500e+03	0.408095e+03
0.151500e+03	0.408095e+03

BR13 Response to BR20 Discharge	
Time (*h*)	**Specific** Pressure ($kPa-s/m^3$)
0.152500e+03	0.414762e+03
0.153500e+03	0.414762e+03
0.154500e+03	0.414762e+03
0.155500e+03	0.414762e+03
0.156500e+03	0.414762e+03
0.157500e+03	0.414762e+03
0.158500e+03	0.414762e+03
0.159500e+03	0.421428e+03
0.160500e+03	0.421428e+03
0.161500e+03	0.421428e+03
0.194500e+03	0.461428e+03
0.195500e+03	0.468095e+03
0.196500e+03	0.468095e+03
0.197500e+03	0.448095e+03
0.198500e+03	0.474762e+03
0.199500e+03	0.474762e+03
0.200500e+03	0.474762e+03
0.201500e+03	0.474762e+03
0.202500e+03	0.474762e+03
0.203500e+03	0.474762e+03
0.204500e+03	0.474762e+03
0.205500e+03	0.481429e+03
0.206500e+03	0.478095e+03
0.207500e+03	0.481429e+03
0.208500e+03	0.481429e+03
0.209500e+03	0.481429e+03
0.210500e+03	0.481429e+03
0.211500e+03	0.481429e+03
0.212500e+03	0.481429e+03
0.213500e+03	0.488095e+03
0.214500e+03	0.481429e+03
0.215500e+03	0.488095e+03
0.216500e+03	0.488095e+03
0.217500e+03	0.484762e+03
0.218500e+03	0.488095e+03
0.219500e+03	0.488095e+03
0.220500e+03	0.488095e+03
0.221500e+03	0.488095e+03
0.222500e+03	0.488095e+03
0.223500e+03	0.488095e+03
0.224500e+03	0.494762e+03
0.225500e+03	0.494762e+03
0.226500e+03	0.494762e+03
0.227500e+03	0.491429e+03
0.228500e+03	0.494762e+03
0.229500e+03	0.494762e+03
0.230500e+03	0.494762e+03
0.231500e+03	0.494762e+03
0.232500e+03	0.494762e+03
0.233500e+03	0.488095e+03
0.234500e+03	0.494762e+03

BR13 Reswnse to BR20 Discharge	
Time (h)	specific Pressure ($kPa-s/m^3$)
0.235500e+03	0.494762e+03
0.236500e+03	0.501429e+03
0.237500e+03	0.501429e+03
0.238500e+03	0.501429e+03
0.239500e+03	0.501429e+03
0.240500e+03	0.508095e+03
0.241500e+03	0.508095e+03
0.242500e+03	0.508095e+03
0.243500e+03	0.508095e+03
0.244500e+03	0.508095e+03
0.245500e+03	0.508095e+03
0.246500e+03	0.508095e+03
0.247500e+03	0.514762e+03
0.248500e+03	0.511429e+03
0.249500e+03	0.514762e+03
0.250500e+03	0.514762e+03
0.251500e+03	0.508095e+03
0.252500e+03	0.514762e+03
0.253500e+03	0.514762e+03
0.254500e+03	0.514762e+03
0.255500e+03	0.518095e+03
0.256500e+03	0.514762e+03
0.258500e+03	0.514762e+03
0.259500e+03	0.514762e+03
0.260500e+03	0.521429e+03
0.261500e+03	0.521429e+03
0.262500e+03	0.528095e+03
0.263500e+03	0.528095e+03
0.264500e+03	0.528095e+03
0.265500e+03	0.528095e+03
0.266500e+03	0.534762e+03
0.267500e+03	0.528095e+03
0.268500e+03	0.534762e+03
0.269500e+03	0.528095e+03
0.270500e+03	0.534762e+03
0.271500e+03	0.534762e+03
0.272500e+03	0.534762e+03
0.273500e+03	0.534762e+03
0.274500e+03	0.541429e+03
0.275500e+03	0.538095e+03
0.276500e+03	0.534762e+03
0.277500e+03	0.541429e+03
0.278500e+03	0.534762e+03
0.279500e+03	0.541429e+03
0.280500e+03	0.548095e+03
0.281500e+03	0.544762e+03
0.282500e+03	0.541429e+03
0.283500e+03	0.548095e+03
0.284500e+03	0.544762e+03
0.285500e+03	0.548095e+03
0.286500e+03	0.554881e+03

BR13 Response to BR20 Discharge	
Time (h)	Specific Pressure ($kPa-s/m^3$)
0.287500e+03	0.554881e+03
0.288500e+03	0.554881e+03
0.289500e+03	0.554881e+03
0.290500e+03	0.558214e+03
0.291500e+03	0.554881e+03
0.292500e+03	0.554881e+03
0.293500e+03	0.561548e+03
0.294500e+03	0.554881e+03
0.295500e+03	0.561548e+03
0.296500e+03	0.561548e+03
0.297500e+03	0.561548e+03
0.298500e+03	0.561548e+03
0.299500e+03	0.561548e+03
0.300500e+03	0.561548e+03
0.301500e+03	0.568214e+03
0.302500e+03	0.561548e+03
0.303500e+03	0.561548e+03
0.304500e+03	0.568214e+03
0.305500e+03	0.568214e+03
0.306500e+03	0.568214e+03
0.307500e+03	0.568214e+03
0.308500e+03	0.568214e+03
0.309500e+03	0.574881e+03
0.310500e+03	0.568214e+03
0.311500e+03	0.574881e+03
0.312500e+03	0.581548e+03
0.313500e+03	0.574881e+03
0.314500e+03	0.574881e+03
0.315500e+03	0.574881e+03
0.316500e+03	0.574881e+03
0.317500e+03	0.574881e+03
0.318500e+03	0.574881e+03
0.319500e+03	0.574881e+03
0.320500e+03	0.574881e+03
0.321500e+03	0.574881e+03
0.322500e+03	0.574881e+03
0.323500e+03	0.574881e+03
0.324500e+03	0.574881e+03
0.325500e+03	0.581548e+03
0.326500e+03	0.574881e+03
0.327500e+03	0.581548e+03
0.328500e+03	0.574881e+03
0.329500e+03	0.574881e+03
0.330500e+03	0.574881e+03
0.331500e+03	0.574881e+03
0.332500e+03	0.581548e+03
0.333500e+03	0.588214e+03
0.334500e+03	0.588214e+03
0.335500e+03	0.584881e+03
0.336500e+03	0.588214e+03
0.337500e+03	0.588214e+03

Time (h)	Specific pressure ($kPa-s/m^3$)
0.338500e+03	0.588214e+03
0.339500e+03	0.588214e+03
0.340500e+03	0.588214e+03
0.341500e+03	0.578214e+03
0.342500e+03	0.568214e+03
0.343500e+03	0.561548e+03
0.344500e+03	0.554881e+03
0.345500e+03	0.541429e+03
0.346500e+03	0.534762e+03
0.347500e+03	0.528095e+03
0.348500e+03	0.514762e+03
0.349500e+03	0.508095e+03
0.350500e+03	0.501429e+03
0.351500e+03	0.494762e+03
0.352500e+03	0.488095e+03
0.353500e+03	0.484762e+03
0.354500e+03	0.474762e+03
0.355500e+03	0.474762e+03
0.356500e+03	0.474762e+03
0.357500e+03	0.474762e+03
0.358500e+03	0.468095e+03
0.359500e+03	0.468095e+03
0.360500e+03	0.461428e+03
0.361500e+03	0.461428e+03
0.362500e+03	0.454762e+03
0.363500e+03	0.454762e+03
0.364500e+03	0.448095e+03
0.365500e+03	0.448095e+03
0.366500e+03	0.441429e+03
0.367500e+03	0.434762e+03
0.368500e+03	0.434762e+03
0.369500e+03	0.428095e+03
0.370500e+03	0.421428e+03
0.371500e+03	0.421428e+03
0.372500e+03	0.421428e+03
0.373500e+03	0.414762e+03
0.374500e+03	0.411429e+03
0.375500e+03	0.408095e+03
0.376500e+03	0.401429e+03
0.377500e+03	0.401429e+03
0.378500e+03	0.401429e+03
0.379500e+03	0.394762e+03
0.407500e+03	0.348095e+03
0.408500e+03	0.348095e+03
0.409500e+03	0.341428e+03
0.410500e+03	0.341428e+03
0.411500e+03	0.341428e+03
0.412500e+03	0.341428e+03
0.413500e+03	0.341428e+03
0.414500e+03	0.334762e+03
0.415500e+03	0.334762e+03

BR13 Response to BR20 Discharge	
Time (*h*)	**Specific** Pressure ($kPa-s/m^3$)
0.416500e+03	0.334762e+03
0.417500e+03	**0.328095e+03**
0.418500e+03	**0.328095e+03**
0.419500e+03	**0.328095e+03**
0.420500e+03	0.321429e+03
0.421500e+03	**0.328095e+03**
0.422500e+03	0.321429e+03
0.423500e+03	0.321429e+03
0.424500e+03	**0.314762e+03**
0.425500e+03	**0.314762e+03**
0.426500e+03	0.314762e+03
0.427500e+03	0.314762e+03
0.428500e+03	0.314762e+03
0.429500e+03	0.314762e+03
0.430500e+03	0.314762e+03
0.431500e+03	0.314762e+03
0.432500e+03	0.314762e+03
0.433500e+03	0.314762e+03
0.434500e+03	**0.308095e+03**
0.435500e+03	**0.308095e+03**
0.436500e+03	**0.308095e+03**
0.437500e+03	**0.308095e+03**
0.438500e+03	0.301429e+03
0.439500e+03	0.301429e+03
0.440500e+03	**0.308095e+03**
0.441500e+03	**0.308095e+03**
0.442500e+03	**0.308095e+03**
0.443500e+03	0.301429e+03
0.444500e+03	0.301429e+03
0.445500e+03	0.301429e+03
0.446500e+03	0.301429e+03
0.447500e+03	0.301429e+03
0.448500e+03	0.301429e+03
0.449500e+03	0.294762e+03
0.450500e+03	0.294762e+03
0.451500e+03	0.294762e+03
0.452500e+03	**0.288095e+03**
0.453500e+03	**0.288095e+03**
0.454500e+03	0.294762e+03
0.455500e+03	0.294762e+03
0.456500e+03	0.294762e+03
0.457500e+03	**0.288095e+03**
0.458500e+03	**0.288095e+03**
0.460500e+03	0.294762e+03
0.461500e+03	**0.288095e+03**
0.462500e+03	**0.288095e+03**
0.463500e+03	**0.288095e+03**
0.464500e+03	**0.288095e+03**
0.465500e+03	**0.288095e+03**
0.466500e+03	0.284762e+03
0.467500e+03	0.281429e+03

BR13 Response to BR20 Discharge	
Time (h)	Specific Pressure ($kPa-s/m^3$)
0.468500e+03	0.281429e+03
0.469500e+03	0.274762e+03
0.470500e+03	0.274762e+03
0.471500e+03	0.274762e+03
0.472500e+03	0.271429e+03
0.473500e+03	0.268095e+03
0.474500e+03	0.268095e+03
0.475500e+03	0.268095e+03
0.476500e+03	0.268095e+03
0.477500e+03	0.274762e+03
0.478500e+03	0.274762e+03
0.479500e+03	0.274762e+03
0.480500e+03	0.274762e+03
0.481500e+03	0.274762e+03
0.482500e+03	0.274762e+03
0.483500e+03	0.268095e+03
0.484500e+03	0.268095e+03
0.485500e+03	0.268095e+03
0.486500e+03	0.261429e+03
0.487500e+03	0.261429e+03
0.488500e+03	0.254762e+03
0.489500e+03	0.254762e+03
0.490500e+03	0.254762e+03
0.491500e+03	0.254762e+03
0.492500e+03	0.254762e+03
0.493500e+03	0.254762e+03
0.494500e+03	0.254762e+03
0.495500e+03	0.254762e+03
0.496500e+03	0.248095e+03
0.497500e+03	0.251429e+03
0.498500e+03	0.248095e+03
0.499500e+03	0.241429e+03
0.500500e+03	0.248095e+03
0.501500e+03	0.248095e+03
0.502500e+03	0.254762e+03
0.503500e+03	0.254762e+03
0.504500e+03	0.254762e+03
0.505500e+03	0.251429e+03
0.506500e+03	0.254762e+03
0.507500e+03	0.254762e+03
0.508500e+03	0.248095e+03
0.509500e+03	0.251429e+03
0.510500e+03	0.248095e+03
0.511500e+03	0.248095e+03
0.512500e+03	0.248095e+03
0.513500e+03	0.248095e+03
0.514500e+03	0.241429e+03
0.515500e+03	0.241429e+03
0.516500e+03	0.241429e+03
0.517500e+03	0.234762e+03
0.518500e+03	0.241429e+03

BR13 Response to BR20 Discharge	
Time (h)	Specific Pressure ($kPa-s/m^3$)
0.519500e+03	0.241429e+03
0.520500e+03	0.241429e+03
0.521500e+03	0.241429e+03
0.522500e+03	0.234762e+03
0.523500e+03	0.234762e+03
0.524500e+03	0.234762e+03
0.525500e+03	0.234762e+03
0.526500e+03	0.241429e+03
0.527500e+03	0.241429e+03
0.528500e+03	0.241429e+03
0.529500e+03	0.241429e+03
0.530500e+03	0.241429e+03
0.531500e+03	0.244762e+03
0.532500e+03	0.241429e+03
0.533500e+03	0.244762e+03
0.534500e+03	0.241429e+03
0.535500e+03	0.241429e+03
0.536500e+03	0.241429e+03
0.537500e+03	0.234762e+03
0.538500e+03	0.234762e+03
0.539500e+03	0.234762e+03
0.540500e+03	0.241429e+03
0.541500e+03	0.234762e+03
0.542500e+03	0.234762e+03
0.543500e+03	0.234762e+03
0.544500e+03	0.234762e+03
0.578500e+03	0.221429e+03
0.579500e+03	0.228095e+03
0.888500e+03	0.185000e+03
0.889500e+03	0.183095e+03
0.890500e+03	0.181190e+03
0.891500e+03	0.181190e+03
0.892500e+03	0.177381e+03
0.893500e+03	0.173452e+03
0.894500e+03	0.177381e+03
0.895500e+03	0.177381e+03
0.896500e+03	0.173452e+03
0.897500e+03	0.173452e+03
0.898500e+03	0.173452e+03
0.899500e+03	0.173452e+03
0.900500e+03	0.173452e+03
0.901500e+03	0.173452e+03
0.902500e+03	0.173452e+03
0.903500e+03	0.177381e+03
0.904500e+03	0.173452e+03
0.905500e+03	0.173452e+03
0.906500e+03	0.173452e+03
0.907500e+03	0.171548e+03
0.908500e+03	0.173452e+03
0.909500e+03	0.173452e+03
0.910500e+03	0.177381e+03

BR13 Response to BR20 Discharge	
Time (h)	specific pressure ($kPa-s/m^3$)
0.911500e+03	0.177381e+03
0.912500e+03	0.181190e+03
0.913500e+03	0.183095e+03
0.914500e+03	0.181190e+03
0.915500e+03	0.185000e+03
0.916500e+03	0.185000e+03
0.917500e+03	0.185000e+03
0.918500e+03	0.181190e+03
0.919500e+03	0.179286e+03
0.920500e+03	0.177381e+03
0.921500e+03	0.177381e+03
0.922500e+03	0.177381e+03
0.923500e+03	0.175357e+03
0.924500e+03	0.173452e+03
0.925500e+03	0.173452e+03
0.926500e+03	0.177381e+03
0.927500e+03	0.177381e+03
0.928500e+03	0.173452e+03
0.929500e+03	0.181190e+03
0.930500e+03	0.183095e+03
0.931500e+03	0.185000e+03
0.932500e+03	0.185000e+03
0.933500e+03	0.192738e+03
0.934500e+03	0.192738e+03
0.935500e+03	0.190833e+03
0.936500e+03	0.188810e+03
0.937500e+03	0.188810e+03
0.938500e+03	0.188810e+03
0.939500e+03	0.188810e+03
0.940500e+03	0.185000e+03
0.941500e+03	0.185000e+03
0.942500e+03	0.185000e+03
0.943500e+03	0.185000e+03
0.944500e+03	0.185000e+03
0.945500e+03	0.185000e+03
0.946500e+03	0.185000e+03
0.947500e+03	0.185000e+03
0.948500e+03	0.185000e+03
0.949500e+03	0.173452e+03
0.950500e+03	0.181190e+03
0.951500e+03	0.181190e+03
0.952500e+03	0.181190e+03
0.953500e+03	0.177381e+03
0.954500e+03	0.181190e+03
0.955500e+03	0.181190e+03
0.956500e+03	0.181190e+03
0.957500e+03	0.185000e+03
0.958500e+03	0.188810e+03
0.959500e+03	0.188810e+03
0.960500e+03	0.188810e+03
0.961500e+03	0.188810e+03

BR13 Response to BR20 Discharge	
Time (*h*)	Specific Pressure ($kPa-s/m^3$)
0.962500e+03	0.185000e+03
0.963500e+03	0.181190e+03
0.964500e+03	0.181190e+03
0.965500e+03	0.177381e+03
0.966500e+03	0.177381e+03
0.967500e+03	0.177381e+03
0.968500e+03	0.181190e+03
0.969500e+03	0.177381e+03
0.970500e+03	0.173452e+03
0.971500e+03	0.169643e+03
0.972500e+03	0.169643e+03
0.973500e+03	0.165833e+03
0.974500e+03	0.165833e+03
0.975500e+03	0.163929e+03
0.976500e+03	0.165833e+03
0.977500e+03	0.162024e+03
0.978500e+03	0.158095e+03
0.979500e+03	0.135000e+03
0.980500e+03	0.165833e+03
0.981500e+03	0.173452e+03
0.982500e+03	0.173452e+03
0.983500e+03	0.177381e+03
0.984500e+03	0.177381e+03
0.985500e+03	0.177381e+03
0.986500e+03	0.173452e+03
0.987500e+03	0.171548e+03
0.988500e+03	0.169643e+03
0.989500e+03	0.165833e+03
0.990500e+03	0.165833e+03
0.991500e+03	0.165833e+03
0.992500e+03	0.158095e+03
0.993500e+03	0.165833e+03
0.994500e+03	0.165833e+03
0.995500e+03	0.162024e+03
0.996500e+03	0.162024e+03
0.997500e+03	0.158095e+03
0.998500e+03	0.158095e+03
0.999500e+03	0.162024e+03
0.100050e+04	0.158095e+03
0.100150e+04	0.158095e+03
0.100250e+04	0.154286e+03
0.100350e+04	0.158095e+03
0.100450e+04	0.158095e+03
0.100550e+04	0.169643e+03
0.100650e+04	0.169643e+03
0.100750e+04	0.173452e+03
0.100850e+04	0.177381e+03
0.100950e+04	0.175357e+03
0.101050e+04	0.173452e+03
0.101150e+04	0.169643e+03
0.101250e+04	0.165833e+03

BR13 Response to BR20 Discharge	
Time (h)	specific pressure ($kPa-s/m^3$)
0.101350e+04	0.162024e+03
0.101450e+04	0.162024e+03
0.101550e+04	0.158095e+03
0.101650e+04	0.160000e+03
0.101750e+04	0.158095e+03
0.101850e+04	0.162024e+03
0.101950e+04	0.158095e+03
0.102050e+04	0.162024e+03
0.102150e+04	0.162024e+03
0.102250e+04	0.165833e+03
0.102350e+04	0.165833e+03
0.102450e+04	0.165833e+03
0.102550e+04	0.165833e+03
0.102650e+04	0.165833e+03
0.102750e+04	0.154286e+03
0.102850e+04	0.169643e+03
0.102950e+04	0.154286e+03
0.103050e+04	0.181190e+03
0.103150e+04	0.181190e+03
0.103250e+04	0.177381e+03
0.103350e+04	0.177381e+03
0.103450e+04	0.177381e+03
0.107850e+04	0.150476e+03
0.107950e+04	0.154286e+03
0.108050e+04	0.158095e+03
0.108150e+04	0.158095e+03
0.108250e+04	0.162024e+03
0.108350e+04	0.158095e+03
0.108450e+04	0.158095e+03
0.108550e+04	0.154286e+03
0.108650e+04	0.154286e+03
0.108750e+04	0.154286e+03
0.108850e+04	0.158095e+03
0.108950e+04	0.154286e+03
0.109050e+04	0.154286e+03
0.109150e+04	0.152381e+03
0.109250e+04	0.150476e+03
0.109350e+04	0.154286e+03
0.109450e+04	0.154286e+03
0.109550e+04	0.154286e+03
0.110150e+04	0.150476e+03
0.110250e+04	0.150476e+03
0.110350e+04	0.158095e+03
0.110450e+04	0.162024e+03
0.110550e+04	0.160000e+03
0.110650e+04	0.158095e+03
0.110750e+04	0.158095e+03
0.110850e+04	0.158095e+03
0.110950e+04	0.154286e+03
0.111050e+04	0.154286e+03
0.111150e+04	0.150476e+03

BR13 Reswnse to BR20 Discharge	
Time (h)	Specific Pressure ($kPa-s/m^3$)
0.111250e+04	0.148452e+03
0.111350e+04	0.150476e+03
0.111450e+04	0.150476e+03
0.111550e+04	0.150476e+03
0.111650e+04	0.150476e+03
0.111750e+04	0.150476e+03
0.111850e+04	0.152381e+03
0.111950e+04	0.154286e+03
0.112050e+04	0.19286e+03
0.112150e+04	0.154286e+03
0.112250e+04	0.154286e+03
0.112350e+04	0.150476e+03
0.112450e+04	0.154286e+03
0.112550e+04	0.158095e+03
0.112650e+04	0.165833e+03
0.112750e+04	0.165833e+03
0.112850e+04	0.165833e+03
0.112950e+04	0.165833e+03
0.113050e+04	0.165833e+03
0.113150e+04	0.162024e+03
0.113250e+04	0.158095e+03
0.113350e+04	0.154286e+03
0.113450e+04	0.150476e+03
0.113550e+04	0.150476e+03
0.113650e+04	0.158095e+03
0.113750e+04	0.158095e+03
0.113850e+04	0.158095e+03
0.113950e+04	0.154286e+03
0.114050e+04	0.154286e+03
0.114150e+04	0.154286e+03
0.114250e+04	0.154286e+03
0.114350e+04	0.150476e+03
0.114450e+04	0.150476e+03
0.114550e+04	0.150476e+03
0.114650e+04	0.150476e+03
0.114750e+04	0.154286e+03
0.114850e+04	0.158095e+03
0.114950e+04	0.158095e+03
0.115050e+04	0.162024e+03
0.115150e+04	0.162024e+03
0.115250e+04	0.162024e+03
0.115350e+04	0.162024e+03
0.115450e+04	0.158095e+03
0.115550e+04	0.158095e+03
0.115650e+04	0.154286e+03
0.115750e+04	0.152381e+03
0.115850e+04	0.150476e+03
0.115950e+04	0.148452e+03
0.116050e+04	0.146548e+03
0.116150e+04	0.146548e+03
0.116250e+04	0.142738e+03

BR13 Response to BR20 Discharge	
Time (*h*)	Specific Pressure ($kPa-s/m^3$)
0.116350e+04	0.146548e+03
0.116450e+04	0.146548e+03
0.116550e+04	0.146548e+03
0.116650e+04	0.142738e+03
0.116750e+04	0.142738e+03
0.116850e+04	0.142738e+03
0.116950e+04	0.146548e+03
0.117050e+04	0.142738e+03
0.117150e+04	0.142738e+03
0.117250e+04	0.142738e+03
0.117350e+04	0.142738e+03
0.117450e+04	0.146548e+03
0.117550e+04	0.146548e+03
0.117650e+04	0.150476e+03
0.117750e+04	0.150476e+03
0.117850e+04	0.150476e+03
0.117950e+04	0.154286e+03
0.118050e+04	0.150476e+03
0.118150e+04	0.154286e+03
0.118250e+04	0.150476e+03
0.118350e+04	0.150476e+03
0.118450e+04	0.150476e+03
0.118550e+04	0.150476e+03
0.118650e+04	0.154286e+03
0.118750e+04	0.150476e+03
0.118850e+04	0.150476e+03
0.118950e+04	0.150476e+03
0.119050e+04	0.142738e+03
0.119150e+04	0.142738e+03
0.119250e+04	0.150476e+03
0.119350e+04	0.150476e+03
0.119450e+04	0.146548e+03
0.119550e+04	0.142738e+03
0.119650e+04	0.146548e+03
0.119750e+04	0.146548e+03
0.119850e+04	0.146548e+03
0.119950e+04	0.146548e+03
0.120050e+04	0.146548e+03
0.120150e+04	0.146548e+03
0.120250e+04	0.146548e+03
0.120350e+04	0.146548e+03
0.120450e+04	0.146548e+03
0.120550e+04	0.146548e+03
0.120650e+04	0.146548e+03
0.120750e+04	0.142738e+03
0.120850e+04	0.146548e+03
0.120950e+04	0.146548e+03
0.121050e+04	0.146548e+03
0.121150e+04	0.146548e+03
0.121250e+04	0.146548e+03
0.121350e+04	0.146548e+03

BR13 Response to BR20 Discharge	
Time (h)	specific pressure ($kPa-s/m^3$)
0.121450e+04	0.146548e+03
0.121550e+04	0.146548e+03
0.121650e+04	0.146548e+03
0.121750e+04	0.146548e+03

TABLE B11

TEST C2: BR23 RESPONSE TO BR20 DISCHARGE

BR23 Response to BR20 Discharge	
Time (h)	Specific Pressure ($kPa-s/m^3$)
0.150000e+01	0.272618e+02
0.250000e+01	0.341666e+02
0.350000e+01	0.546428e+02
0.450000e+01	0.614286e+02
0.550000e+01	0.819046e+02
0.650000e+01	0.819046e+02
0.750000e+01	0.955952e+02
0.850000e+01	0.102500e+03
0.950000e+01	0.116071e+03
0.105000e+02	0.116071e+03
0.115000e+02	0.122976e+03
0.125000e+02	0.136667e+03
0.545000e+02	0.293809e+03
0.695000e+02	0.328095e+03
0.705000e+02	0.328095e+03
0.715000e+02	0.334881e+03
0.725000e+02	0.334881e+03
0.735000e+02	0.334881e+03
0.745000e+02	0.334881e+03
0.755000e+02	0.334881e+03
0.765000e+02	0.341667e+03
0.775000e+02	0.348571e+03
0.785000e+02	0.341667e+03
0.795000e+02	0.348571e+03
0.805000e+02	0.348571e+03
0.815000e+02	0.355357e+03
0.825000e+02	0.355357e+03
0.835000e+02	0.362262e+03
0.845000e+02	0.362262e+03
0.855000e+02	0.362262e+03
0.865000e+02	0.365714e+03
0.875000e+02	0.362262e+03
0.885000e+02	0.369048e+03
0.895000e+02	0.369048e+03
0.905000e+02	0.369048e+03
0.915000e+02	0.375952e+03
0.925000e+02	0.375952e+03
0.935000e+02	0.375952e+03
0.945000e+02	0.375952e+03
0.955000e+02	0.382738e+03
0.965000e+02	0.382738e+03
0.975000e+02	0.382738e+03
0.985000e+02	0.386191e+03
0.995000e+02	0.382738e+03
0.100500e+03	0.389643e+03

BR23 Response to BR20 Discharge	
Time (*h*)	specific Pressure ($kPa-s/m^3$)
0.101500e+03	0.389643e+03
0.102500e+03	0.389643e+03
0.103500e+03	0.389643e+03
0.104500e+03	0.389643e+03
0.105500e+03	0.396429e+03
0.106500e+03	0.396429e+03
0.107500e+03	0.403333e+03
0.108500e+03	0.403333e+03
0.109500e+03	0.403333e+03
0.110500e+03	0.403333e+03
0.111500e+03	0.410119e+03
0.112500e+03	0.403333e+03
0.113500e+03	0.410119e+03
0.114500e+03	0.410119e+03
0.115500e+03	0.410119e+03
0.116500e+03	0.410119e+03
0.117500e+03	0.410119e+03
0.118500e+03	0.416905e+03
0.119500e+03	0.410119e+03
0.120500e+03	0.416905e+03
0.121500e+03	0.410119e+03
0.122500e+03	0.416905e+03
0.123500e+03	0.416905e+03
0.124500e+03	0.420357e+03
0.125500e+03	0.423809e+03
0.126500e+03	0.423809e+03
0.127500e+03	0.423809e+03
0.128500e+03	0.423809e+03
0.129500e+03	0.423809e+03
0.130500e+03	0.430595e+03
0.131500e+03	0.423809e+03
0.132500e+03	0.430595e+03
0.133500e+03	0.430595e+03
0.134500e+03	0.430595e+03
0.135500e+03	0.437500e+03
0.136500e+03	0.437500e+03
0.137500e+03	0.437500e+03
0.138500e+03	0.437500e+03
0.139500e+03	0.437500e+03
0.140500e+03	0.440952e+03
0.141500e+03	0.437500e+03
0.142500e+03	0.437500e+03
0.143500e+03	0.444286e+03
0.144500e+03	0.437500e+03
0.145500e+03	0.444286e+03
0.146500e+03	0.444286e+03
0.147500e+03	0.444286e+03
0.148500e+03	0.444286e+03
0.149500e+03	0.444286e+03
0.150500e+03	0.451190e+03
0.151500e+03	0.451190e+03

BR23 Response to BR20 Discharge	
Time (*h*)	Specific Pressure ($kPa-s/m^3$)
0.152500e+03	0.451190e+03
0.153500e+03	0.451190e+03
0.154500e+03	0.457976e+03
0.155500e+03	0.451190e+03
0.156500e+03	0.457976e+03
0.157500e+03	0.457976e+03
0.158500e+03	0.457976e+03
0.159500e+03	0.457976e+03
0.160500e+03	0.461428e+03
0.161500e+03	0.464881e+03
0.194500e+03	0.499048e+03
0.195500e+03	0.499048e+03
0.196500e+03	0.499048e+03
0.197500e+03	0.499048e+03
0.198500e+03	0.499048e+03
0.199500e+03	0.505952e+03
0.200500e+03	0.505952e+03
0.201500e+03	0.505952e+03
0.202500e+03	0.505952e+03
0.203500e+03	0.505952e+03
0.204500e+03	0.505952e+03
0.205500e+03	0.505952e+03
0.206500e+03	0.505952e+03
0.207500e+03	0.505952e+03
0.208500e+03	0.505952e+03
0.209500e+03	0.512738e+03
0.210500e+03	0.509405e+03
0.211500e+03	0.505952e+03
0.212500e+03	0.512738e+03
0.213500e+03	0.512738e+03
0.214500e+03	0.512738e+03
0.215500e+03	0.512738e+03
0.216500e+03	0.509405e+03
0.217500e+03	0.512738e+03
0.218500e+03	0.512738e+03
0.219500e+03	0.512738e+03
0.220500e+03	0.512738e+03
0.221500e+03	0.512738e+03
0.222500e+03	0.516190e+03
0.223500e+03	0.512738e+03
0.224500e+03	0.512738e+03
0.225500e+03	0.512738e+03
0.226500e+03	0.519643e+03
0.227500e+03	0.519643e+03
0.228500e+03	0.519643e+03
0.229500e+03	0.512738e+03
0.230500e+03	0.519643e+03
0.231500e+03	0.519643e+03
0.232500e+03	0.519643e+03
0.233500e+03	0.519643e+03
0.234500e+03	0.519643e+03

BR23 Response to BR20 Discharge	
Time (h)	specific pressure ($kPa-s/m^3$)
0.235500e+03	0.519643e+03
0.236500e+03	0.519643e+03
0.237500e+03	0.519643e+03
0.238500e+03	0.522976e+03
0.239500e+03	0.519643e+03
0.240500e+03	0.519643e+03
0.241500e+03	0.519643e+03
0.242500e+03	0.519643e+03
0.243500e+03	0.522976e+03
0.244500e+03	0.526429e+03
0.245500e+03	0.526429e+03
0.246500e+03	0.519643e+03
0.247500e+03	0.526429e+03
0.248500e+03	0.526429e+03
0.249500e+03	0.526429e+03
0.250500e+03	0.519643e+03
0.251500e+03	0.526429e+03
0.252500e+03	0.533333e+03
0.253500e+03	0.526429e+03
0.254500e+03	0.526429e+03
0.255500e+03	0.533333e+03
0.256500e+03	0.533333e+03
0.258500e+03	0.536667e+03
0.259500e+03	0.533333e+03
0.260500e+03	0.533333e+03
0.261500e+03	0.533333e+03
0.262500e+03	0.533333e+03
0.263500e+03	0.533333e+03
0.264500e+03	0.533333e+03
0.265500e+03	0.540119e+03
0.266500e+03	0.540119e+03
0.267500e+03	0.533333e+03
0.268500e+03	0.540119e+03
0.269500e+03	0.540119e+03
0.270500e+03	0.547024e+03
0.271500e+03	0.540119e+03
0.272500e+03	0.543571e+03
0.273500e+03	0.547024e+03
0.274500e+03	0.547024e+03
0.275500e+03	0.547024e+03
0.276500e+03	0.547024e+03
0.277500e+03	0.547024e+03
0.278500e+03	0.547024e+03
0.279500e+03	0.553810e+03
0.280500e+03	0.547024e+03
0.281500e+03	0.547024e+03
0.282500e+03	0.553810e+03
0.283500e+03	0.553810e+03
0.284500e+03	0.553810e+03
0.285500e+03	0.547024e+03
0.286500e+03	0.547024e+03

Time (h)	Specific Pressure ($kPa-s/m^3$)
0.287500e+03	0.547024e+03
0.288500e+03	0.553810e+03
0.289500e+03	0.553810e+03
0.290500e+03	0.553810e+03
0.291500e+03	0.553810e+03
0.292500e+03	0.553810e+03
0.293500e+03	0.553810e+03
0.294500e+03	0.553810e+03
0.295500e+03	0.560714e+03
0.296500e+03	0.557262e+03
0.297500e+03	0.560714e+03
0.298500e+03	0.560714e+03
0.299500e+03	0.553810e+03
0.300500e+03	0.560714e+03
0.301500e+03	0.553810e+03
0.302500e+03	0.560714e+03
0.303500e+03	0.560714e+03
0.304500e+03	0.560714e+03
0.305500e+03	0.560714e+03
0.306500e+03	0.560714e+03
0.307500e+03	0.560714e+03
0.308500e+03	0.564047e+03
0.309500e+03	0.560714e+03
0.310500e+03	0.567500e+03
0.311500e+03	0.567500e+03
0.312500e+03	0.567500e+03
0.313500e+03	0.567500e+03
0.314500e+03	0.567500e+03
0.315500e+03	0.567500e+03
0.316500e+03	0.567500e+03
0.317500e+03	0.560714e+03
0.318500e+03	0.567500e+03
0.319500e+03	0.567500e+03
0.320500e+03	0.567500e+03
0.321500e+03	0.567500e+03
0.322500e+03	0.567500e+03
0.323500e+03	0.567500e+03
0.324500e+03	0.567500e+03
0.325500e+03	0.567500e+03
0.326500e+03	0.574405e+03
0.327500e+03	0.567500e+03
0.328500e+03	0.567500e+03
0.329500e+03	0.567500e+03
0.330500e+03	0.567500e+03
0.331500e+03	0.567500e+03
0.332500e+03	0.574405e+03
0.333500e+03	0.574405e+03
0.334500e+03	0.567500e+03
0.335500e+03	0.574405e+03
0.336500e+03	0.574405e+03
0.337500e+03	0.574405e+03

BR23 Response to BR20 Discharge	
Time (h)	specific pressure ($kPa-s/m^3$)
0.338500e+03	0.574405e+03
0.339500e+03	0.567500e+03
0.340500e+03	0.560714e+03
0.341500e+03	0.547024e+03
0.342500e+03	0.533333e+03
0.343500e+03	0.519643e+03
0.344500e+03	0.505952e+03
0.345500e+03	0.492262e+03
0.346500e+03	0.485357e+03
0.347500e+03	0.478571e+03
0.348500e+03	0.471667e+03
0.349500e+03	0.464881e+03
0.350500e+03	0.457976e+03
0.351500e+03	0.451190e+03
0.352500e+03	0.444286e+03
0.353500e+03	0.444286e+03
0.354500e+03	0.437500e+03
0.355500e+03	0.430595e+03
0.356500e+03	0.430595e+03
0.357500e+03	0.423809e+03
0.358500e+03	0.423809e+03
0.359500e+03	0.416905e+03
0.360500e+03	0.410119e+03
0.361500e+03	0.410119e+03
0.362500e+03	0.403333e+03
0.363500e+03	0.403333e+03
0.364500e+03	0.396429e+03
0.365500e+03	0.396429e+03
0.366500e+03	0.389643e+03
0.367500e+03	0.389643e+03
0.368500e+03	0.382738e+03
0.369500e+03	0.382738e+03
0.370500e+03	0.375952e+03
0.371500e+03	0.369048e+03
0.372500e+03	0.369048e+03
0.373500e+03	0.369048e+03
0.374500e+03	0.362262e+03
0.375500e+03	0.362262e+03
0.376500e+03	0.362262e+03
0.377500e+03	0.355357e+03
0.378500e+03	0.355357e+03
0.379500e+03	0.348571e+03
0.407500e+03	0.287024e+03
0.408500e+03	0.287024e+03
0.409500e+03	0.287024e+03
0.410500e+03	0.287024e+03
0.411500e+03	0.283571e+03
0.412500e+03	0.280119e+03
0.413500e+03	0.280119e+03
0.414500e+03	0.273333e+03
0.415500e+03	0.273333e+03

BR23 Response to BR20 Discharge	
Time (*h*)	Specific Pressure ($kPa-s/m^3$)
0.416500e+03	0.273333e+03
0.417500e+03	0.273333e+03
0.418500e+03	0.266548e+03
0.419500e+03	0.266548e+03
0.420500e+03	0.266548e+03
0.421500e+03	0.266548e+03
0.422500e+03	0.266548e+03
0.423500e+03	0.266548e+03
0.424500e+03	0.266548e+03
0.425500e+03	0.259643e+03
0.426500e+03	0.252857e+03
0.427500e+03	0.259643e+03
0.428500e+03	0.252857e+03
0.429500e+03	0.252857e+03
0.430500e+03	0.252857e+03
0.431500e+03	0.252857e+03
0.432500e+03	0.252857e+03
0.433500e+03	0.245952e+03
0.434500e+03	0.245952e+03
0.435500e+03	0.249405e+03
0.436500e+03	0.245952e+03
0.437500e+03	0.245952e+03
0.438500e+03	0.245952e+03
0.439500e+03	0.245952e+03
0.440500e+03	0.245952e+03
0.441500e+03	0.245952e+03
0.442500e+03	0.239167e+03
0.443500e+03	0.239167e+03
0.444500e+03	0.242619e+03
0.445500e+03	0.239167e+03
0.446500e+03	0.239167e+03
0.447500e+03	0.239167e+03
0.448500e+03	0.239167e+03
0.449500e+03	0.239167e+03
0.450500e+03	0.239167e+03
0.451500e+03	0.239167e+03
0.452500e+03	0.232262e+03
0.453500e+03	0.235714e+03
0.454500e+03	0.232262e+03
0.455500e+03	0.232262e+03
0.456500e+03	0.232262e+03
0.457500e+03	0.232262e+03
0.458500e+03	0.232262e+03
0.460500e+03	0.232262e+03
0.461500e+03	0.232262e+03
0.462500e+03	0.232262e+03
0.463500e+03	0.232262e+03
0.464500e+03	0.232262e+03
0.465500e+03	0.232262e+03
0.466500e+03	0.232262e+03
0.467500e+03	0.225476e+03

BR23 Response to BR20 Discharge	
Time (h)	specific pressure ($kPa-s/m^3$)
0.468500e+03	0.225476e+03
0.469500e+03	0.225476e+03
0.470500e+03	0.218690e+03
0.471500e+03	0.218690e+03
0.472500e+03	0.218690e+03
0.473500e+03	0.218690e+03
0.474500e+03	0.218690e+03
0.475500e+03	0.211786e+03
0.476500e+03	0.211786e+03
0.477500e+03	0.211786e+03
0.478500e+03	0.211786e+03
0.479500e+03	0.211786e+03
0.480500e+03	0.211786e+03
0.481500e+03	0.208452e+03
0.482500e+03	0.205000e+03
0.483500e+03	0.205000e+03
0.484500e+03	0.205000e+03
0.485500e+03	0.205000e+03
0.486500e+03	0.205000e+03
0.487500e+03	0.205000e+03
0.488500e+03	0.198095e+03
0.489500e+03	0.198095e+03
0.490500e+03	0.198095e+03
0.491500e+03	0.198095e+03
0.492500e+03	0.198095e+03
0.493500e+03	0.198095e+03
0.494500e+03	0.198095e+03
0.495500e+03	0.198095e+03
0.496500e+03	0.198095e+03
0.497500e+03	0.191309e+03
0.498500e+03	0.191309e+03
0.499500e+03	0.191309e+03
0.500500e+03	0.191309e+03
0.501500e+03	0.191309e+03
0.502500e+03	0.191309e+03
0.503500e+03	0.191309e+03
0.504500e+03	0.184405e+03
0.505500e+03	0.191309e+03
0.506500e+03	0.191309e+03
0.507500e+03	0.191309e+03
0.508500e+03	0.191309e+03
0.509500e+03	0.191309e+03
0.510500e+03	0.191309e+03
0.511500e+03	0.191309e+03
0.512500e+03	0.191309e+03
0.513500e+03	0.184405e+03
0.514500e+03	0.191309e+03
0.515500e+03	0.184405e+03
0.516500e+03	0.184405e+03
0.517500e+03	0.184405e+03
0.518500e+03	0.184405e+03

BR23 Response to BR20 Discharge	
Time (h)	Specific Pressure ($kPa-s/m^3$)
0.519500e+03	0.184405e+03
0.520500e+03	0.184405e+03
0.521500e+03	0.184405e+03
0.522500e+03	0.184405e+03
0.523500e+03	0.184405e+03
0.524500e+03	0.184405e+03
0.525500e+03	0.184405e+03
0.526500e+03	0.184405e+03
0.527500e+03	0.184405e+03
0.528500e+03	0.177619e+03
0.529500e+03	0.177619e+03
0.530500e+03	0.184405e+03
0.531500e+03	0.177619e+03
0.532500e+03	0.177619e+03
0.533500e+03	0.177619e+03
0.534500e+03	0.177619e+03
0.535500e+03	0.177619e+03
0.536500e+03	0.177619e+03
0.537500e+03	0.177619e+03
0.538500e+03	0.170833e+03
0.539500e+03	0.177619e+03
0.540500e+03	0.177619e+03
0.541500e+03	0.170833e+03
0.542500e+03	0.170833e+03
0.543500e+03	0.177619e+03
0.544500e+03	0.177619e+03
0.578500e+03	0.150357e+03
0.579500e+03	0.150357e+03

TABLE B12

TEST C3: BR34 RESPONSE TO BR20 DISCHARGE

Time (h)	Specific Pressure ($kPa-s/m^3$)
0.250000e+01	0.214277e+01
0.450000e+01	0.428590e+01
0.550000e+01	0.428590e+01
0.650000e+01	0.214277e+01
0.750000e+01	0.428590e+01
0.850000e+01	0.428590e+01
0.950000e+01	0.642867e+01
0.105000e+02	0.857144e+01
0.115000e+02	0.857144e+01
0.125000e+02	0.857144e+01
0.545000e+02	0.100357e+03
0.695000e+02	0.136667e+03
0.705000e+02	0.136667e+03
0.715000e+02	0.140952e+03
0.725000e+02	0.140952e+03
0.735000e+02	0.145238e+03
0.745000e+02	0.145238e+03
0.755000e+02	0.145238e+03
0.765000e+02	0.149524e+03
0.775000e+02	0.149524e+03
0.785000e+02	0.153810e+03
0.795000e+02	0.153810e+03
0.805000e+02	0.158095e+03
0.815000e+02	0.158095e+03
0.825000e+02	0.162381e+03
0.835000e+02	0.166667e+03
0.845000e+02	0.170833e+03
0.855000e+02	0.170833e+03
0.865000e+02	0.175 119e+03
0.875000e+02	0.175119e+03
0.885000e+02	0.179405e+03
0.895000e+02	0.179405e+03
0.905000e+02	0.183690e+03
0.915000e+02	0.183690e+03
0.925000e+02	0.187976e+03
0.935000e+02	0.187976e+03
0.945000e+02	0.192262e+03
0.955000e+02	0.192262e+03
0.965000e+02	0.192262e+03
0.975000e+02	0.196548e+03
0.985000e+02	0.200833e+03
0.995000e+02	0.200833e+03
0.100500e+03	0.205119e+03
0.101500e+03	0.205 119e+03
0.102500e+03	0.205 119e+03

BR34 Response to BR20 Discharge	
Time (h)	specificpressure ($kPa-s/m^3$)
0.103500e+03	0.205119e+03
0.104500e+03	0.209405e+03
0.105500e+03	0.213691e+03
0.106500e+03	0.213691e+03
0.107500e+03	0.217976e+03
0.108500e+03	0.217976e+03
0.109500e+03	0.217976e+03
0.110500e+03	0.222262e+03
0.111500e+03	0.222262e+03
0.112500e+03	0.226428e+03
0.113500e+03	0.230714e+03
0.114500e+03	0.230714e+03
0.115500e+03	0.232857e+03
0.116500e+03	0.235000e+03
0.117500e+03	0.237143e+03
0.118500e+03	0.239286e+03
0.119500e+03	0.239286e+03
0.120500e+03	0.243571e+03
0.121500e+03	0.243571e+03
0.122500e+03	0.243571e+03
0.123500e+03	0.247857e+03
0.124500e+03	0.247857e+03
0.125500e+03	0.247857e+03
0.126500e+03	0.252143e+03
0.127500e+03	0.252143e+03
0.128500e+03	0.252143e+03
0.129500e+03	0.256429e+03
0.130500e+03	0.256429e+03
0.131500e+03	0.260714e+03
0.132500e+03	0.260714e+03
0.133500e+03	0.260714e+03
0.134500e+03	0.265000e+03
0.135500e+03	0.265000e+03
0.136500e+03	0.265000e+03
0.137500e+03	0.267143e+03
0.138500e+03	0.269286e+03
0.139500e+03	0.269286e+03
0.140500e+03	0.269286e+03
0.141500e+03	0.273572e+03
0.142500e+03	0.273572e+03
0.143500e+03	0.277857e+03
0.144500e+03	0.277857e+03
0.145500e+03	0.277857e+03
0.146500e+03	0.286309e+03
0.147500e+03	0.286309e+03
0.148500e+03	0.286309e+03
0.149500e+03	0.288453e+03
0.150500e+03	0.290595e+03
0.151500e+03	0.290595e+03
0.152500e+03	0.294881e+03
0.153500e+03	0.290595e+03

BR34 Response to BR20 Discharge	
Time (h)	specific Pressure ($kPa-s/m^3$)
0.154500e+03	0.294881e+03
0.155500e+03	0.294881e+03
0.156500e+03	0.299167e+03
0.157500e+03	0.299167e+03
0.158500e+03	0.301310e+03
0.159500e+03	0.301310e+03
0.160500e+03	0.303452e+03
0.161500e+03	0.307738e+03
0.194500e+03	0.363333e+03
0.195500e+03	0.359167e+03
0.196500e+03	0.363333e+03
0.197500e+03	0.363333e+03
0.198500e+03	0.363333e+03
0.199500e+03	0.363333e+03
0.200500e+03	0.363333e+03
0.201500e+03	0.367619e+03
0.202500e+03	0.369762e+03
0.203500e+03	0.367619e+03
0.204500e+03	0.371905e+03
0.205500e+03	0.371905e+03
0.206500e+03	0.371905e+03
0.207500e+03	0.376191e+03
0.208500e+03	0.376191e+03
0.209500e+03	0.380476e+03
0.210500e+03	0.380476e+03
0.211500e+03	0.380476e+03
0.212500e+03	0.384762e+03
0.213500e+03	0.384762e+03
0.214500e+03	0.384762e+03
0.215500e+03	0.384762e+03
0.216500e+03	0.384762e+03
0.217500e+03	0.389048e+03
0.218500e+03	0.389048e+03
0.219500e+03	0.389048e+03
0.220500e+03	0.391191e+03
0.221500e+03	0.391191e+03
0.222500e+03	0.393333e+03
0.223500e+03	0.393333e+03
0.224500e+03	0.393333e+03
0.225500e+03	0.395476e+03
0.226500e+03	0.397619e+03
0.227500e+03	0.397619e+03
0.228500e+03	0.397619e+03
0.229500e+03	0.397619e+03
0.230500e+03	0.397619e+03
0.231500e+03	0.401905e+03
0.232500e+03	0.399762e+03
0.233500e+03	0.406190e+03
0.234500e+03	0.406190e+03
0.235500e+03	0.408333e+03
0.236500e+03	0.410476e+03

BR34 Response to BR20 Discharge	
Time (*h*)	Specific pressure ($kPa-s/m^3$)
0.237500e+03	0.410476e+03
0.238500e+03	0.410476e+03
0.239500e+03	0.410476e+03
0.240500e+03	0.414762e+03
0.241500e+03	0.414762e+03
0.242500e+03	0.414762e+03
0.243500e+03	0.414762e+03
0.244500e+03	0.416905e+03
0.245500e+03	0.419048e+03
0.246500e+03	0.419048e+03
0.247500e+03	0.421191e+03
0.248500e+03	0.419048e+03
0.249500e+03	0.419048e+03
0.250500e+03	0.419048e+03
0.251500e+03	0.423333e+03
0.252500e+03	0.423333e+03
0.253500e+03	0.427619e+03
0.254500e+03	0.427619e+03
0.255500e+03	0.429762e+03
0.256500e+03	0.431905e+03
0.258500e+03	0.431905e+03
0.259500e+03	0.431905e+03
0.260500e+03	0.436191e+03
0.261500e+03	0.436191e+03
0.262500e+03	0.436191e+03
0.263500e+03	0.436191e+03
0.264500e+03	0.440476e+03
0.265500e+03	0.436191e+03
0.266500e+03	0.440476e+03
0.267500e+03	0.444762e+03
0.268500e+03	0.444762e+03
0.269500e+03	0.444762e+03
0.270500e+03	0.444762e+03
0.271500e+03	0.444762e+03
0.272500e+03	0.444762e+03
0.273500e+03	0.449048e+03
0.274500e+03	0.449048e+03
0.275500e+03	0.449048e+03
0.276500e+03	0.453333e+03
0.277500e+03	0.453333e+03
0.278500e+03	0.453333e+03
0.279500e+03	0.457619e+03
0.280500e+03	0.453333e+03
0.281500e+03	0.457619e+03
0.282500e+03	0.461905e+03
0.283500e+03	0.461905e+03
0.284500e+03	0.464048e+03
0.285500e+03	0.466191e+03
0.286500e+03	0.466191e+03
0.287500e+03	0.470476e+03
0.288500e+03	0.466191e+03

BR34 Response to BR20 Discharge	
Time (h)	Specific Pressure ($kPa-s/m^3$)
0.289500e+03	0.470476e+03
0.290500e+03	0.470476e+03
0.291500e+03	0.470476e+03
0.292500e+03	0.470476e+03
0.293500e+03	0.474762e+03
0.294500e+03	0.470476e+03
0.295500e+03	0.474762e+03
0.296500e+03	0.474762e+03
0.297500e+03	0.474762e+03
0.298500e+03	0.479048e+03
0.299500e+03	0.479048e+03
0.300500e+03	0.479048e+03
0.301500e+03	0.479048e+03
0.302500e+03	0.483214e+03
0.303500e+03	0.479048e+03
0.304500e+03	0.483214e+03
0.305500e+03	0.485357e+03
0.306500e+03	0.483214e+03
0.307500e+03	0.487500e+03
0.308500e+03	0.487500e+03
0.309500e+03	0.491786e+03
0.310500e+03	0.491786e+03
0.311500e+03	0.491786e+03
0.312500e+03	0.491786e+03
0.313500e+03	0.491786e+03
0.314500e+03	0.491786e+03
0.315500e+03	0.491786e+03
0.316500e+03	0.496072e+03
0.317500e+03	0.496072e+03
0.318500e+03	0.496072e+03
0.319500e+03	0.496072e+03
0.320500e+03	0.500357e+03
0.321500e+03	0.500357e+03
0.322500e+03	0.504643e+03
0.323500e+03	0.500357e+03
0.324500e+03	0.504643e+03
0.325500e+03	0.504643e+03
0.326500e+03	0.504643e+03
0.327500e+03	0.500357e+03
0.328500e+03	0.504643e+03
0.329500e+03	0.506786e+03
0.330500e+03	0.508929e+03
0.331500e+03	0.508929e+03
0.332500e+03	0.508929e+03
0.333500e+03	0.508929e+03
0.334500e+03	0.513214e+03
0.335500e+03	0.508929e+03
0.336500e+03	0.513214e+03
0.337500e+03	0.513214e+03
0.338500e+03	0.513214e+03
0.339500e+03	0.513214e+03

BR34 Response to BR20 Discharge	
Time (*h*)	Specific Pressure ($kPa-s/m^3$)
0.340500e+03	0.513214e+03
0.341500e+03	0.513214e+03
0.342500e+03	0.513214e+03
0.343500e+03	0.517500e+03
0.344500e+03	0.508929e+03
0.345500e+03	0.513214e+03
0.346500e+03	0.513214e+03
0.347500e+03	0.515357e+03
0.348500e+03	0.513214e+03
0.349500e+03	0.513214e+03
0.350500e+03	0.513214e+03
0.351500e+03	0.508929e+03
0.352500e+03	0.508929e+03
0.353500e+03	0.508929e+03
0.354500e+03	0.504643e+03
0.355500e+03	0.504643e+03
0.356500e+03	0.504643e+03
0.357500e+03	0.504643e+03
0.358500e+03	0.500357e+03
0.359500e+03	0.500357e+03
0.360500e+03	0.500357e+03
0.361500e+03	0.496072e+03
0.362500e+03	0.493928e+03
0.363500e+03	0.491786e+03
0.364500e+03	0.491786e+03
0.365500e+03	0.489643e+03
0.366500e+03	0.487500e+03
0.367500e+03	0.487500e+03
0.368500e+03	0.485357e+03
0.369500e+03	0.483214e+03
0.370500e+03	0.483214e+03
0.371500e+03	0.481191e+03
0.372500e+03	0.479048e+03
0.373500e+03	0.474762e+03
0.374500e+03	0.474762e+03
0.375500e+03	0.474762e+03
0.376500e+03	0.470476e+03
0.377500e+03	0.470476e+03
0.378500e+03	0.466191e+03
0.379500e+03	0.466191e+03
0.407500e+03	0.419048e+03
0.408500e+03	0.419048e+03
0.409500e+03	0.414762e+03
0.410500e+03	0.414762e+03
0.411500e+03	0.410476e+03
0.412500e+03	0.410476e+03
0.413500e+03	0.410476e+03
0.414500e+03	0.410476e+03
0.415500e+03	0.406190e+03
0.416500e+03	0.406190e+03
0.417500e+03	0.401905e+03

BR34 Response to BR20 Discharge	
Time (*h*)	Specific Pressure ($kPa-s/m^3$)
0.418500e+03	0.401905e+03
0.419500e+03	0.401905e+03
0.420500e+03	0.401905e+03
0.421500e+03	0.397619e+03
0.422500e+03	0.397619e+03
0.423500e+03	0.397619e+03
0.424500e+03	0.393333e+03
0.425500e+03	0.393333e+03
0.426500e+03	0.389048e+03
0.427500e+03	0.389048e+03
0.428500e+03	0.389048e+03
0.429500e+03	0.389048e+03
0.430500e+03	0.384762e+03
0.431500e+03	0.384762e+03
0.432500e+03	0.382619e+03
0.433500e+03	0.380476e+03
0.434500e+03	0.380476e+03
0.435500e+03	0.380476e+03
0.436500e+03	0.376191e+03
0.437500e+03	0.376191e+03
0.438500e+03	0.374048e+03
0.439500e+03	0.371905e+03
0.440500e+03	0.371905e+03
0.441500e+03	0.369762e+03
0.442500e+03	0.367619e+03
0.443500e+03	0.367619e+03
0.444500e+03	0.367619e+03
0.445500e+03	0.363333e+03
0.446500e+03	0.363333e+03
0.447500e+03	0.363333e+03
0.448500e+03	0.359167e+03
0.449500e+03	0.359167e+03
0.450500e+03	0.357024e+03
0.451500e+03	0.354881e+03
0.452500e+03	0.354881e+03
0.453500e+03	0.354881e+03
0.454500e+03	0.350595e+03
0.455500e+03	0.350595e+03
0.456500e+03	0.348452e+03
0.457500e+03	0.346309e+03
0.458500e+03	0.346309e+03
0.460500e+03	0.342024e+03
0.461500e+03	0.342024e+03
0.462500e+03	0.342024e+03
0.463500e+03	0.342024e+03
0.464500e+03	0.337738e+03
0.465500e+03	0.333453e+03
0.466500e+03	0.333453e+03
0.467500e+03	0.337738e+03
0.468500e+03	0.333453e+03
0.469500e+03	0.337738e+03

Time (h)	Specific Pressure ($kPa-s/m^3$)
0.470500e+03	0.333453e+03
0.471500e+03	0.333453e+03
0.472500e+03	0.329167e+03
0.473500e+03	0.331309e+03
0.474500e+03	0.329167e+03
0.476500e+03	0.320595e+03
0.479500e+03	0.320595e+03
0.480500e+03	0.320595e+03
0.481500e+03	0.320595e+03
0.482500e+03	0.320595e+03
0.483500e+03	0.316310e+03
0.484500e+03	0.316310e+03
0.485500e+03	0.316310e+03
0.486500e+03	0.314167e+03
0.487500e+03	0.312024e+03
0.488500e+03	0.312024e+03
0.489500e+03	0.307738e+03
0.490500e+03	0.307738e+03
0.491500e+03	0.307738e+03
0.492500e+03	0.307738e+03
0.493500e+03	0.307738e+03
0.494500e+03	0.307738e+03
0.495500e+03	0.307738e+03
0.496500e+03	0.303452e+03
0.497500e+03	0.303452e+03
0.498500e+03	0.303452e+03
0.499500e+03	0.303452e+03
0.500500e+03	0.303452e+03
0.501500e+03	0.303452e+03
0.502500e+03	0.299167e+03
0.503500e+03	0.299167e+03
0.504500e+03	0.297024e+03
0.505500e+03	0.294881e+03
0.506500e+03	0.294881e+03
0.507500e+03	0.294881e+03
0.508500e+03	0.294881e+03
0.509500e+03	0.294881e+03
0.510500e+03	0.290595e+03
0.511500e+03	0.290595e+03
0.512500e+03	0.290595e+03
0.513500e+03	0.288453e+03
0.514500e+03	0.286309e+03
0.515500e+03	0.290595e+03
0.516500e+03	0.290595e+03
0.517500e+03	0.286309e+03
0.518500e+03	0.288453e+03
0.519500e+03	0.286309e+03
0.520500e+03	0.286309e+03
0.521500e+03	0.286309e+03
0.522500e+03	0.288453e+03
0.523500e+03	0.286309e+03

BR34 Response to BR20 Discharge	
Time (h)	Specific Pressure ($kPa-s/m^3$)
0.524500e+03	0.286309e+03
0.525500e+03	0.284286e+03
0.526500e+03	0.282143e+03
0.527500e+03	0.282143e+03
0.528500e+03	0.282143e+03
0.529500e+03	0.282143e+03
0.530500e+03	0.282143e+03
0.531500e+03	0.277857e+03
0.532500e+03	0.277857e+03
0.533500e+03	0.277857e+03
0.534500e+03	0.277857e+03
0.535500e+03	0.277857e+03
0.536500e+03	0.273572e+03
0.537500e+03	0.273572e+03
0.538500e+03	0.277857e+03
0.539500e+03	0.273572e+03
0.540500e+03	0.273572e+03
0.541500e+03	0.273572e+03
0.542500e+03	0.273572e+03
0.543500e+03	0.273572e+03
0.544500e+03	0.273572e+03
0.578500e+03	0.252143e+03
0.579500e+03	0.247857e+03